Probing New Physics with Flavour, Collider, and Molecular Physics

From Supersymmetry to a Light Dark Sector

Zur Erlangung des akademischen Grades eines

Doktors der Naturwissenschaften (Dr. rer. nat.)

von der KIT-Fakultät für Physik
des Karlsruher Instituts für Technologie (KIT)

genehmigte

Dissertation

von

M.Sc. Mustafa Tabet

geboren in Karlsruhe

Abstract

In this thesis the recent anomalous measurements in $b \to sll$ transitions are studied. In particular, a solution within the R-parity conserving Minimal Supersymmetric Standard Model with non-holomorphic couplings is worked out. Constraints coming from theory and experiment are analysed. Eventually, correlations between these anomalies and effects in $b \to dll$ transitions are briefly discussed.

Furthermore, a two-Higgs-doublet model with spontaneous CP violation is analysed. Theoretical constraints make the derivation of upper bounds on the masses of the additional Higgs fields possible. A sum rule for the charged-Higgs couplings to bottom quarks is obtained and lower bounds on the very same couplings are determined. This implies in particular non-standard collider signatures which are subsequently analysed.

The last part of this work studies the constraints coming from molecular spectroscopy of hydrogen isotopologues on various light New Physics models.

Zusammenfassung

In dieser Dissertation werden die jüngsten anomalen Messungen in $b \to sll$ Übergängen untersucht. Im Speziellen wird eine Lösung im Rahmen des minimalen supersymmetrischen Standardmodells mit R-Paritätserhaltung und nicht holomorphen Kopplungen erarbeitet. Theoretische und experimentelle Einschränkungen an dieses Modell werden analysiert. Schließlich werden Korrelationen zwischen diesen Anomalien und Effekte in $b \to dll$ Übergängen diskutiert.

Weiter wird ein Zwei-Higgs-Dublett Modell mit spontaner CP-Verletzung untersucht. Theoretische Einschränkungen erlauben es Obergrenzen an die Massen der zusätzlichen Higgs-Felder zu bestimmen. Sowohl eine Summenregel für die Kopplungen des geladenen Higgs-Bosons an die Bottom-Quarks als auch Untergrenzen an jene Kopplungen werden bestimmt. Das impliziert im Speziellen Nichtstandard-Signaturen in der Kolliderphysik, welche, darauf aufbauend, analysiert werden.

Der letzte Teil dieser Arbeit befasst sich mit den Einschränkungen an unterschiedliche Modelle leichter neuer Physik durch molekulare Spektroskopie von Wasserstoff-Isotopologen.

Contents

Part IV   Appendices

List of Figures

List of Tables

Abbreviations

2HDM two-Higgs-doublet model

CARS Coherent Anti-Stokes Raman Scattering Spectroscopy

CKM Cabibbo–Kobayashi–Maskawa

DVR discrete value representation

HL-LHC High-Luminosity Large Hadron Collider

KM Kobayashi–Maskawa

LCDA light-cone distribution amplitude

LCSR light-cone sum rule

LEP Large Electron–Positron Collider

LHC Large Hadron Collider

LSP lightest supersymmetric particle

MSSM Minimal Supersymmetric Standard Model

NAPT non-adiabatic perturbation theory

NLO next-to-leading order

NNLO next-to-next-to-leading order

NRQED non-relativistic QED

OPE operator product expansion

QCD quantum chromodynamics

QCDF QCD factorisation

QED quantum electrodynamics

vev vacuum expectation value

Introduction

The formulation of the Standard Model, which encodes all known interactions besides gravity, might be the biggest success within the framework of quantum field theory. Not only have all predicted particles been observed with the Higgs boson being the latest one discovered at the Large Hadron Collider (LHC) in 2012, but also do most theoretical predictions match the experimental measurements to a high precision. However, not all predictions and measurements agree perfectly. Even better for our inquiring minds, we *know* that there must be physics beyond the Standard Model. First, astronomical observations show that the largest part of the mass in the universe does not come from the matter described within the Standard Model. There has to be additional gravitationally interacting matter that we do not observe, hence these unknown particles are termed *dark matter*. On top of this, the observed matter-antimatter asymmetry cannot be explained within the Standard Model, additional sources of CP violation are needed. Beside these shortcomings of the Standard Model, there are strong evidences and hints for physics beyond the Standard Model, for instance there is the long-standing deviation between the prediction and measurement of the anomalous magnetic moment of the muon or the recent anomalous measurements in $b \to sll$[1] transitions, respectively. All these discrepancies have to be resolved, but this is not the end of the story. There are the so-called Standard Model puzzles: Questions that one may ask which could have an answer, but with our current understanding of Nature might as well just be like that. In other words, these are by no means problems or flaws of the Standard Model that require a solution but might serve as clues for the nature of the yet unknown physics beyond the Standard Model. For example the flavour puzzle, namely the question why there is such a large hierarchy between the fermion masses and the elements of the quark mixing matrix within the Standard Model. This might as well be connected to a more fundamental question: The Standard Model without neutrino masses has 19 free parameters, and the question that now arises is whether all these parameters follow from a more fundamental theory with fewer free parameters. Further, there is the so-called strong CP puzzle[2] namely the question why the θ parameter in the quantum chromodynamics (QCD) Lagrangian is so close to, or even exactly, zero. It is these puzzles and questions that keep our curiosity

---

[1]Unless noted otherwise, $ll \equiv l^+l^-$ is implicitly understood.
[2]Note that we refrain from terming it a problem as it is widely done in the literature due to our clear distinction between problem and puzzle.

driving and from now on it is this yet unknown physics beyond the Standard Model that we generically refer to as *New Physics*.

How does this New Physics look like? Beyond the rules set by quantum field theory and the constraints from experimental measurements, the only boundaries are set by the limits of our creativity. Actually, even the former assumption might be dropped as quantum field theory in its current form is incompatible with gravity. Nevertheless, we know phenomenologically that the energy scales we consider in this work are sufficiently well described by quantum field theories. It even goes beyond that: The Standard Model has established itself as a very successful theory, and thus, often serves as the starting point for, or limit of, a New Physics model.

The difficulty lies in determining the New Physics model realised in Nature which further is complicated by the absence of any direct detection. Nevertheless, New Physics models can still be extensively constrained. For example the non-observation itself excludes New Physics models that contrary to the observation predict a detectable effect. The approach here is twofold: On the one hand, constraints on New Physics models come from the non-observation at direct detection experiments, for instance performed at the LHC. On the other hand, the absence of any deviations in precision measurements performed at high and low energies puts severe limits on the New Physics. In particular the latter approach has proven valuable in the past and allowed for example to predict the top quark mass within a certain mass window. Another significant advantage of precision measurements is the reach up to the PeV scale in excluding New Physics—far above the current and near future reach of direct searches. Furthermore, deviations between the Standard Model predictions and the measurements require New Physics to bring the theory in line with experiments. This is exactly what is tackled in this thesis. We examine several New Physics scenarios from high to low energy proposed to overcome the shortcomings of the Standard Model in the context of current direct and indirect constraints as well as anomalous measurements.

First, we investigate the recent anomalies in the $b \to sll$ transition, the so-called b anomalies, where the recent measurement provides a hint for New Physics. This is done in the context of the Minimal Supersymmetric Standard Model (MSSM)—a Standard Model extension which for example is able to provide a dark matter candidate, to unify the gauge couplings at the grand unification scale, and to circumvent the hierarchy puzzle. The latter appears in the context of New Physics models where the Higgs boson mass is calculable. In this case one expects corrections to the Higgs boson mass that are quadratically in the scale at which the New Physics is expected to arise. However, the Higgs boson has a mass around the electroweak scale, but without a tuning of the parameters this is unexpected in the presence of new heavy particles which would push the Higgs boson mass far above the electroweak scale. In the MSSM this is circumvented by the presence of the so-called superpartners such that corrections of heavy particles are cancelled by the contribution of the postulated superpartners. However, with the non-observation of particles beyond the ones present in the Standard Model at the LHC, the popularity of this model is decreasing. The fate of the MSSM worsened by the recent b anomalies as it is widely claimed that the MSSM[1] is not able to accommodate the difference between theory and experiment in the measured quantities. In case of a confirmation of the anomalies, this highly disfavours the MSSM as a Standard Model extension. However, the analyses discussing the MSSM in the context of the b anomalies overlook a non-negligible parameter region which might be able to actually explain the anomalies. Thus, we provide the last stepping stone of this

---

[1]Actually the *R*-parity conserving MSSM, this is discussed further below.

discussion and thoroughly analyse whether the MSSM is able to explain the anomalous measurements. In this case we provide a clear phenomenological direction for a future detection of supersymmetric particles. A non-detection, on the other hand, implies that the MSSM is indeed highly disfavoured as an explanation of the $b \to sll$ anomalies. This is done in Part I.

While the MSSM is able to tackle many problems and puzzles of the Standard Model, one major shortcoming cannot be solved: the baryon asymmetry. This can be addressed in other models with additional sources of CP violation as for example in a two-Higgs-doublet model (2HDM). For instance in the general 2HDM with spontaneous CP violation, new CP violating interactions arise from the mixing of CP-even and CP-odd Higgs states [1] beside the ones induced by the complex Cabibbo–Kobayashi–Maskawa (CKM) matrix. Initially, this model has been proposed to explain the observed CP violation in Nature. Nonetheless, the Kobayashi-Maskawa mechanism became established. Together with the large flavour violating couplings that arise at tree-level which are not observed in experiments, this model has lost in popularity. However, it is not yet ruled out—meaning that CP might still be spontaneously broken in Nature—and for this reason interesting features and phenomenology have been overlooked. Thus, in Part II we investigate the general 2HDM with spontaneous CP violation. We first introduce the model in Chapter 5, and determine a sum rule for the charged-Higgs couplings, which has crucial implications on collider phenomenology. Thus, in Chapter 6 we examine the constraints coming from direct searches and pave the way for near future experiments. The main results are summarised in Chapter 7.

So far we have only discussed New Physics beyond the electroweak scale for example the MSSM in Part I or New Physics around the electroweak scale for instance the 2HDM with spontaneous CP violation in Part II. However, in particular in the context of dark matter or of solutions to the CP puzzle, there is a plethora of New Physics models at energies below the electroweak scale. Thus, in Part III we derive model-independent constraints on classes of New Physics models at low energy. This is done with the help of molecular spectroscopy, which as a laboratory experiment is crucial since it directly excludes New Physics in a parameter region which otherwise is only indirectly accessible by astrophysical and cosmological observations. First, we introduce the theoretical and experimental framework in Chapter 8, and subsequently perform the New Physics analyses in Chapter 9. The results are summarised in Chapter 10.

Finally, we conclude the main results of this thesis in Chapter 11.

A New Physics Analysis of the $b \to sll$ Anomalies

In this part we provide a solution for the $b \to sll$ anomalies within the R-parity conserving Minimal Supersymmetric Standard Model in Chapter 2. For this we examine the parameter space where the fermion masses are generated radiatively. Hence, non-holomorphic soft breaking terms have to be kept in the scalar potential, and strong constraints from experiment and theory, in particular from vacuum stability are expected. In Chapter 3 we study the effect of New Physics in the $b \to dll$ transition. This helps to map out the flavour structure of the underlying model provided the anomalies in the $b \to sll$ sector are confirmed in future experiments. Finally, we conclude this part in Chapter 4.

A Supersymmetric Solution to the $R_{K^{(*)}}$ Anomalies

The recent measurement by the LHCb experiment provides evidence for a lepton flavour non-universal interaction in the transition $b \to sll$ with $l = e, \mu$ [2]. This violation of lepton flavour universality is already present in the Standard Model. However, it is only broken by the tiny Yukawa couplings of the Higgs boson to electrons and muons, and hence, negligible. Therefore, the ratio of the branching fractions

$$R_M^{[q_{min}, q_{max}]} = \frac{\int_{q_{min}}^{q_{max}} dq^2 \, dBR(B \to M\mu^+\mu^-)/dq^2}{\int_{q_{min}}^{q_{max}} dq^2 \, dBR(B \to Me^+e^-)/dq^2} , \qquad M = K^+, K^{0*}, \qquad (2.1)$$

is a powerful tool to test the Standard Model. While the QCD corrections cancel in this ratio, the quantum electrodynamics (QED) ones do not. The latter can yield up to a 10 % correction in the bins with small q^2 due to $\log(m_l)$ enhanced terms, however, they are controlled by the experimental cuts which keep the uncertainty at the 1 % level [3,4]. This renders the ratio $R_{K^{(*)}}$ theoretically clean, and any deviation from $R_K^{(*)} = 1 \pm 0.01$ for $q_{min} \geq 1.1 \, \text{GeV}^2$ is a clear sign of physics beyond the Standard Model.

The first measurements of the ratios $R_{K^{(*)}}^{[1.1,6]}$ and $R_{K^*}^{[0.045,1.1]}$ by the LHCb experiment point towards a 2.1–2.6 σ downward deviation from the Standard Model prediction [4,5]. Previous and current measurements of this ratio and branching fractions by the Belle and BaBar experiment are compatible with the Standard Model prediction within 1σ [6–10]. However, due to the much lower statistics of these experiments, the uncertainties of the measurements are much higher than the ones provided by the LHCb collaboration, see Figure 2.1. Interestingly, deviations in the decay $B \to K^{0*}\mu^+\mu^-$ were already observed in 2013 by the LHCb experiment in form-factor independent observables, in particular in the angular observable P_5' [11,12]. These observables were specifically designed to be theoretically clean and to provide a high New Physics sensitivity. In this work we focus on the $R_{K^{(*)}}$ anomalies.[1] The current measurements by the LHCb experiment read [2,5]

$$R_K^{[1.1,6]} = 0.846^{+0.042 \, +0.013}_{-0.039 \, -0.012} , \quad R_{K^*}^{[0.045,1.1]} = 0.66^{+0.11}_{-0.07} \pm 0.03 , \quad R_{K^*}^{[1.1,6]} = 0.69^{+0.11}_{-0.07} \pm 0.05 ,$$
$$(2.2)$$

---

[1]Nonetheless, deviations seen in other observables are taken implicitly into account by comparing with the Wilson coefficients obtained in the global analyses. Approximate expressions for the angular observables as a function of the New Physics Wilson coefficients can be found in Reference [13].
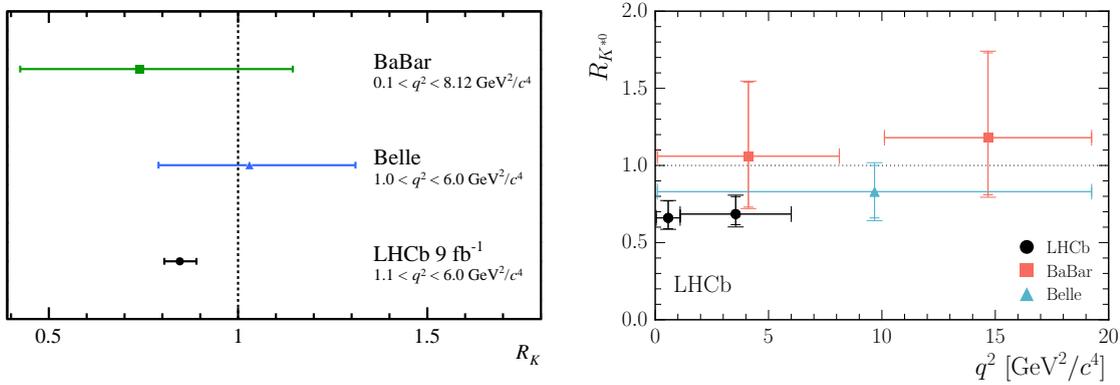
Figure 2.1.: Measurements of the ratio R_K (left) and R_{K^*} (right) by the Belle, BaBar and LHCb experiments [2, 5]. Note that the Belle measurement of R_{K^*} is superseded by Reference [9]. Nevertheless, the updated measurement remains compatible with the Standard Model prediction.

where the first uncertainty is statistical and the second systematic. While the measurements of R_{K^*} deviate more than $2\,\sigma$ from the Standard Model prediction, the measurement of R_K provides an evidence for lepton flavour non-universality with a significance of $3.1\,\sigma$.

Taking into account all measured observables of the $b \to sll$ transition, model-independent fits were performed favouring the New Physics hypothesis over the Standard Model hypothesis with a significance of over $5\,\sigma$ [14, 15]. For a detailed discussion of the global analysis see Reference [16]. Various New Physics models have been proposed to explain these deviations like the R-parity violating MSSM [17–19], models with leptoquarks [20, 21] or Z' bosons [22–26]. A review can be found in Reference [27].

The R-parity *conserving* MSSM as an otherwise popular New Physics model did not gain much impetus since early estimates showed that even for an $\mathcal{O}(1)$ squark mixing no sizeable contributions can be generated [13, 28]. There, contributions from higgsino boxes were neglected which are suppressed by the tiny Yukawa coupling of the muon. However, the tree-level relation between the mass m_μ and Yukawa coupling y_μ, $m_\mu \propto v y_\mu$, is broken by radiative corrections to the fermion masses. If those are generated at one-loop level, the corresponding Yukawa couplings can be as large as $\mathcal{O}(1)$, and the loop suppression will be responsible for the smallness of the fermion masses. In this case, the contribution coming from higgsino box diagrams cannot be neglected any longer.

The outline of this chapter is as follows: We introduce the MSSM with non-holomorphic couplings where we discuss the field content and the softly broken superpotential. We see that setting the vacuum expectation value (vev) of the second Higgs doublet v_d to $v_d = 0$ renders the Yukawa couplings of the down-type quarks and charged leptons into free parameters. This in turn can be used to generate sizeable higgsino contributions to R_K and R_{K^*} which is done in Section 2.2. In Section 2.3, we examine the allowed parameter space by taking into account experimental constraints and flavour constraints in particular. The radiative generation of fermion masses is analysed in Section 2.4. Next, we investigate the most imporant theoretical constraint, namely the effect of vacuum stability on the experimentally allowed parameter region needed to explain the deviation in $R_{K^{(*)}}$. A combined numerical analysis is performed in Section 2.6. Finally, we summarise the results in Section 2.7.

Table 2.1.: Standard Model matter fields with their scalar superpartners together with the Higgs bosons and their fermionic superpartners [30]. Convention adapted to Reference [29].

name	spin 0	spin 1/2	$SU(3)_C$	$SU(2)_L$	$U(1)_Y$
sleptons, leptons	$L_i = (\tilde{\nu}_i, \tilde{e}_{L,i}^-)^T$	$\left(\nu_{L,i}, e_{L,i}^-\right)^T$	1	2	-1
	$R_i = \tilde{e}_{R,i}^+$	$\left(e_{L,i}^-\right)^c$	1	1	2
squarks, quark	$Q_i = (\tilde{u}_{L,i}, \tilde{d}_{L,i})^T$	$(u_{L,i}, d_{L,i})^T$	3	2	1/3
	$U_i = \tilde{u}_{R,i}^*$	$(u_{L,i})^c$	$\bar{3}$	2	$-4/3$
	$D_i = \tilde{d}_{R,i}^*$	$(d_{L,i})^c$	$\bar{3}$	2	2/3
Higgs, higgsino	$H_u = (h_u^+, h_u^0)$	$\psi_{H_u} = (\tilde{h}_u^1, \tilde{h}_u^2)$	1	2	1
	$H_d = (h_d^0, h_d^-)$	$\psi_{H_d} = (\tilde{h}_d^1, \tilde{h}_d^2)$	1	2	-1

Table 2.2.: Standard Model gauge fields with their fermionic superpartners [30].

name	spin 1/2	spin 1	$SU(3)_C \times SU(2)_L \times U(1)_Y$
gluinos, gluons	$\tilde{g}^a$	G_μ^a	$(8, 1, 0)$
winos, W bosons	$\tilde{W}^i$	W_μ^i	$(1, 3, 0)$
bino, B boson	$\tilde{B}$	B_μ	$(1, 1, 0)$

2.1. The MSSM with Non-Holomorphic Couplings

Aside from minor notational differences, we follow the convention of Reference [29]. The most general Lagrangian of the MSSM, $\mathcal{L}_{\text{MSSM}}$, can be written compactly as

$$\mathcal{L}_{\text{MSSM}} = \mathcal{L}_{\text{free}+\text{gauge}} + \mathcal{L}_{\text{Yukawa}} - V + \mathcal{L}_{\text{soft}}. \tag{2.3}$$

In the following, we briefly discuss each term. For an extensive review see for instance Reference [30].

$\mathcal{L}_{\text{free}+\text{gauge}}$ contains the (gauge-)kinetic terms of the Standard Model fields, and the gauge self interaction. In addition it contains the kinetic terms for the supersymmetric partners of the Standard Model fields. In case of the fermions, they are scalars called sfermions while the spin 1/2 fermionic superpartners of the Standard Model gauge bosons are called gauginos, see Table 2.1 and Table 2.2, respectively, for their representation under the Standard Model gauge group. Consequently, $\mathcal{L}_{\text{free}+\text{gauge}}$ contains the interaction of the sfermion and gaugino fields with the gauge bosons, as well as a sfermion-fermion-gaugino interaction vertex.

The remaining non-gauge interaction terms can be described conveniently by the superpotential W which by construction has to be a holomorphic function of the scalar fields. Thus, a second Higgs doublet with an opposite hypercharge is required, see Table 2.1. Therefore, the most general, holomorphic and gauge invariant superpotential is given by [29]

$$W = \mu \epsilon_{ij} H_d^i H_u^j + \epsilon_{ij} Y_l H_d^i L^j R + \epsilon_{ij} Y_d H_d^i Q^j D + \epsilon_{ij} Y_u H_u^i Q^j U + W_{\not{R}}, \tag{2.4}$$

with $\epsilon_{12} = -\epsilon_{21} = -1$, the left-handed slepton field L^i, right-handed charged slepton R, the left- and right-handed squark fields Q^i, D and U, respectively. The term $W_{\not{R}}$ contains additional interactions which break the (accidental) lepton and baryon number conservation of the Standard Model. Such terms are strongly constrained by experimental measurements especially by the non-observation of a proton decay. They can be forbidden by charging all particles under an additional global symmetry called R-parity[1] [31]

$$R = (-1)^{3B+L+2s}\,, \tag{2.5}$$

with the spin s, baryon number B and lepton number L of the respective particle. With this definition the Standard Model particles and both Higgs doublets are even under R-parity while all supersymmetric particles are odd. This also means that the lightest supersymmetric particle (LSP) is stable and might serve as a dark matter candidate [32–34].

Finally, the Yukawa interactions $\mathcal{L}_{\text{Yukawa}}$ and the scalar potential V can be written as

$$\mathcal{L}_{\text{Yukawa}} = -\frac{1}{2}\frac{\partial^2 W}{\partial A_i \partial A_j}\psi_i \psi_j + \text{h.c.}\,, \qquad\qquad V = \frac{1}{2}D^a D^a + F_i^* F_i\,, \tag{2.6}$$

with the scalar fields A_i and their fermionic partners ψ_i. The F- and D-terms are given by

$$F_i = \frac{\partial W}{\partial A_i}\,, \qquad\qquad D^a = \sum_{\substack{\text{gauge groups}}} g A_i^* T_{ij}^a A_j\,, \tag{2.7}$$

where g denotes the gauge coupling and T^a the generators of the gauge group.

All terms discussed so far respect supersymmetry, i.e a scalar field has the same mass as its corresponding Standard Model field. However, such particles would have already been observed in Nature which means that supersymmetry must be broken if it is realised. For this reason one has to introduce the soft breaking terms $\mathcal{L}_{\text{soft}}$:

$$\begin{aligned}
\mathcal{L}_{\text{soft}} = &- m_{H_1}^2 H_d^{i*} H_d^i - m_{H_2}^2 H_u^{i*} H_u^i - m_L^2 L_i^* L_i - m_R^2 R^* R - m_Q^2 Q_i^* Q_i - m_D^2 D^* D - m_U^2 U^* U \\
&+ \frac{M_1}{2}\tilde{B}\tilde{B} + \frac{M_2}{2}\tilde{W}^i\tilde{W}^i + \frac{M_3}{2}\tilde{g}^a\tilde{g}^a + \text{h.c.} \\
&+ m_{12}^2 \epsilon_{ij} H_d^i H_u^j + \epsilon_{ij} A_l H_d^i L^j R + \epsilon_{ij} A_d H_d^i Q^j D + \epsilon_{ij} A_u H_u^i Q^j U + \text{h.c.} \\
&+ A_l' H_u^{i*} L^i R + A_d' H_u^{i*} Q^i D + A_u' H_d^{i*} Q^i U + \text{h.c.}\,, \tag{2.8}
\end{aligned}$$

where the first two lines contain the mass terms of the scalar fields and gauginos. The third and fourth line contain the holomorphic and non-holomorphic trilinear couplings of the scalar fields, respectively. Note that the former has the same structure as the superpotential W with the replacements $Y_f \to A_f$ and $\mu \to m_{12}$. The latter contains the interactions with the complex conjugate Higgs fields and for this reason they are called non-holomorphic. These non-holomorphic couplings are often neglected in the literature since they are often suppressed in high-scale supersymmetric breaking scenarios [35], however, they turn out to be crucial in our case. In general, the free 3×3 matrices $A_f^{(\prime)}$ can be complex, but since it does not affect any conclusion we choose them to be real.

We work in the super-CKM basis, i.e. a simultaneous rotation of the quark and squark fields is performed such that the Yukawa couplings are diagonal. Note that in general, the sfermion mass matrices remain non-diagonal [29, 36], and the CKM matrix V appears in

---

[1]Note the coinciding notation with the right-handed slepton fields R, however, since the meaning is apparent from the context, we refrain from changing the notation.

the sup (or sdown) sector. Analytic expressions in the sfermion and gaugino mass basis are often lengthy or lack insight since they involve the diagonalisation of large matrices. For this reason calculations are often performed in the mass insertion approximation [37–39] which is a diagrammatic expansion in the off-diagonal elements of the sfermion and gaugino mass matrices. This results in quadratic mixing terms in the interaction Lagrangian. Technically, we will make use of the Flavour Expansion Theorem [40, 41]. This allows us to perform the calculation in the mass basis and avoid the cumbersome diagrammatic expansion while still benefiting from an expansion in terms of the mass insertions Δ. We consider a supersymmetric mass scale M_{SUSY} of $\mathcal{O}(1\,\text{TeV})$ which is a reasonable assumption considering the non-observation of supersymmetric particles at the LHC [42–59].

Higgs Sector

In general, the Higgs fields acquire the vevs

$$\langle H_d \rangle = \begin{pmatrix} v_d \\ 0 \end{pmatrix}, \qquad\qquad \langle H_u \rangle = \begin{pmatrix} 0 \\ v_u \end{pmatrix}, \qquad (2.9)$$

with

$$\sqrt{v_d^2 + v_u^2} = v \approx 174\,\text{GeV}, \quad v_d = v c_\beta \equiv v\cos\beta, \quad v_u = v s_\beta \equiv v\sin\beta, \quad \tan\beta = v_u/v_d. \qquad (2.10)$$

Inspecting Equations (2.4) and (2.6), one sees that the tree-level mass of the down-type quarks and charged leptons f_i is given by

$$m_{f_i} = -Y_{f,ii} v_d. \qquad (2.11)$$

Therefore, for $v_d = 0$—or equivalently $\tan\beta \to \infty$—the Yukawa couplings of the down-type quarks and charged leptons are not fixed by the mass of that particle anymore.[1] Instead the observed mass of these particles has to be generated radiatively. This renders the Yukawa couplings Y_d and Y_l into free parameters only bounded by perturbativity.[2] Of course the Yukawa couplings enter the interactions of the fermions with the Higgs bosons and higgsinos, and therefore, they also re-enter the higher-order contributions to the fermion masses. However, this still leaves freedom in the choice of the Yukawa couplings and will be analysed further in Section 2.4. For now let us investigate the supersymmetric sector in this particular limit.

As usual, inserting the vevs into the Higgs potential yields the following vacuum conditions, see for example Reference [29]

$$\left(\frac{e^2}{4c_W^2 s_W^2}(v_d^2 - v_u^2) + m_{H_1}^2 + |\mu|^2 \right) v_d = -m_{12}^2 v_u,$$

$$\left(\frac{-e^2}{4c_W^2 s_W^2}(v_d^2 - v_u^2) + m_{H_2}^2 + |\mu|^2 \right) v_u = -m_{12}^2 v_d, \qquad (2.12)$$

---

[1]Even though we work in the limit $v_d = 0$, everything holds true for $v_d \ll 1$ ($\tan\beta \gg 100$).
[2]Here we use a tight, $y < \sqrt{2\pi}$, and loose, $y < \sqrt{4\pi}$, perturbativity constraint. An actual analysis based on partial-wave unitary [60] suggests an upper bound of $m_q < 500\,\text{GeV}$ and $m_l < 1\,\text{TeV}$ for quarks and leptons, respectively. While the former is close to our tight bound, we are well below the latter for leptons.

where s_W and c_W denote the sine and cosine of the weak mixing angle θ_W, respectively. In our case with $v_d = 0$, this simplifies to

$$m_{12}^2 = 0,$$

$$m_{H_2}^2 = -|\mu|^2 - \frac{e^2}{4c_W^2 s_W^2} v^2. \tag{2.13}$$

Interestingly, the free mass parameter has to be $m_{H_1}^2$ in contrast to the case with a non-vanishing vev v_d where the mass parameter m_{12}^2 can be chosen to be free instead. Therefore, the Higgs fields decouple for $m_{H_1}^2 \gg v$. Note that Equation (2.13) receives radiative corrections. In that case, the vevs are chosen to minimise the loop corrected potential. This might require additional fine-tuning of the mass parameters in particular m_{12}^2, such that $v_d \approx 0$. However, compared to the fine-tuning needed for the electroweak scale the additional tuning should be only of order $m_{12}^2/v^2 \sim g^2/(16\pi^2)$.

Diagonalising the charged Higgs mass matrix by the rotation Z_H [29]

$$\begin{pmatrix} h_d^+ \\ h_u^+ \end{pmatrix} = Z_H \begin{pmatrix} H^+ \\ G^+ \end{pmatrix}, \qquad Z_H = \frac{1}{v} \begin{pmatrix} v_u & -v_d \\ v_d & v_u \end{pmatrix} = \begin{pmatrix} s_\beta & -c_\beta \\ c_\beta & s_\beta \end{pmatrix}, \tag{2.14}$$

leads to the charged Higgs mass

$$m_{H^\pm}^2 = m_W^2 + m_{H_1}^2 + m_{H_2}^2 + 2|\mu|^2, \tag{2.15}$$

where $m_{H_2}^2$ is fixed by Equation (2.13).

The neutral Higgs mass matrix factorises into a CP-even and a CP-odd block and the neutral pseudoscalar fields A^0 and G^0 are given by the same rotation Z_H as in Equation (2.14) [29]:

$$\text{Im}\left\{ \begin{pmatrix} h_d^0 \\ h_u^0 \end{pmatrix} \right\} = Z_H \begin{pmatrix} A^0 \\ G^0 \end{pmatrix}, \tag{2.16}$$

with the mass of the physical pseudoscalar particle A^0 given by [29]

$$m_{A^0}^2 = m_{H^\pm}^2 - m_W^2. \tag{2.17}$$

In general, the CP-even mass block M_H of the physical Higgs fields H_i^0 has to be diagonalised. However, in the case $v_d = 0$, this mass matrix simplifies to

$$M_H^2 = \begin{pmatrix} m_{H_1}^2 + |\mu|^2 - \dfrac{e^2 v^2}{4 s_W^2 c_W^2} & 0 \\ 0 & \dfrac{e^2 v^2}{2 s_W^2 c_W^2} \end{pmatrix}, \tag{2.18}$$

and the masses can be read off

$$m_{H_1^0} = \sqrt{m_{H_1}^2 + |\mu|^2 - \frac{e^2 v^2}{4 s_W^2 c_W^2}}, \qquad m_{H_2^0} \equiv m_{h_{SM}} = m_Z = \frac{ev}{\sqrt{2} s_W c_W}. \tag{2.19}$$

Note that the tree-level mass $m_{h_{SM}}$ of the light CP-even Higgs is fixed to be exactly the Z boson mass m_Z, while in the general case the Higgs mass is only bounded from above by the mass m_Z. The general expressions can be found in Appendix A together with the discussion of the gaugino sector. If not mentioned otherwise, we work in the limit $v_d = 0 \Rightarrow v_u = v$.[1]

---

[1]For the health of this limit, see for example Reference [61].

Sfermion Sector

We will briefly review the sfermion mass matrices in the presence of the non-holomorphic couplings since they are less often considered in the literature. As before, we work in the limit $v_d = 0$ and drop terms that are of $\mathcal{O}(v^2/M_{\text{SUSY}}^2)$. In this case, the charged slepton mass matrix reads [29]

$$M_L^2 = \begin{pmatrix} (M_L^2)_{LL} & (M_L^2)_{LR} \\ (M_L^2)_{LR}^\dagger & (M_L^2)_{RR} \end{pmatrix}, \tag{2.20}$$

with

$$\left(M_L^2\right)_{LL} = \left(m_L^2\right)^T, \qquad \left(M_L^2\right)_{RR} = m_R^2, \qquad \left(M_L^2\right)_{LR} = v_u \left(Y_l \mu^* - A_l'\right), \tag{2.21}$$

as introduced in Equation (2.8). We adopt the following notation for the off-diagonal elements of the mass matrices

$$\Delta_{XY,ij}^f = \left[\left(M_f^2\right)_{XY}\right]_{ij}. \tag{2.22}$$

Without influencing any conclusion, the matrices in Equation (2.21) can be chosen diagonal, i.e. $\Delta_{XY,ij}^L = 0$. Similarly one has for the sdown mass matrices [29]

$$\left(M_D^2\right)_{LL} = \left(m_Q^2\right)^T, \qquad \left(M_D^2\right)_{RR} = m_D^2, \qquad \left(M_D^2\right)_{LR} = v_u \left(Y_d \mu^* - A_d'\right), \tag{2.23}$$

where again the matrices can be chosen diagonal with the exception of m_D^2. As we are interested in a possible explanation of the anomalies in the $b \rightarrow sll$ transition, we allow for sstrange–sbottom mixing by setting

$$\left(m_D^2\right)_{23} = \Delta_{RR,23}^D. \tag{2.24}$$

Another possibility would be to introduce the mixing through the non-holomorphic coupling $A_{23(32)}'$. This is commented on at the end of the chapter.

Finally, the sup mass matrices are given by [29]

$$\left(M_U^2\right)_{LL} = \left(V m_Q^2 V^\dagger\right)^T, \qquad \left(M_U^2\right)_{RR} = m_U^2, \qquad \left(M_U^2\right)_{LR} = -v_u A_u, \tag{2.25}$$

up to contributions with a relative suppression of $\mathcal{O}(v^2/M_{\text{SUSY}}^2)$.

2.2. The Semileptonic Transition $b \rightarrow sll$

The effective Hamiltonian for the $b \rightarrow sll$ transition reads

$$\mathcal{H}_{\text{eff}} = \sum_i C_i O_i. \tag{2.26}$$

The Standard Model contributions can be inferred from the discussion in Chapter 3. There, the dominant contribution comes from C_9 and C_{10}. Here instead, we focus on the New Physics contribution which in addition to the vector operators can enter through four scalar and two tensor operators. However, the scalar operators are strongly constrained by the branching ratio $\text{BR}(B_s \rightarrow \mu\mu)$, and can therefore not yield sizeable contributions to $R_{K^{(*)}}$. Note that the same holds for the lepton flavour universal contribution C_7 which is
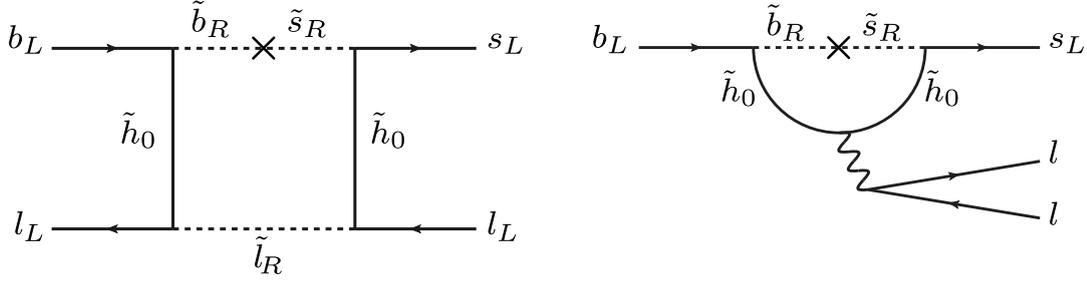
Figure 2.2.: Two types of diagrams that contribute to $b \to sll$: box (left) and penguin contributions (right).

constrained by $\mathrm{BR}(B \to X_s \gamma)$. Leading contributions through tensor operators vanish in the parameter space we are considering. This leaves us with the following set of relevant operators

$$O_{9,l} = (\bar{s}\gamma^\mu P_L b)\left(\bar{l}\gamma_\mu l\right), \qquad\qquad O_{9,l'} = (\bar{s}\gamma^\mu P_R b)\left(\bar{l}\gamma_\mu l\right),$$
$$O_{10,l} = (\bar{s}\gamma^\mu P_L b)\left(\bar{l}\gamma_\mu\gamma_5 l\right), \qquad\qquad O_{10,l'} = (\bar{s}\gamma^\mu P_R b)\left(\bar{l}\gamma_\mu\gamma_5 l\right), \qquad (2.27)$$

where we will consider the case $l = \mu$ since the latest measurement favours New Physics to the ratio $R_{K^{(*)}}$ through the transition $b \to s\mu\mu$ [62]. We also drop the index $l = \mu$ for brevity. The supersymmetric contributions to these operators can be divided into two classes: box and penguin diagrams, see Figure 2.2. In the following we will only discuss the dominant contributions to the Wilson coefficients to determine the interesting parameter space. The full contributions are taken into account in the numerical analysis in Section 2.6.

Box Contributions   Box contributions stem from diagrams with charged Higgs bosons, charginos, or neutralinos running in the loop. Choosing $m_{H_1}^2 \gg \mathcal{O}(1\,\mathrm{TeV}^2)$, we can safely neglect the charged Higgs contributions to $C_{9^{(\prime)}}$ and $C_{10^{(\prime)}}$. Even though this choice seems to be made out of convenience, it will turn out that this is actually necessary. In any case, the Goldstone and charged Higgs-Goldstone boson contributions vanish for $v_d = 0$. The exact contributions to the Wilson coefficients can be adapted from References [63–65].

The chargino box contribution to $C_{9^{(\prime)}}$ and $C_{10^{(\prime)}}$, up to corrections of $\mathcal{O}(e^2 v^2 / M_{\mathrm{SUSY}}^2)$, reads

$$64\pi^2 C_n^{\mathrm{box},\chi} = + c_n^\chi \sum_{i=1}^3 V_{i3} V_{i2}^* D_2(m_{\chi_1}^2, m_{\chi_1}^2, m_{Q,i}'^2, m_{L,\tilde{\mu}}^2)$$
$$+ c_n^\chi \sum_{\substack{i,j=1\\i\neq j}}^3 V_{i3} V_{j2}^* \Delta_{LL,ij}^U \frac{D_2(m_{\chi_1}^2, m_{\chi_1}^2, m_{Q,i}'^2, m_{L,\tilde{\mu}}^2) - D_2(m_{\chi_1}^2, m_{\chi_1}^2, m_{Q,j}'^2, m_{L,\tilde{\mu}}^2)}{m_{Q,i}'^2 - m_{Q,j}'^2}$$
$$- d_n^\chi |y_\mu|^2 \sum_{i=1}^3 V_{i3} V_{i2}^* |y_{u_i}|^2 m_{\chi_2}^2 D_0(m_{\chi_2}^2, m_{\chi_2}^2, m_{U,3+i}^2, m_{L,\tilde{\mu}}^2), \qquad (2.28)$$

for $n = 9^{(\prime)}, 10^{(\prime)}$ with the coefficients c_n^χ and d_n^χ listed in Table 2.3. The loop functions can be found in Appendix B. Note that Equation (2.28) still holds in the case of degenerate squark masses. Due to the analyticity of the loop functions, the limit $m_{Q,i}'^2 \to m_{Q,j}'^2$ is well defined, see also Reference [40].

Table 2.3.: Coefficients c_n^χ, d_n^χ with $n = 9^{(\prime)}, 10^{(\prime)}$ for the chargino contribution $C_n^{\text{box},\chi}$ in Equation (2.28).

	$n = 9$	$n = 10$	$n = 9'$	$n = 10'$
c_n^χ	$e^4/(2s_W^4)$	$-e^4/(2s_W^4)$	$\|y_\mu\|^2 y_s^* y_b$	$-\|y_\mu\|^2 y_s^* y_b$
d_n^χ	1	1	0	0

The neutralino contributions to C_9 and C_{10} reads

$$
C_{9(10)}^{\text{box},\chi^0} = (\overset{+}{-}) \frac{|y_\mu|^2 y_b y_s^*}{128\pi^2} \frac{\Delta_{RR,32}^D}{m_{D,\tilde{s}}^2 - m_{D,\tilde{b}}^2}
$$
$$
\times \left[D_2(m_{\chi_3^0}^2, m_{\chi_3^0}^2, m_{D,\tilde{s}}^2, m_{R,\tilde{\mu}}^2) - D_2(m_{\chi_3^0}^2, m_{\chi_3^0}^2, m_{D,\tilde{b}}^2, m_{R,\tilde{\mu}}^2) \right.
$$
$$
\left. (\overset{+}{-}) D_2(m_{\chi_3^0}^2, m_{\chi_3^0}^2, m_{D,\tilde{s}}^2, m_{L,\tilde{\mu}}^2) (\overset{+}{-}) D_2(m_{\chi_3^0}^2, m_{\chi_3^0}^2, m_{D,\tilde{b}}^2, m_{L,\tilde{\mu}}^2) \right] , \quad (2.29)
$$

up to corrections of $\mathcal{O}(v^2/M_{\text{SUSY}}^2)$, whereas the contribution to the chirality flipped coefficients is given by

$$
C_{9'(10')}^{\text{box},\chi^0} = (\overset{+}{-}) \frac{e^4}{288\pi^2 c_W^4} \frac{\Delta_{RR,32}^D}{m_{D,\tilde{s}}^2 - m_{D,\tilde{b}}^2}
$$
$$
\times \left[D_2^0(m_{\chi_1^0}^2, m_{\chi_1^0}^2, m_{D,\tilde{s}}^2, m_{R,\tilde{\mu}}^2) - D_2^0(m_{\chi_1^0}^2, m_{\chi_1^0}^2, m_{D,\tilde{b}}^2, m_{R,\tilde{\mu}}^2) \right.
$$
$$
\left. (\overset{+}{-}) \frac{1}{4} \left(D_2^0(m_{\chi_1^0}^2, m_{\chi_1^0}^2, m_{D,\tilde{s}}^2, m_{L,\tilde{\mu}}^2) - D_2^0(m_{\chi_1^0}^2, m_{\chi_1^0}^2, m_{D,\tilde{b}}^2, m_{L,\tilde{\mu}}^2) \right) \right] .
$$
$$
(2.30)
$$

The loop function D_2^0 can be found in Appendix B. Inspecting Table 2.3 and Equations (2.29)–(2.30), we can immediately identify the contributions that can become sizeable. First, contributions to $C_{9'(10')}^{\text{box},\chi^0}$ are negligible since they are strongly suppressed by the electroweak coupling to the fourth power. The same holds for the chargino contributions $C_{9(10)}^{\text{box},\chi}$ that are proportional to c_n^χ. This leaves us with the neutralino contributions to $C_{9(10)}^{\text{box},\chi^0}$, and with the chargino contributions to $C_{9'(10')}^{\text{box},\chi}$ as well as the ones $\propto d_n^\chi$. The former can become sizeable $C_9^{\text{box},\chi^0} \sim C_{10}^{\text{box},\chi^0} \sim \mathcal{O}(1)$[1] for $y_{l,d,s} \sim \mathcal{O}(1)$ and $m_{R,\tilde{\mu}} \sim m_{D,\tilde{s}(\tilde{b})} \sim \mu \sim \mathcal{O}(1\,\text{TeV})$. Additionally if $m_{L,\tilde{\mu}} \gg m_{R,\tilde{\mu}}$, one has $C_9^{\text{box},\chi^0} \approx -C_{10}^{\text{box},\chi^0}$. As it will turn out, $m_{L,\tilde{\mu}} \gg m_{R,\tilde{\mu}}$ is a particularly favourable choice not only because this scenario is favoured with respect to C_9^{NP} only [67]. In this case, the chargino contributions are subleading to the neutralino ones due to the heavy left-handed slepton running in the loop and the CKM suppression. Moreover, the sup squark masses are yet to determine which can suppress this contribution further. Otherwise there would be additional contributions to all loop processes mediated by a W boson and fermion.

Let us compare this with the global analysis of the $b \to sll$ observables: In Reference [15] a model-independent fit to $b \to sll$ observables is performed. There, various New Physics

---

[1]Note the change in the normalisation compared to the definition in Equation (2.26) and the formulae in Equations (2.28)–(2.30). Whenever we refer to the Wilson coefficients in the text, we convert our result to the more common normalisation of the effective Hamiltonian—as for example in Reference [66]—for easier comparison.

hypotheses are parametrised in terms of the Wilson coefficients $C_{10^{(\prime)}}^{\mathrm{NP}}$, $C_{9^{(\prime)}}^{\mathrm{NP}}$ and $C_{7^{\prime}}^{\mathrm{NP}}$. Among them is the hypothesis $C_9^{\mathrm{NP}} = -C_{10}^{\mathrm{NP}}$ which we just found to be feasible in our scenario. This hypothesis has a best fit point of $C_9^{\mathrm{NP}} = -0.44$, a p-value of 22.8 % and a pull of $6.2\,\sigma$ with respect to the Standard Model [15].

PENGUIN CONTRIBUTIONS   Penguin contributions as depicted in Figure 2.2 are lepton flavour universal, and hence, contribute equally to $C_{9^{(\prime)},\mu}$ ($C_{10^{(\prime)},\mu}$) and $C_{9^{(\prime)},e}$ ($C_{10^{(\prime)},e}$). Actually, additional lepton flavour universal contributions to $R_{K^{(*)}}$ are even slightly favoured by the experimental data [14, 67, 68]. Nevertheless, these contributions are subleading in the parameter space we are interested in: Z penguins mediated by gluinos are negligible without left–right mixing [64, 69], and neutralino and chargino loops are suppressed by the electroweak couplings. In any case, the electroweak penguins lack the enhancement due to the missing large Yukawa coupling of the muon. Contributions to $C_{9^{(\prime)}}$ are additionally suppressed by the small factor $(1 - 4s_W^2) \approx 0.08$. Furthermore, photon penguins decouple much faster than the Z penguins [69]. For this reason we do not expect sizeable contributions, which are taken care off in the numerical analysis anyway. Further and extensive discussions on these contributions can be found in the literature [13, 28, 69–73].

INTERMEDIATE RESULT   We found that the anomalies in the $b \to sll$ transition can be explained with the following mass spectrum

$$y_{\mu,d,s} \sim \mathcal{O}(1)\,, \qquad m_{R,\tilde{\mu}} \sim m_{D,\tilde{s}(\tilde{b})} \sim \mu \sim \mathcal{O}(1\,\mathrm{TeV})\,, \qquad m_{R,\tilde{\mu}} \ll m_{L,\tilde{\mu}}\,, \qquad (2.31)$$

which yields $C_9 \approx -C_{10}$ as favoured by the global analyses. In the following, we examine the flavour constraints to determine the allowed parameter space for which the feasibility of this spectrum is analysed: Yukawa couplings of $\mathcal{O}(1)$ are only possible if the masses can be generated radiatively within the parameter space of interest.

2.3. Flavour Constraints

In this section we examine the allowed parameter space in the context of the experimental constraints from precision measurements. First we consider the anomalous magnetic moment of the muon a_μ which is expected to significantly restrict the allowed parameter space. Chirality flipped contributions are greatly enhanced by the Yukawa coupling of the muon $y_\mu \sim \mathcal{O}(1)$ and the vev $v_u = v$. Higgsino box diagrams are several orders of magnitude enhanced, and therefore, they could be severely constrained by B_s–$\bar{B}_s$ mixing. Further, bounds coming from $B_s \to \mu^+\mu^-$ and $B \to X_s\gamma$ are investigated. Finally, taking these constraints into account, we show the allowed regions of the parameters in Equation (2.31).

Anomalous Magnetic Moment of the Muon a_μ

The precise measurement of the anomalous magnetic moment of the muon a_μ provides a stringent constraint on the parameter space of New Physics: The latest measurement exhibits a $3.3\,\sigma$ deviation from the SM prediction [74]. Combined with the previous measurement at Brookhaven [75] this corresponds to a significance of $4.2\,\sigma$ yielding strong evidence for New Physics beyond the Standard Model [74]. Therefore, every part of the parameter space pointing in the wrong direction is highly disfavoured. The combined measurements read [74]

$$a_{\mu,\mathrm{exp}} = 116592061(41) \times 10^{-11}\,, \qquad (2.32)$$
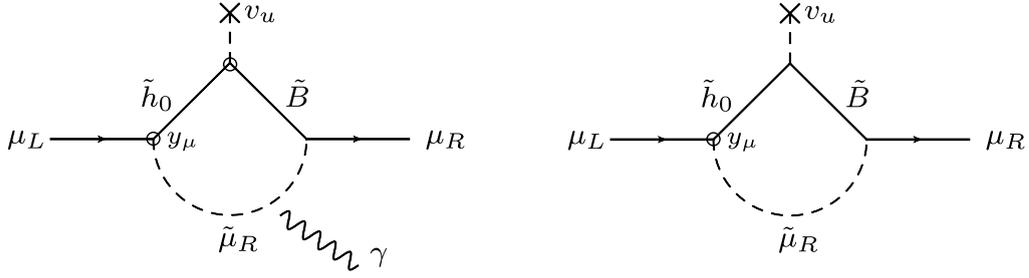
Figure 2.3.: Dominant contribution to a_μ for $m_{L,\tilde{\mu}} \gg m_{R,\tilde{\mu}}$ (left). Without the photon attached to the diagram, it is the dominant contribution to the muon mass (right)

while the Standard Model prediction is given by [76]

$$a_{\mu,\mathrm{SM}} = 116591810(43) \times 10^{-11}.$$ (2.33)

which corresponds to a deviation Δa_μ of

$$\Delta a_\mu = a_{\mu,\mathrm{exp}} - a_{\mu,\mathrm{SM}} = 251(59) \times 10^{-11}.$$ (2.34)

The dominant contributions mediated by charginos a_μ^χ and neutralinos $a_\mu^{\chi^0}$ read to first order in the mass insertions [77] (note that all supersymmetric parameters are chosen real from now on, see also Appendix A)

$$a_\mu^\chi = \frac{e^2 m_\mu v y_\mu}{24\pi^2 s_W^2} \frac{\mu M_2}{m_{L\tilde{\mu}}^2} \frac{F_2^C\left(M_2^2/m_{L,\tilde{\mu}}^2\right) - F_2^C\left(\mu^2/m_{L,\tilde{\mu}}^2\right)}{M_2^2 - \mu^2},$$

$$a_\mu^{\chi^0} = \frac{e^2 m_\mu v y_\mu}{96\pi^2 c_W^2} \frac{\mu M_1}{m_{L\tilde{\mu}}^2} \frac{F_2^N\left(M_1^2/m_{L,\tilde{\mu}}^2\right) - F_2^N\left(\mu^2/m_{L,\tilde{\mu}}^2\right)}{M_1^2 - \mu^2}$$

$$- \frac{e^2 m_\mu v y_\mu}{96\pi^2 c_W^2} \frac{\mu M_2}{m_{L\tilde{\mu}}^2} \frac{F_2^N\left(M_2^2/m_{L,\tilde{\mu}}^2\right) - F_2^N\left(\mu^2/m_{L,\tilde{\mu}}^2\right)}{M_2^2 - \mu^2}$$

$$- \frac{e^2 m_\mu v y_\mu}{48\pi^2 c_W^2} \frac{\mu M_1}{m_{R\tilde{\mu}}^2} \frac{F_2^N\left(M_1^2/m_{R,\tilde{\mu}}^2\right) - F_2^N\left(\mu^2/m_{R,\tilde{\mu}}^2\right)}{M_1^2 - \mu^2}$$

$$+ \frac{e^2 m_\mu v \left(y_\mu \mu - A'_{\tilde{\mu}}\right) M_1}{48\pi^2 c_W^2} \frac{F_2^N\left(M_1^2/m_{L,\tilde{\mu}}^2\right)/m_{L,\tilde{\mu}}^2 - F_2^N\left(M_1^2/m_{R,\tilde{\mu}}^2\right)/m_{R,\tilde{\mu}}^2}{m_{L,\tilde{\mu}}^2 - m_{R,\tilde{\mu}}^2},$$ (2.35)

and indeed, contributions to the anomalous magnetic moment are greatly enhanced by the factor $v y_\mu$, cf. Figure 2.3. For the loop functions $F_2^{C(N)}$ see Reference [77]. Considering the limit $m_{L,\tilde{\mu}} \gg m_{R,\tilde{\mu}}$, the chargino contribution a_μ^χ becomes subleading compared to the one mediated by the neutralinos $a_\mu^{\chi^0}$. The latter simplifies to

$$a_\mu^{\chi^0} = - \frac{e^2 m_\mu v y_\mu}{48\pi^2 c_W^2} \frac{\mu M_1}{m_{R,\tilde{\mu}}^2} \frac{F_2^N\left(M_1^2/m_{R,\tilde{\mu}}^2\right) - F_2^N\left(\mu^2/m_{R,\tilde{\mu}}^2\right)}{M_1^2 - \mu^2},$$ (2.36)

which for $y_\mu \sim \mathcal{O}(1)$ and $m_{R,\tilde{\mu}} \sim \mathcal{O}(1\,\mathrm{TeV})$ yields the required size Δa_μ to resolve the tension between the measurement and the theory value given that $\mathrm{sign}(\mu M_1) = -1$ and
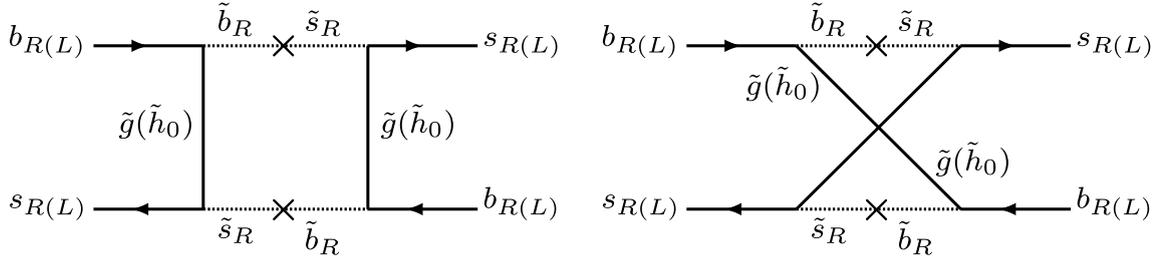
Figure 2.4.: Some box contributions to B_s–$\overline{B}_s$ mixing. Note that the crossed (right) higgsino contributions is relatively suppressed by v^2/M_{SUSY}^2 compared to the uncrossed (left) while for the gluino both diagrams cancel partially for $m_{\tilde{g}} \geq 3/2 m_{\tilde{q}}$.

$m_{L,\tilde{\mu}}^2 \gg M_2^2 \sim M_1^2 > \mu^2 \approx m_{R,\tilde{\mu}}^2$. Remarkably, this is the same hierarchy as needed to explain the anomalies in the $b \to sll$ transitions, see Equation (2.31).[1]

Neutral B_s Meson Mixing

Neutral B_s–$\overline{B}_s$ mixing receives enhanced contributions from higgsino box diagrams which are often neglected due to the smallness of the Yukawa couplings, see Figure 2.4. To constrain the parameter space we use the complex ratio

$$C_{B_s} e^{2i\phi_{B_s}} = 1 + \frac{\langle B_s | \mathcal{H}_{\text{eff}}^{\text{NP}} | \overline{B}_s \rangle}{\langle B_s | \mathcal{H}_{\text{eff}}^{\text{SM}} | \overline{B}_s \rangle}, \tag{2.37}$$

with the New Physics contribution $\langle B_s | \mathcal{H}_{\text{eff}}^{\text{NP}} | \overline{B}_s \rangle$ to the B_s meson mixing amplitude. Details of the calculation can be found in Reference [1]. We demand the absolute value, C_{B_s}, and phase ϕ_{B_s} to stay within 1σ around the online update of the UTfit result [79,80]

$$C_{B_s} = 1.110 \pm 0.090, \qquad\qquad \phi_{B_s} = (0.42 \pm 0.89)^{\circ}, \tag{2.38}$$

where the correlation between C_{B_s} and ϕ_{B_s} can be neglected. The relevant Wilson coefficients to second order in the mass insertions read [81]

$$C_1^{\chi^0} = \frac{y_b^2 y_s^2}{128\pi^2} \left(\frac{\Delta_{RR,23}^D}{m_{D,\tilde{s}}^2 - m_{D,\tilde{b}}^2} \right)^2 \left[D_2 \left(m_{D,\tilde{s}}^2, m_{D,\tilde{s}}^2, \mu^2, \mu^2 \right) + D_2 \left(m_{D,\tilde{b}}^2, m_{D,\tilde{b}}^2, \mu^2, \mu^2 \right) \right.$$
$$\left. -2D_2 \left(m_{D,\tilde{s}}^2, m_{D,\tilde{b}}^2, \mu^2, \mu^2 \right) \right],$$

$$C_4^{\chi^0} = -\frac{e^2 y_b y_s}{144\pi^2 c_W^2} \left(\frac{\Delta_{RR,23}^D}{m_{D,\tilde{s}}^2 - m_{D,\tilde{b}}^2} \right)^2 \left[D_2 \left(m_{D,\tilde{s}}^2, m_{D,\tilde{s}}^2, M_1^2, \mu^2 \right) + D_2 \left(m_{D,\tilde{b}}^2, m_{D,\tilde{b}}^2, M_1^2, \mu^2 \right) \right.$$
$$\left. -2D_2 \left(m_{D,\tilde{s}}^2, m_{D,\tilde{b}}^2, M_1^2, \mu^2 \right) \right]. \tag{2.39}$$

Note that the crossed higgsino box diagram, see Figure 2.4, is suppressed by v^2/M_{SUSY}^2. An explicit evaluation of this contribution shows that both higgsino contributions cancel to leading order in the mass insertions. This is unlike the gluino contribution where the crossed and uncrossed diagrams cancel to a great extent given $m_{\tilde{g}} \geq 3/2 m_{\tilde{q}}$ [82].

---

[1]During the finishing of this thesis, I came across Reference [78] where the authors also explain $(g-2)_{\mu}$ for $\tan\beta \to \infty$.

Assuming the same mass spectrum as discussed earlier to resolve the $R_{K^{(*)}}$ and $(g-2)_\mu$ anomalies, the dominant contribution is given by $C_1^{\chi^0}$. The contribution to the Wilson coefficient $C_4^{\chi^0}$ is subleading due to the suppression by the electroweak coupling, and since the $(g-2)_\mu$ anomaly favours a bino mass $M_1^2 > \mu^2$. As long as all other contributions to the Wilson coefficients are suppressed the contribution to the Wilson coefficient $C_1^{\chi^0}$ pushes the mass difference Δm_s to the upper limit of the $1\,\sigma$ interval around the experimental value. This only holds as long as one wants to explain the ratio $R_{K^{(*)}}$ within $1\,\sigma$, and can be relaxed by taking moderate gluino masses $m_{\tilde{g}}^2 \gtrsim M_1^2$: The gluino-neutralino boxes can be of similar order and the corresponding contribution to C_5 has the opposite sign.

Rare B Decay: $B_s \rightarrow \mu^+\mu^-$

The decay $B_s \rightarrow \mu^+\mu^-$ is experimentally well measured and theoretically clean. In the Standard Model this process is strongly suppressed as it is generated at one loop level and requires a helicity flip. In the model considered in this chapter, some contributions are greatly enhanced by the large Yukawa couplings, which might put severe constraints on the parameter space. The experimental measurement is given by [83]

$$\mathrm{BR_{exp}}(B_s \rightarrow \mu^+\mu^-) = (3.0 \pm 0.4) \times 10^{-9}\,, \tag{2.40}$$

and the Standard Model prediction reads [84]

$$\mathrm{BR_{SM}}(B_s \rightarrow \mu^+\mu^-) = (3.65 \pm 0.23) \times 10^{-9}\,. \tag{2.41}$$

The missing Wilson coefficients for this decay are $C_{S^{(\prime)}}$ and $C_{P^{(\prime)}}$, see Section 2.2. To first order in the mass insertions they read [63]

$$
\begin{aligned}
C_S = C_P = {} & -\frac{e^2 y_\mu y_b}{96\pi^2 c_W^2} \Delta_{RR,23}^D \frac{D_2\left(\mu^2, M_1^2, m_{R,\tilde{b}}^2, m_{R,\tilde{\mu}}^2\right) - D_2\left(\mu^2, M_1^2, m_{R,\tilde{s}}^2, m_{R,\tilde{\mu}}^2\right)}{m_{R,\tilde{b}}^2 - m_{R,\tilde{s}}^2} \\
& + \frac{e^2 y_\mu y_b}{192\pi^2 c_W^2} \Delta_{RR,23}^D \frac{D_2\left(\mu^2, M_1^2, m_{R,\tilde{b}}^2, m_{L,\tilde{\mu}}^2\right) - D_2\left(\mu^2, M_1^2, m_{R,\tilde{s}}^2, m_{L,\tilde{\mu}}^2\right)}{m_{R,\tilde{b}}^2 - m_{R,\tilde{s}}^2}\,, \\
C_{S'} = C_{P'} = {} & -\frac{e^2 y_\mu y_s}{96\pi^2 c_W^2} \Delta_{RR,23}^D \frac{D_2\left(\mu^2, M_1^2, m_{R,\tilde{b}}^2, m_{R,\tilde{\mu}}^2\right) - D_2\left(\mu^2, M_1^2, m_{R,\tilde{s}}^2, m_{R,\tilde{\mu}}^2\right)}{m_{R,\tilde{b}}^2 - m_{R,\tilde{s}}^2} \\
& + \frac{e^2 y_\mu y_s}{192\pi^2 c_W^2} \Delta_{RR,23}^D \frac{D_2\left(\mu^2, M_1^2, m_{R,\tilde{b}}^2, m_{L,\tilde{\mu}}^2\right) - D_2\left(\mu^2, M_1^2, m_{R,\tilde{s}}^2, m_{L,\tilde{\mu}}^2\right)}{m_{R,\tilde{b}}^2 - m_{R,\tilde{s}}^2}\,. \tag{2.42}
\end{aligned}
$$

These contributions are suppressed by the weak coupling and given the large experimental uncertainty of $\approx 13\,\%$, there is no additional constraint on the parameter space determined from the previous observables given that the New Physics contributions point in a way that loosens the small tension between the measurement and prediction.

Radiative B decay: $B \rightarrow X_s\gamma$

Similar to $B_s \rightarrow \mu\mu$, the radiative decay $B \rightarrow X_s\gamma$ is precisely measured and theoretically clean. Therefore, this decay puts stringent constraints on New Physics contributions. The

experimental measurement of the CP and isospin averaged branching ratio extrapolated to a photon energy threshold E_γ^B of $1.6\,\mathrm{GeV}$ is given by the Belle collaboration [85]

$$\mathrm{BR}_{\exp}^{E_\gamma^B > 1.6}(B \to X_s \gamma) = (3.12 \pm 0.23) \times 10^{-4}\,. \tag{2.43}$$

The state of the art Standard Model prediction reads [86][1]

$$\mathrm{BR}_{\mathrm{SM}}^{\mathrm{NNLO},E_\gamma^B > 1.6}(B \to X_s \gamma) = (3.36 \pm 0.23) \times 10^{-4}\,. \tag{2.44}$$

The dominant Wilson coefficient for this decay is C_7 where the main MSSM contribution to first order in the mass insertions is given by [64]

$$
\begin{aligned}
C_7^{\chi^0} ={}& -\frac{y_b y_s}{6 V_{ts}^* V_{tb} (e/s_{\mathrm{W}})^2} \frac{m_W^2}{\mu^2} \frac{\Delta_{RR,23}^D}{m_{D,\tilde{s}}^2 - m_{D,\tilde{b}}^2} \left[f_3(m_{D,\tilde{s}}^2/\mu^2) - f_3\left(m_{D,\tilde{b}}^2/\mu^2\right) \right] \\
& - \frac{(s_{\mathrm{W}}/c_{\mathrm{W}})^2}{9 V_{ts}^* V_{tb}} \frac{v y_s m_W^2}{m_b} \frac{\mu M_1}{M_1^2 - \mu^2} \frac{\Delta_{RR,23}^D}{m_{D,\tilde{s}}^2 - m_{D,\tilde{b}}^2} \\
& \times \left[\frac{f_4(m_{D,\tilde{s}}^2/M_1^2)}{M_1^2} - \frac{f_4\left(m_{D,\tilde{b}}^2/M_1^2\right)}{M_1^2} - \frac{f_4(m_{D,\tilde{s}}^2/\mu^2)}{\mu^2} + \frac{f_4\left(m_{D,\tilde{b}}^2/\mu^2\right)}{\mu^2} \right]\,, \\
C_7^{\chi} ={}& -\frac{1}{6 V_{ts}^* V_{tb}} \frac{m_W^2}{M_2^2} \sum_{i=1}^3 V_{i2}^* V_{i3} f_1\left(m_{U,i}^2/M_2^2\right) \\
& + \frac{1}{6 V_{ts}^* V_{tb}} \frac{m_W^2}{\mu^2} \sum_{i=1}^3 V_{i2}^* V_{i3} |y_{u_i}|^2 f_1\left(m_{U,i}^2/M_2^2\right) \\
& + \frac{v y_b}{3 V_{ts}^* V_{tb} m_b} \frac{\mu M_2}{\mu^2 - M_2^2} \sum_{i=1}^3 V_{i2}^* V_{i3} \left[\frac{m_W^2}{\mu^2} f_2\left(m_{U,i}^2/\mu^2\right) - \frac{m_W^2}{M_2^2} f_2\left(m_{U,i}^2/M_2^2\right) \right]\,. \tag{2.45}
\end{aligned}
$$

Note that contributions proportional to the comparably small Δ_{ij}^U are neglected for the sake of clarity. In the Standard Model, contributions to the Wilson coefficient $C_{7'}$ are suppressed by m_s/m_b. However, in scenarios with non-minimal flavour violation $C_{7'}$ can become sizeable. They are obtained by interchanging $L \leftrightarrow R$ in C_7. To first order in the mass insertions the dominant contributions read

$$
\begin{aligned}
C_{7'}^{\chi^0} ={}& -\frac{(s_{\mathrm{W}}/c_{\mathrm{W}})^2}{9 V_{ts}^* V_{tb}} \frac{v y_b m_W^2}{m_b} \frac{\mu M_1}{M_1^2 - \mu^2} \frac{\Delta_{RR,23}^D}{m_{D,\tilde{s}}^2 - m_{D,\tilde{b}}^2} \\
& \times \left[\frac{f_4(m_{D,\tilde{s}}^2/M_1^2)}{M_1^2} - \frac{f_4\left(m_{D,\tilde{b}}^2/M_1^2\right)}{M_1^2} - \frac{f_4(m_{D,\tilde{s}}^2/\mu^2)}{\mu^2} + \frac{f_4\left(m_{D,\tilde{b}}^2/\mu^2\right)}{\mu^2} \right]\,, \\
C_{7'}^{\chi} ={}& -\frac{y_b y_s}{6 V_{ts}^* V_{tb} (e/s_{\mathrm{W}})^2} \frac{m_W^2}{\mu^2} \sum_{i=1}^3 V_{i2}^* V_{i3} f_1\left(m_{U,i}/\mu^2\right) \\
& + \frac{v y_s}{3 V_{ts}^* V_{tb} m_b} \frac{\mu M_2}{M_2^2 - \mu^2} \sum_{i=1}^3 V_{i2}^* V_{i3} \left[\frac{m_W^2}{M_2^2} f_1\left(m_{U,i}/M_2^2\right)/M_2^2 - \frac{m_W^2}{\mu^2} f_1\left(m_{U,i}/\mu^2\right)/\mu^2 \right]\,. \tag{2.46}
\end{aligned}
$$

---

[1]After this analysis had been performed an updated prediction with a reduced theoretical uncertainty was published, see Reference [87]. This does not alter any conclusion and has very little influence on the numerical analysis later on.
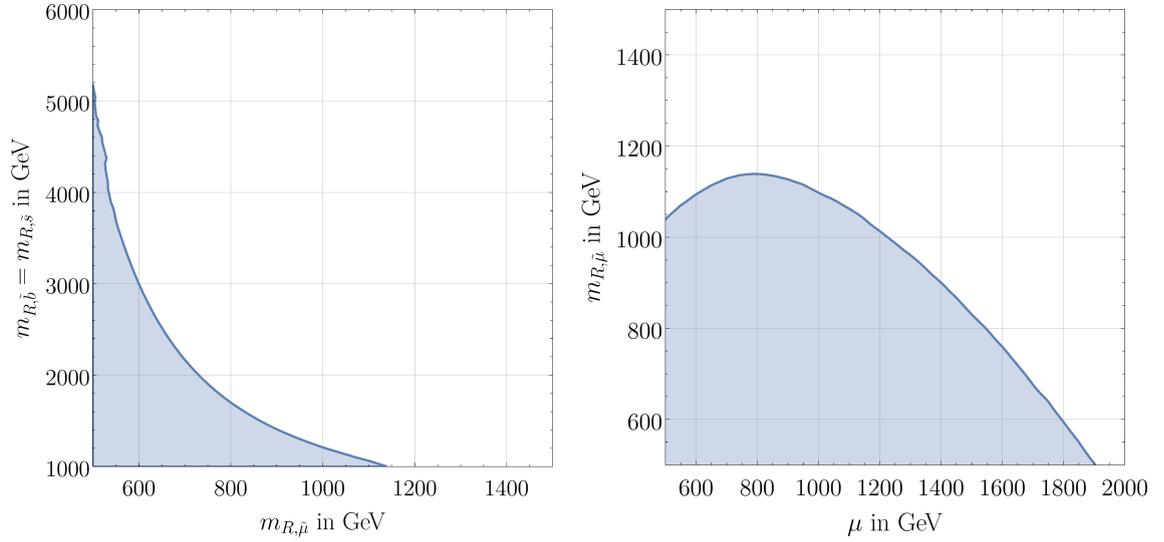
Figure 2.5.: Allowed regions at 68 % C.L. on the mass planes taking all constraints discussed in Section 2.3 into account.

Focusing on the neutralino contribution $C_{7^{(\prime)}}^{\chi^0}$, we see that similar to $C_1^{\chi^0}$ there is a contribution which one cannot get rid off: Unlike $C_{7'}^{\chi^0}$ which can be suppressed for large bino masses M_1, the first line of Equation (2.45) is fixed by the Yukawa couplings, the higgsino mass μ, and the right-handed masses and mixing of the squarks which are all needed to explain the $R_{K^{(*)}}$ anomalies. The interplay of all constraints will be analysed further in the next subsection.

Combined Constraints

We will use this subsection to provide an intermediate scan of all previously discussed constraints. We determine the allowed region for the Yukawa couplings y_f, the masses of the right-handed squarks $m_{R,\tilde{s}(\tilde{b})}$, the smuon $m_{R,\tilde{\mu}}$, the higgsino μ, and bino M_1. All other mass scales are set high enough to forbid any additional contributions. The scan is performed over the following ranges to comply with current collider searches

$$\mu, m_{R,\tilde{\mu}} > 500\,\text{GeV} \qquad m_{R,\tilde{s}} = m_{R,\tilde{b}}, |M_1| > 1\,\text{TeV}, \qquad 0 > y_\mu, y_s = y_b > -\sqrt{4\pi}. \qquad (2.47)$$

The allowed regions at 68 % C.L. on the μ–$m_{R,\tilde{\mu}}$ plane, the $m_{R,\tilde{\mu}}$–$m_{R,\tilde{b}}$ plane, the M_1–μ, and on the y_s–y_b plane are shown in Figure 2.5 and 2.6. Note that in this case, the deviation d_i of any considered observable O_i is defined as

$$d_i = \frac{O_{i,\text{theo}} - O_{i,\text{exp}}}{\sigma_{i,\text{tot}}}, \qquad (2.48)$$

within the allowed regions is also below 2. One can see that the Yukawa couplings have to be $-y_{s,b,\mu} \gtrsim 0.5$, while the higgsino mass μ and right-handed smuon mass $m_{R,\tilde{\mu}}$ have to stay below $\lesssim 2\,\text{TeV}$ and $\lesssim 1\,\text{TeV}$, respectively. The right-handed sstrange and sbottom squark masses can be as large as 5 TeV, however, they drop quickly for increasing right-handed smuon masses. The allowed region on the bino mass, $4\,\text{TeV} \lesssim -M_1 \lesssim 10\,\text{TeV}$, comes from the experimental constraints, in particular it is due to the anomalous magnetic moment of the muon.

In the next section, we examine the possibility of generating the fermion masses radiatively within the allowed parameter region.
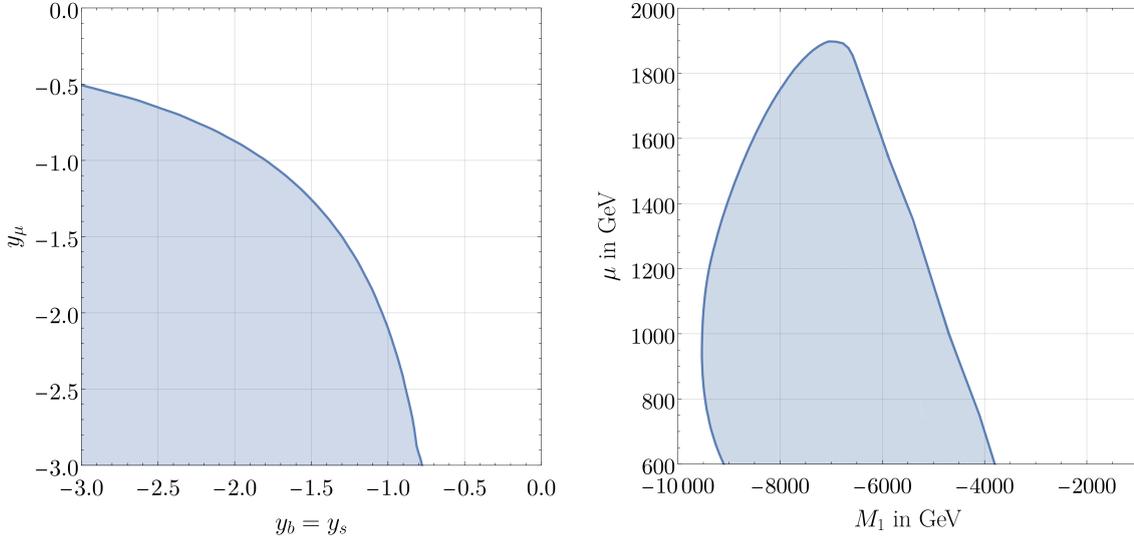
Figure 2.6.: Allowed regions at 68 % C.L. on the mass and coupling planes taking all constraints discussed in Section 2.3 into account.

2.4. Radiative Generation of Lepton and Down Quark Masses

Since the vev v_d of the Higgs field H_d which couples to the leptons and down quarks vanishes, the corresponding masses must be generated radiatively at one-loop. In general, the self energies and the physical fermion masses are related by [88]

$$m_{f,ij} = -Y_{f_i}^{(0)} \delta_{ij} v_d + \Sigma_{f,ij} \,, \qquad\qquad f = d, l \,, \qquad (2.49)$$

where we closely follow the convention and notation of Reference [88]. There, the self energy $\Sigma_{f,ij}$ is decomposed as

$$\Sigma_{f,ij}(p) = \left(\Sigma_{f,ij}^{LR}(p^2) + \not{p}\, \Sigma_{f,ij}^{RR}(p^2) \right) P_R + \left(\Sigma_{f,ij}^{RL}(p^2) + \not{p}\, \Sigma_{f,ij}^{LL}(p^2) \right) P_L \,, \qquad (2.50)$$

where the superscripts denote the chirality of the incoming and outgoing quark line. We consider the chirally enhanced part $\Sigma_{f,ij}^{LR}$ which is the dominant contribution for large $\tan\beta$, and we decompose it further as

$$\Sigma_{f,ij}^{LR} \equiv \Sigma_{f,ij}^{LR}(0) = \sum_{\tilde{p}_1, \tilde{p}_2, \dots} \Sigma_{LR,f,ij}^{\tilde{p}_1 \tilde{p}_2, \dots} = \Sigma_{f,ij}^{A} + \Sigma_{f,ij}^{A'} \,. \qquad (2.51)$$

where $\Sigma_{LR,f,ij}^{\tilde{p}_1 \tilde{p}_2, \dots}$ refers to the chirality changing self energy with the particles $\tilde{p}_1, \tilde{p}_2, \dots$ running in the loop. The contributions $\Sigma_{f,ij}^{A}$ and $\Sigma_{f,ij}^{A'}$ refer to the part of the chirality changing self energies that are proportional to v_d and v_u, respectively.

Finally, in the limit $v_d = 0$ Equation (2.49) simplifies to

$$m_{f,ij} = \Sigma_{f,ij}^{A'} \,, \qquad (2.52)$$

and there are no contributions from the chirally conserving self energies at this level due to vanishing tree-level masses. Note that this contribution is finite since no corresponding interaction appears in the Lagrangian at tree-level. For this reason, we follow Reference [89] and work in a minimal renormalisation scheme, thus, no counterterms are
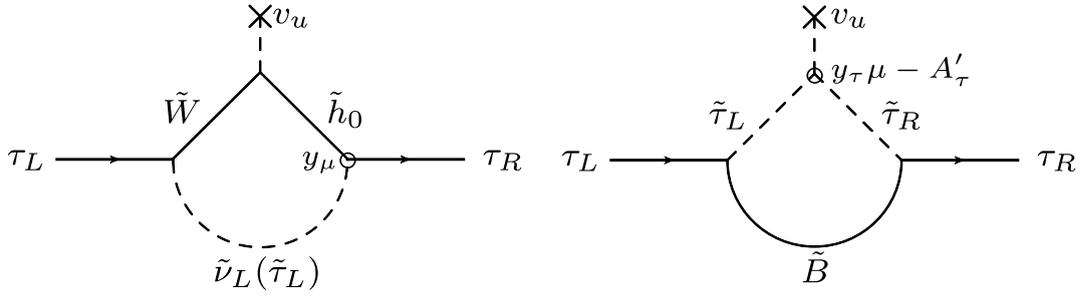
Figure 2.7.: Some leading contributions to the tau mass.

needed in contrast to an on-shell renormalisation scheme for the fermion masses [90]. Note that this choice is already apparent in Equation (2.49) since no counterterm was given there. This also means that the bare Yukawa couplings $Y_{f_i}^{(0)}$ coincide with the renormalised ones Y_{f_i} [89].

First we consider the charged lepton masses. Note, if it is possible to generate the muon or tau mass radiatively with Yukawa couplings of $\mathcal{O}(1)$, the electron mass can also be generated by downscaling the corresponding free parameters in the (s)electron sector, for instance the Yukawa coupling y_e.[1]

Lepton Masses

The dominant contributions are in general the charged wino-higgsino-slepton loops $\Sigma_{LR,l}^{\bar{W}\tilde{h}\tilde{l}}$, the bino-slepton loops $\Sigma_{LR,l}^{\tilde{B}\tilde{l}}$, and the neutral wino/bino-higgsino-slepton loops $\Sigma_{LR,l}^{\tilde{W}/\tilde{B}\tilde{h}\tilde{l}}$. Diagrams contributing to the tau and muon masses can be found in Figure 2.7 and Figure 2.3, respectively.

For a heavy left-handed smuon mass $m_{L,\tilde{\mu}} \gg m_{R,\tilde{\mu}}$ and $y_\mu \sim \mathcal{O}(1)$, the only dominant contribution is the bino-higgsino-slepton loop which is given by

$$\Sigma_{LR,\mu}^{\tilde{B}\tilde{h}\tilde{\mu}} = \frac{e^2}{16\pi^2 c_W^2} \frac{v y_\mu \mu M_1}{M_1^2 - \mu^2} \left[B_0\left(\mu^2, m_{R,\tilde{\mu}}^2\right) - B_0\left(M_1^2, m_{R,\tilde{\mu}}^2\right) \right]$$
$$\approx 7 \times 10^{-4} \times \mathcal{O}(10^2) \times \mathcal{O}(1)$$
$$\approx 7 \times \mathcal{O}(10^{-2}), \tag{2.53}$$

with the two-point function B_0 defined in Appendix B. And indeed, for the parameter space we are considering, the self energy $\Sigma_{LR,\mu}^{\tilde{B}\tilde{h}\tilde{\mu}}$ can be of the required size. Since the tau lepton is much heavier than the muon, the question arises, whether the tau mass can also be generated radiatively. For a stau spectrum similar to the smuon sector, the required size of the tau Yukawa coupling would be far above the perturbativity limit. Thus, we discuss all contributions to the tau mass in more detail. They read

$$\Sigma_{LR,\tau}^{\bar{W}\tilde{h}\tilde{\mu}} = \frac{e^2}{16\pi^2 s_W^2} \frac{v y_\tau \mu M_2}{M_2^2 - \mu^2} \left[B_0\left(\mu^2, m_{L,\tilde{\tau}}^2\right) - B_0\left(M_2^2, m_{L,\tilde{\tau}}^2\right) \right]$$
$$\lesssim 1, \tag{2.54}$$

---

[1]The same holds for the down quark mass m_d.

where, for now, $y_\tau \lesssim \sqrt{2\pi}$, $m_{L,\tilde{\tau}} > 100\,\text{GeV}$[1], and—in order to explain $R_{K^{(*)}}$—$\mu < 1.5\,\text{TeV}$. The remaining contributions read

$$\Sigma_{LR,\tau}^{\tilde{B}\tilde{\mu}} = \frac{e^2}{16\pi^2 c_W^2} \frac{v\,(y_\tau \mu - A_{\tilde{\tau}}')\,M_1}{m_{L,\tilde{\tau}}^2 - m_{R,\tilde{\tau}}^2} \left[B_0\left(M_1^2, m_{L,\tilde{\tau}}^2\right) - B_0\left(M_1^2, m_{R,\tilde{\tau}}^2\right) \right]$$

$$\Sigma_{LR,\tau}^{\tilde{W}/\tilde{B}\tilde{h}\tilde{\mu}} = \frac{e^2}{32\pi^2 c_W^2} \frac{v y_\tau \mu M_1}{M_1^2 - \mu^2} \left[B_0\left(M_1^2, m_{L,\tilde{\tau}}^2\right) - B_0\left(\mu^2, m_{L,\tilde{\tau}}^2\right) \right]$$

$$+ \frac{e^2}{32\pi^2 c_W^2} \frac{v y_\tau \mu M_2}{M_2^2 - \mu^2} \left[B_0\left(\mu^2, m_{L,\tilde{\tau}}^2\right) - B_0\left(M_2^2, m_{L,\tilde{\tau}}^2\right) \right]$$

$$- \frac{e^2}{16\pi^2 c_W^2} \frac{v y_\tau \mu M_1}{M_1^2 - \mu^2} \left[B_0\left(M_1^2, m_{R,\tilde{\tau}}^2\right) - B_0\left(\mu^2, m_{R,\tilde{\tau}}^2\right) \right] . \tag{2.55}$$

Taking a careful look at these contributions, one sees that in order to recover the tau mass, μ has to be large, i.e. $|\mu| \approx 1.5\,\text{TeV}$ and $M_2 \approx \mu$. The last contribution to the self energy $\Sigma_{LR,\tau}^{\tilde{W}/\tilde{B}\tilde{h}\tilde{\mu}}$ has an opposite sign compared to $\Sigma_{LR,\tau}^{\tilde{B}\tilde{\mu}}$ leading to a reduction of the tau mass. This contribution can be suppressed by a large right-handed stau mass. However, this also reduces the positive contribution $\Sigma_{LR,\tau}^{\tilde{B}\tilde{\mu}}$. Anyway, a light left-handed stau mass is favoured in order to not suppress the additionally needed contributions in Equation (2.55). In this case the sum of both self energies is positive, and hence, light right-handed stau masses are also favoured. However, the stau masses are naively constrained by the vacuum stability to be $m_{L,\tilde{\tau}}^2 + m_{R,\tilde{\tau}}^2 \geq |y_\tau \mu - A_{\tilde{\tau}}'|^2/2$[2]. Since the left-handed mass has to be light, we again end up with heayy right-handed staus. Under the constraints $y_\tau < \sqrt{2\pi}$, $m_{L,\tilde{\tau}} > 100\,\text{GeV}$, and $\mu < 1.5\,\text{TeV}$ the only possibility to get the heavy tau mass is a light bino mass. However, a light bino mass leads to a large muon mass and the contribution in Equation (2.53) has to be cancelled by taking a lighter left-handed smuon mass $m_{L,\tilde{\mu}}$ which in turn enhances $B_s \to \mu^+\mu^-$ and $(g-2)_\mu$. Therefore, the only possibility to get a sizeable contribution to the tau mass is allowing the tau Yukawa coupling y_τ to be as large as $y_\tau \approx 3 < \sqrt{4\pi}$ while $m_{L,\tilde{\tau}} \lesssim 500\,\text{GeV}$. As a result, the right-handed stau has to be heavy in order to maintain the vacuum stability for such a large Yukawa coupling.[3]

The hierarchy $m_{L,\tilde{\tau}} < m_{R,\tilde{\tau}}$ is also favoured, since otherwise the LSP would be a right-handed stau, which as a charged particle is experimentally forbidden.

Interestingly, the resulting allowed parameter space implies

$$\text{sign}(y_\tau y_\mu) = -1, \qquad C_{9,\tau}^{\text{NP}} \approx C_{10,\tau}^{\text{NP}}, \qquad \left| \frac{C_{9,\tau}^{\text{NP}}}{C_{9,\mu}^{\text{NP}}} \right| \approx \left(\frac{y_\tau}{y_\mu} \right)^2 \sim \mathcal{O}(1), \tag{2.56}$$

while the supersymmetric contribution to the scalar Wilson coefficients $C_{S^{(\prime)}(P^{(\prime)}),\tau}$, relevant for $B_s \to \tau^+\tau^-$ might even receive a suppression for $y_\tau < 2y_\mu$

$$\frac{C_{S^{(\prime)}(P^{(\prime)}),\tau}}{C_{S^{(\prime)}(P^{(\prime)}),\mu}} \approx \frac{y_\tau}{2y_\mu} \sim \mathcal{O}\left(\frac{1}{2} \right). \tag{2.57}$$

In particular the latter are a distinctive feature compared to the more popular leptoquark models where these processes receive large enhancements [93–97].
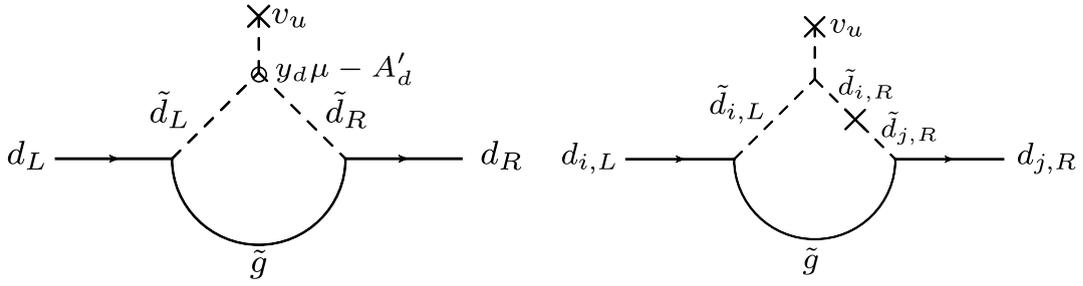
Figure 2.8.: Dominant contributions to the down quark masses and flavour changing self energy.

Down Quark Masses

Now we consider the contributions to down quark masses. The dominant contribution given by the gluino loop reads

$$\Sigma_{LR,d_i}^{\tilde{g}\tilde{d}_i} = \frac{g_s^2}{6\pi^2} \frac{v\left(y_{d_i}\mu - A'_{\tilde{d}_i}\right)m_{\tilde{g}}}{m_{D,\tilde{d}_i}^2 - m_{Q,\tilde{u}_i}^2} \left[B_0\left(m_{D,\tilde{d}_i}^2, m_{\tilde{g}}^2\right) - B_0\left(m_{Q,\tilde{u}_i}^2, m_{\tilde{g}}^2\right)\right], \qquad (2.58)$$

cf. Figure 2.8. Assuming heavy gluino, left-handed squark masses $\gtrsim 10\,\text{TeV}$ and light right-handed squark masses as afore-mentioned, the bottom mass can be generated radiatively for $|y_b\mu - A'_b|^2 \lesssim 2m_{Q,\tilde{t}}^2$. The latter is chosen to naively maintain vacuum stability for now. In general this choice can be relaxed which only proves our point further, cf. Section 2.5. While one has $\text{sign}(y_b\mu) = -\text{sign}(A'_b)$ in order to enhance the contribution to the bottom mass, one needs $\text{sign}(y_s\mu) = \text{sign}(A'_s)$ to cancel the large contribution $\propto y_s\mu$ such that the small strange quark mass is obtained.

Due to the off-diagonal sdown mass matrix element $\Delta_{RR,23}^D$, there are flavour changing self energies, $\Sigma_{LR,sb}^{\tilde{g}\tilde{c}\tilde{s}\tilde{b}}$ and $\Sigma_{LR,bs}^{\tilde{g}\tilde{t}\tilde{b}\tilde{s}}$, which in general can become sizeable, and therefore, enhance all previously discussed contributions to flavour observables, see Figure 2.8. Since the smallness of the strange quark mass requires a smaller trilinear coupling $A'_{\tilde{s}} < A'_{\tilde{b}}$, the dominant flavour changing self energy is

$$\Sigma_{LR,bs}^{\tilde{g}\tilde{t}\tilde{b}\tilde{s}} = \frac{g_s^2}{6\pi^2} \frac{v\left(y_b\mu - A'_b\right)\Delta_{RR,23}^D m_{\tilde{g}}}{(m_{Q,\tilde{t}}^2 - m_{D,\tilde{s}}^2)(m_{Q,\tilde{t}}^2 - m_{D,\tilde{b}}^2)(m_{D,\tilde{s}}^2 - m_{D,\tilde{b}}^2)} \tilde{B}_0\left(m_{Q,\tilde{t}}^2, m_{D,\tilde{s}}^2, m_{D,\tilde{b}}^2, m_{\tilde{g}}^2\right), \quad (2.59)$$

where the loop function $\tilde{B}_0$ can be found in Appendix B. In general, the bottom and strange quark masses are then obtained by diagonalising the matrix

$$\left(m_{d,ij}\right)_{i,j>1} = \begin{pmatrix} \Sigma_{ss}^{LR} & \Sigma_{sb}^{LR} \\ \Sigma_{bs}^{LR} & \Sigma_{bs}^{LR} \end{pmatrix}, \qquad (2.60)$$

with the total self-energy contributions $\Sigma_{d,ij}^{LR}$ as defined in Equation (2.51), see also Equation (2.49). For a very heavy gluino and heavy left-handed squark masses, which is favoured for our explanation of the $R_{K^{(*)}}$ anomalies, the flavour changing self energies are of $\mathcal{O}(10^{-3})$ and the effect to the previously discussed flavour observables is subleading.

---

[1]We will comment on this mass bound at the end of the chapter.
[2]This follows from $2(m_{L,\tilde{\tau}}^2 + m_{R,\tilde{\tau}}^2) \geq |\mu|^2$ [91,92] $\rightarrow m_{L,\tilde{\tau}}^2 + m_{R,\tilde{\tau}}^2 \geq |y_\tau\mu - A'_{\tilde{\tau}}|^2/2$
[3]The Yukawa coupling enters the scalar potential via a trilinear coupling in a term $\propto y_\tau\mu^*$.
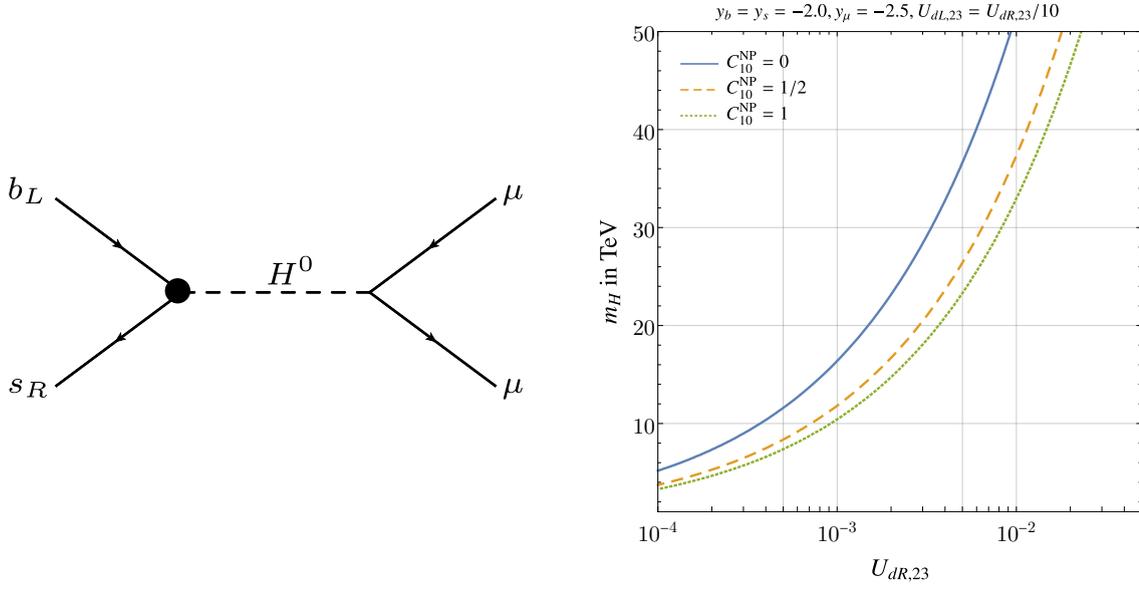
Figure 2.9.: *Left*: Effective tree-level Higgs contribution to $B_s \to \mu\mu$.
Right: Lower limit on the heavy neutral Higgs mass as a function of typical values of the flavour changing self energies and for different New Physics contributions to the Wilson coefficient C_{10}^{NP}. Limit is set for maximal values of the Yukawa couplings.

However, it can induce a Higgs penguin, cf. Figure 2.9, and due to $y_\mu \sim \mathcal{O}(1)$ it severely enhances the branching ratio of $B_s \to \mu\mu$. This in turn, sets a stringent lower bound on the heavy Higgs masses justifying our choice in the very beginning of Section 2.2. To determine this lower limit on the mass, we first consider the effective Yukawa Lagrangian.

Effective Yukawa Lagrangian

To estimate the effect of the afore-mentioned Higgs penguin, we closely follow Reference [82]. In general, the effective neutral-Higgs couplings to down-type quarks and leptons read [88]

$$
L = -\bar{d}_{L,i} \left[\left(-Y_{d_j}^{(0)} \delta_{ij} + \frac{\Sigma_{d,ij}^A}{v_d} \right) H_d^{1*} + \frac{\Sigma_{d,ij}^{A'}}{v_u} H_u^2 \right] d_{R,j}
$$
$$
- \bar{l}_{L,i} \left[\left(-Y_{l_j}^{(0)} \delta_{ij} + \frac{\Sigma_{l,ij}^A}{v_d} \right) H_d^{1*} + \frac{\Sigma_{l,ij}^{A'}}{v_u} H_u^2 \right] l_{R,j} + \text{h.c.} .
\tag{2.61}
$$

with the bare Yukawa couplings $Y_f^{(0)}$, the holomorphic part $\Sigma_{f,ij}^A$ and the non-holomorphic part $\Sigma_{f,ij}^{A'}$ of the chirality changing self energy $\Sigma_{f,ij}^{LR}$. The neutral Higgs fields H_d^1 and H_u^2 are related to the physical Higgs fields by [88]

$$
H_d^1 = \frac{1}{\sqrt{2}} \left(\cos(\alpha) H^0 - \sin(\alpha) h^0 + i \sin(\beta) A \right) ,
$$
$$
H_u^2 = \frac{1}{\sqrt{2}} \left(\sin(\alpha) H^0 + \cos(\alpha) h^0 + i \cos(\beta) A \right) .
\tag{2.62}
$$

In the limit $v_d = 0$ the Lagrangian in Equation (2.61) simplifies to

$$L = -\frac{1}{\sqrt{2}}\bar{d}_{L,i}\left[-Y_{d_j}^{(0)}\delta_{ij}\left(H^0 - iA\right) + \frac{\Sigma_{d,ij}^{A'}}{v}h^0\right]d_{R,j}$$
$$-\frac{1}{\sqrt{2}}\bar{l}_{L,i}\left[-Y_{l_j}^{(0)}\delta_{ij}\left(H^0 - iA\right) + \frac{\Sigma_{l,ij}^{A'}}{v}h^0\right]l_{R,j} + \text{h.c.}.\tag{2.63}$$

Taking Equation (2.52) and changing to the fermion mass basis by

$$U_{fL}^\dagger m_f U_{fR} = \text{diag}(m_{f_1}, m_{f_2}, m_{f_3}),\tag{2.64}$$

yields the following neutral-Higgs couplings to fermions

$$L = -\frac{1}{\sqrt{2}}\bar{d}_{L,i}\left[-Y'_{d,ij}\left(H^0 - iA\right) + \frac{m_{d_j}}{v}\delta_{ij}h^0\right]d_{R,j}$$
$$-\frac{1}{\sqrt{2}}\bar{l}_{L,i}\left[-Y'_{l,ij}\left(H^0 - iA\right) + \frac{m_{l_j}}{v}\delta_{ij}h^0\right]l_{R,j} + \text{h.c.},\tag{2.65}$$

with

$$Y'_f = U_{fL}^\dagger Y_f^{(0)} U_{fR},\tag{2.66}$$

and we can read off the couplings of the neutral Higgs fields to the fermions

$$\Gamma_{d_f d_i}^{LRH_k^0} = x_k^d Y'_{d,fi} + x_k^{u*}\frac{m_{d_i}}{v}\delta_{fi},$$
$$\Gamma_{l_f l_i}^{LRH_k^0} = x_k^d Y'_{d,fi} + x_k^{u*}\frac{m_{d_i}}{v}\delta_{fi},\tag{2.67}$$

with

$$H_k^0 = \left(H^0, h^0, A\right), \qquad x_k^u = \left(0, -\frac{1}{\sqrt{2}}, 0\right), \qquad x_k^d = \left(\frac{1}{\sqrt{2}}, 0, -\frac{i}{\sqrt{2}}\right).\tag{2.68}$$

which finally leads us to the neutral Higgs contributions to $B_s \to \mu\mu$.

Neutral Higgs Contribution to $B_s \to \mu^+\mu^-$

The neutral Higgs contributions to the scalar Wilson coefficients relevant for the decay $B_s \to \mu^+\mu^-$ read [98]

$$C_S = \sum_{k=1}^3 \frac{1}{m_{H_k^0}^2}\left(\Gamma_{\mu\mu}^{LRH_k^0} + \Gamma_{\mu\mu}^{RLH_k^0}\right)\Gamma_{bs}^{RLH_k^0}, \quad C_P = \sum_{k=1}^3 \frac{1}{m_{H_k^0}^2}\left(\Gamma_{\mu\mu}^{LRH_k^0} - \Gamma_{\mu\mu}^{RLH_k^0}\right)\Gamma_{bs}^{RLH_k^0},$$

$$C_{S'} = \sum_{k=1}^3 \frac{1}{m_{H_k^0}^2}\left(\Gamma_{\mu\mu}^{LRH_k^0} + \Gamma_{\mu\mu}^{RLH_k^0}\right)\Gamma_{bs}^{LRH_k^0}, \quad C_{P'} = \sum_{k=1}^3 \frac{1}{m_{H_k^0}^2}\left(\Gamma_{\mu\mu}^{LRH_k^0} - \Gamma_{\mu\mu}^{RLH_k^0}\right)\Gamma_{bs}^{LRH_k^0}.\tag{2.69}$$

In our case the flavour changing couplings Y'_l and Y'_d are given by

$$Y'_l = Y_l^{(0)},$$

$$Y_d' = U_{dL}^\dagger Y_d^{(0)} U_{dR} \approx \begin{pmatrix} y_d^{(0)} & 0 & 0 \\ 0 & y_s^{(0)} & \dfrac{\Sigma_{LR,bs}^{\tilde{g}\tilde{t}\tilde{b}\tilde{s}}}{m_b} y_s^{(0)} - \dfrac{\Sigma_{LR,sb}^{\tilde{g}\tilde{c}\tilde{s}\tilde{b}}}{m_b} y_b^{(0)} \\ 0 & -\dfrac{\Sigma_{LR,bs}^{\tilde{g}\tilde{t}\tilde{b}\tilde{s}}}{m_b} y_b^{(0)} + \dfrac{\Sigma_{LR,sb}^{\tilde{g}\tilde{c}\tilde{s}\tilde{b}}}{m_b} y_s^{(0)} & y_b^{(0)} \end{pmatrix}. \quad (2.70)$$

Demanding the prediction $\mathrm{BR}_{\mathrm{theo}}(B_s \to \mu^+\mu^-)$ to stay within 2σ around the measurement for different values of $C_{10,\mu}$ sets a lower limit on the heavy Higgs masses as a function of typical values of the flavour changing self energies $\Sigma_{LR,ij}$, cf. Figure 2.9. We see that the measurement of $\mathrm{BR}(B_s \to \mu^+\mu^-)$ puts a stringent lower limit on the additional neutral Higgs fields of $\mathcal{O}(10\,\mathrm{TeV})$.

2.5. Theoretical Constraints: Vacuum Stability

The relevant part of the scalar potential, see Equations (2.6)–(2.8), reads

$$
\begin{aligned}
V =\ & m_{H_1}^2 h_d^{0*} h_d^0 + m_{H_2}^2 h_u^{0*} h_u^0 + |\mu|^2 h_d^{0*} h_d^0 + |\mu|^2 h_u^{0*} h_u^0 \\
& + m_{L,\tilde{l}}^2 \tilde{l}_L^+ \tilde{l}_L^- + m_{R,\tilde{l}}^2 \tilde{l}_R^+ \tilde{l}_R^- + m_{L,\tilde{c}}^2 \tilde{s}_L^* \tilde{s}_L + m_{R,\tilde{s}}^2 \tilde{s}_R^* \tilde{s}_R + m_{L,\tilde{t}}^2 \tilde{b}_L^* \tilde{b}_L + m_{R,\tilde{b}}^2 \tilde{b}_R^* \tilde{b}_R \\
& + \Delta_{RR,23}^D \left(\tilde{b}_R^* \tilde{s}_R + \tilde{s}_R^* \tilde{b}_R \right) \\
& + y_b^2 \left(\tilde{b}_L^* \tilde{b}_L \tilde{b}_R^* \tilde{b}_R + h_d^{0*} h_d^0 \tilde{b}_L^* \tilde{b}_L + h_d^{0*} h_d^0 \tilde{b}_R^* \tilde{b}_R \right) + y_s^2 \left(\tilde{s}_L^* \tilde{s}_L \tilde{s}_R^* \tilde{s}_R + h_d^{0*} h_d^0 \tilde{s}_L^* \tilde{s}_L + h_d^{0*} h_d^0 \tilde{s}_R^* \tilde{s}_R \right) \\
& + y_l^2 \left(\tilde{l}_L^+ \tilde{l}_L^- \tilde{l}_R^+ \tilde{l}_R^- + h_d^{0*} h_d^0 \tilde{l}_L^+ \tilde{l}_L^- + h_d^{0*} h_d^0 \tilde{l}_R^+ \tilde{l}_R^- \right) \\
& + y_l y_b \left(\tilde{b}_L \tilde{b}_R^* \tilde{l}_L^+ \tilde{l}_R^- + \mathrm{h.c.} \right) + y_l y_s \left(\tilde{s}_L \tilde{s}_R^* \tilde{l}_L^+ \tilde{l}_R^- + \mathrm{h.c.} \right) \\
& + y_b y_s \left(\tilde{b}_L^* \tilde{s}_L \tilde{b}_R \tilde{s}_R^* + \mathrm{h.c.} \right) + y_\mu y_\tau \left(\tilde{\mu}_L^+ \tilde{\tau}_L^- \tilde{\mu}_R^- \tilde{\tau}_R^+ + \mathrm{h.c.} \right) \\
& + h_u^{0*} \left(y_l \mu - A_{\tilde{l}}' \right) \tilde{l}_L^- \tilde{l}_R^+ + h_u^{0*} \left(y_s \mu - A_{\tilde{s}}' \right) \tilde{s}_L \tilde{s}_R^* + h_u^{0*} \left(y_b \mu - A_{\tilde{b}}' \right) \tilde{b}_L \tilde{b}_R^* + \mathrm{h.c.} \\
& + \frac{1}{8} g_1^2 \left(\frac{1}{3} \tilde{b}_L^* \tilde{b}_L + \frac{1}{3} \tilde{s}_L^* \tilde{s}_L - \tilde{l}_L^+ \tilde{l}_L^- + \frac{2}{3} \tilde{b}_R^* \tilde{b}_R + \frac{2}{3} \tilde{s}_R^* \tilde{s}_R + 2 \tilde{l}_R^+ \tilde{l}_R^- - h_d^{0*} h_d^0 + h_u^{0*} h_u^0 \right)^2 \\
& + \frac{1}{8} g_2^2 \left(\tilde{b}_L^* \tilde{b}_L + \tilde{s}_L^* \tilde{s}_L + \tilde{l}_L^+ \tilde{l}_L^- - h_d^{0*} h_d^0 + h_u^{0*} h_u^0 \right)^2 \\
& + \frac{1}{8} g_3^2 \left(\tilde{b}_L^* \tilde{b}_L + \tilde{s}_L^* \tilde{s}_L - \tilde{b}_R^* \tilde{b}_R - \tilde{s}_R^* \tilde{s}_R \right)^2,
\end{aligned} \quad (2.71)
$$

with $l = \mu, \tau$. Note that the scalar potential is bounded from below due to supersymmetry, and that the term proportional to m_{12}^2 vanishes for $v_d = 0$, cf. Equation (2.13). The trilinear terms stem from the non-holomorphic couplings that can generate lower minima in the scalar potential. These minima can in addition break colour or charge. One has to consider this potential as a function of 10 scalar fields ($\tilde{b}_{L,R}$, $\tilde{s}_{L,R}$, $\tilde{\mu}_{L,R}$, $\tilde{\tau}_{L,R}$ and $h_{1,2}$), and hence, there are no closed or analytical expressions to avoid such minima. Therefore, lower vacuum configurations are avoided by explicitly checking that the physical vacuum $v = 174\,\mathrm{GeV}$ remains the global minimum for a given set of potential parameters. In this case the vacuum conditions turn into polynomial equations and *all*[1] isolated stationary points can be found using polynomial homotopy continuation [99], see References [100–102] for similar applications.

Of course, there can be long-lived metastable configurations. However, a precise numerical calculation is computationally too expensive, and instead, we follow the approach of Reference [102], which is briefly summarised in the following: The starting point is a

---

[1]Notice that in practice, there might be numerical instabilities.

renormalisable potential $V(\vec{\phi})$ of n real scalar fields $\vec{\phi} = (\phi_1, \ldots, \phi_n)$ which is expanded around the vacuum $\vec{\phi} = \vec{\phi}_v + \vec{\varphi}$ [102]

$$V(\vec{\varphi}) = \lambda'_{abcd} \varphi_a \varphi_b \varphi_c \varphi_d + A'_{abc} \varphi_a \varphi_b \varphi_c + m'^2_{ab} \varphi_a \varphi_b \,. \tag{2.72}$$

Rewriting the scalar fields $\vec{\varphi} \to \varphi \hat{\varphi}$ in terms of the unit vector $\hat{\varphi}$, the potential reads [102]

$$V(\varphi, \hat{\varphi}) = \lambda(\hat{\varphi}) \varphi^4 - A(\hat{\varphi}) \varphi^3 + m^2(\hat{\varphi}) \varphi^2 \,. \tag{2.73}$$

In order to determine the vacuum stability, one has to calculate the bounce action B which is defined as follows: Given the euclidean equation of motion of a scalar ϕ in a potential U with the boundary conditions [102,103]

$$\lim_{\rho \to \infty} \phi(\rho) = \phi_v \,, \qquad\qquad \frac{\mathrm{d}\phi}{\mathrm{d}\rho} \bigg|_0 = 0 \,, \tag{2.74}$$

the bounce action is then the euclidean action of the corresponding solution [103]. The relationship of the bounce action and the decay rate Γ of a metastable vacuum state per spatial volume V_S reads [102–104]

$$\frac{\Gamma}{V_S} = K e^{-B} \,, \tag{2.75}$$

with a dimensionful parameter K.[1] Numerical methods to estimate the bounce action, can be found for instance in References [105–110]. Here instead, we approximate the bounce action by a semi-analytical result [102,107]

$$B = \frac{\pi^2}{3\lambda} (2 - \delta)^{-3} \left(13.832\,\delta - 10.819\,\delta^2 + 2.0765\,\delta^3 \right) \,, \qquad \delta = \frac{8\lambda m^2}{A^2} \,, \tag{2.76}$$

and a long-lived vacuum is given for $B > 440$ [102].

Note that this method explicitly refers to real scalar fields, thus, all fields in the potential (2.71) should be expanded into real and imaginary part, and rescaled such that the kinetic terms are normalised canonically [102].

2.6. Numerical Analysis and Final Remarks

Here we perform a numerical scan taking into account the exact one-loop expressions of all previously discussed experimental constraints. The vacuum stability is checked explicitly as discussed in Sections 2.5. The flavour changing self energies are resummed, closely following Reference [23]. The scan is done over the parameter regions

$$\begin{aligned}
m_{Q(D),\tilde{q}} &> 1\,\mathrm{TeV}\,, & m_{L,\tilde{\mu}} &> 5\,\mathrm{TeV}\,, & m_{R,\tilde{\mu}} &> 0.5\,\mathrm{TeV}\,, \\
m_{\tilde{g}} &> 2\,\mathrm{TeV}\,, & |y_b| = |y_s| &< 2\,, & |y_\mu| &< 2.5\,, \\
-M_1 &> 1\,\mathrm{TeV}\,, & M_2 &> 0.5\,\mathrm{TeV}\,, & \mu &> 0.5\,\mathrm{TeV}\,,
\end{aligned} \tag{2.77}$$

where we optimised the selected regions, through our intermediate result in Section 2.3, see also Figure 2.5 and 2.6. To minimise the computational expense, the non-holomorphic couplings $A'_{s,b,\mu}$ are determined for a given set of parameters such that the charged

---

[1]Since the value of K is irrelevant for our application, we refrain from going further into detail, and instead direct the interested reader to Reference [102] and the references therein, and of course to the original Reference [104].

lepton and down quark masses are obtained. Non-holomorphic couplings A'_f or right-handed squark mixing $\Delta^D_{RR,23}$ yielding a tachyonic mass spectrum or generating a vacuum instability are discarded.

We provide a benchmark point, defined as the parameter point minimising

$$\chi^2 = \sum_{ij} \left(O_{i,\text{theo}} - O_{i,\text{exp}} \right) V_{ij} \left(O_{j,\text{theo}} - O_{j,\text{exp}} \right) ,$$

with the covariance matrix V and within the regions in Equation (2.77). For this point, a set of masses and couplings, $(m_{L,\tilde\tau}, m_{R,\tilde\tau}, A'_\tau, y_\tau)$, to generate the tau mass is determined such that the vacuum remains (meta-)stable. Of course this is not a sophisticated statistical procedure, but it helps us to determine a point in the MSSM parameter space where we can explain the anomalies in $R_{K^{(*)}}$ without violating any experimental measurement which is exactly what we want to show.

BENCHMARK POINT   We obtain the following best fit point:

$$
\begin{aligned}
m_{Q,\tilde c} &= 18\,\text{TeV}\,, & m_{Q,\tilde t} &= 6.2\,\text{TeV}\,, & m_{D,\tilde s} &= 1.1\,\text{TeV}\,, & m_{D,\tilde b} &= 2.3\,\text{TeV}\,, \\
m_{L,\tilde\mu} &= 19\,\text{TeV}\,, & m_{R,\tilde\mu} &= 0.58\,\text{TeV}\,, & m_{L,\tilde\tau} &= 0.3\,\text{TeV}\,, & m_{R,\tilde\tau} &= 8.0\,\text{TeV}\,, \\
M_1 &= -7.1\,\text{TeV}\,, & M_2 &= 2.7\,\text{TeV}\,, & \mu &= 1.6\,\text{TeV}\,, & m_{\tilde g} &= 5.6\,\text{TeV}\,,
\end{aligned}
\tag{2.78}
$$

while the trilinear couplings A'_f, squark mixing $\Delta^D_{RR,23}$, and Yukawa couplings y_f read

$$
\begin{aligned}
\Delta^D_{RR,23} &= 0.79\,\text{TeV}^2\,, & A'_s &= -2.7\,\text{TeV}\,, & A'_b &= 3.8\,\text{TeV}\,, & A'_\mu &= -17\,\text{GeV}\,, \\
y_b = y_s &= -2.0\,, & y_\mu &= -2.5\,,
\end{aligned}
\tag{2.79}
$$

with $\chi^2_{\min} \approx 1.67$. The New Physics contributions to C_9 and C_{10} are

$$C_9^{\text{NP}} = -0.41\,, \qquad\qquad\qquad C_{10}^{\text{NP}} = 0.44\,, \tag{2.80}$$

very close to the best-fit obtained in Reference [14]

$$C_9 = -C_{10} = -0.44^{+0.07}_{-0.08}\,, \tag{2.81}$$

based on the *full* set of data, which also includes angular observables like P'_5, in the $b \to sll$ transition. For the value of $R_{K^{(*)}}$ and other observables see Table 2.4. There we also list their deviations from the experimental measurements. And indeed, we see a very good agreement between theory and experiment with most deviations well below $1\,\sigma$.

As already explained one can determine a set of parameters $(m_{L,\tilde\tau}, m_{R,\tilde\tau}, A'_\tau, y_\tau)$ to generate the tau mass radiatively. Note that the non-holomorphic coupling A'_τ enters the tau mass correction as $\propto (\mu y_\tau - A'_\tau)$, and hence, it has to be of order $A'_\tau \sim -\mu y_\tau \sim 4\,\text{TeV}$ to have a noticeable effect on the tau mass. Nonetheless, the effect is at most $\lesssim 10\,\%$ since all other contributions are dominated by $y_\tau\mu$, cf. Equations (2.54) and (2.55). However, the trilinear coupling enters the radiative corrections to the lightest Higgs mass $m_{h_{\text{SM}}}$ and due to the large tau Yukawa coupling, there is a non-negligible cancellation with the stop and top contributions for $A'_\tau \sim \mathcal{O}(10\,\text{TeV})$. For this reason we choose $A'_\tau = 0$ and show the allowed region for $y_\tau = 3$ in the stau mass plane in Figure 2.10. There, we also show the naive vacuum stability constraint as hashed region.

Before summarising the main results of this chapter, we comment on some questions that emerged.

Table 2.4.: Parameter point with the lowest sum of the squared deviations of all considered observables.

observable O_i	value	exp	$d_i = (O_{i,\text{theo}} - O_{i,\text{exp}})/\sigma_{i,\text{tot}}$
$R_K^{[1.1,6]}$	0.828	0.846 ± 0.043	0.41
$R_{K^*}^{[1.1,6]}$	0.80	0.69 ± 0.10	1.08
$\text{BR}(B_s \to \mu^+\mu^-) \times 10^9$	3.06	3.00 ± 0.46	0.12
$\text{BR}(B \to X_s\gamma) \times 10^4$	3.2	3.0 ± 0.4	0.31
C_{B_s}	1.08	1.11 ± 0.09	0.29
$\phi_{B_s} \times 10^3$	1	7 ± 16	0.38
$\Delta a_\mu \times 10^9$	2.53	2.51 ± 0.59	0.03

COMMENT ON THE STANDARD MODEL HIGGS MASS   As discussed in Section 2.1 the Standard Model like Higgs field has a mass of m_Z much below the measured value of 125 GeV. For this reason the radiative corrections have to account for the difference between the measurement and tree-level prediction. Usually the dominant contributions are mediated by the stop and the heavy top quark. However, in our case, there are additional important contributions: The sdown quarks and charged sleptons couple with the large Yukawa couplings $y_{s,b,\mu,\tau} \sim 1$ and the non-holomorphic couplings $A'_{s,b,\mu,\tau}$ to the 'wrong' Higgs field via $v_u = v$. This yields an important constraint on the still undetermined right-handed stop mass $m_{R,\tilde{t}}$ and the holomorphic coupling A_t. All these contributions can be determined with the help of the known one-loop effective potential. Requiring the Standard Model like Higgs mass to be $m_{h_{\text{SM}}} = 125 \pm 5$ GeV, the allowed region on the A_t–$m_{R,\tilde{t}}$ plane is shown exemplary for the benchmark point in Figure 2.10.

COMMENT ON COLLIDER CONSTRAINTS   Most parameters are chosen $\gtrsim 1$ TeV, and therefore, current collider constraints are evaded. However, as it has turned out, in order to generate the tau mass radiatively, the left-handed stau mass has to be $\lesssim 500$ GeV, and the question arises if such low masses are not ruled out yet. The left-handed slepton predominantly decays into an off-shell W boson and a left-handed sneutrino, for this reason not even the Large Electron–Positron Collider (LEP) bound of $\lesssim 100$ GeV applies in that case. There, the bound on the sleptons comes from the decay into a lepton and neutralino resulting into two non-back-to-back leptons and missing momentum [83]. This also holds for the LHC searches, where the limits do not apply anyway for $m_{\chi_1^0} > 130$ GeV [83]. Moreover the pair production of sleptons is strongly suppressed compared to the coloured particles and still significantly smaller than the production cross section of charginos and neutralinos [83]. The (mono-)jet searches focus on the squark sector and are not suitable due to the small mass difference between the left-handed stau and sneutrino resulting in low transverse momentum or energy of the decay products and thus inundated by the huge Standard Model background. For the left-handed sneutrino LSP, the relevant constraint comes from the Z width measurement excluding $m_{L,\tilde{t}} < 45$ GeV [83]. For an extensive review see Reference [83].

COMMENT ON SDOWN MIXING THROUGH NON-HOLOMORPHIC COUPLINGS   As mentioned in Section 2.1, another possibility to introduce flavour violation in the $b \to s$ transition is through left–right mixing. However, large left–right mixing $\Delta^D_{LR,23(32)}$ yields large flavour violating self energy contributions which have to be resummed. Values for which the
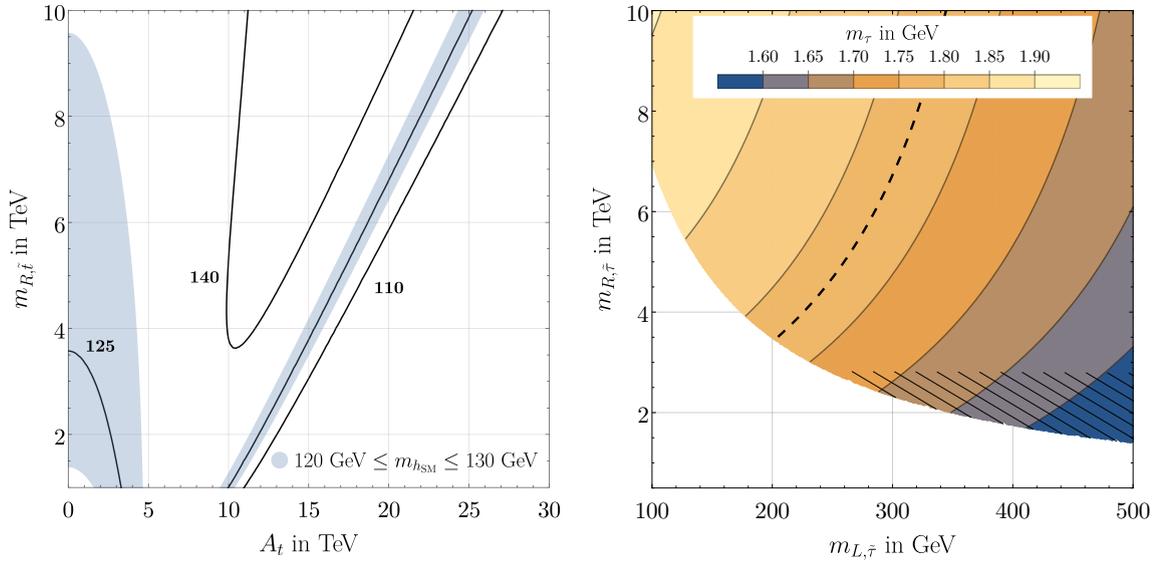
Figure 2.10.: *Left*: Mass of the Standard Model like Higgs field as a function of the stop quark mass $m_{R,\tilde{t}}$ and the holomorphic coupling A_t for the benchmark point, cf. Equations (2.78) and (2.79). The contours are in units of GeV.
Right: Tau mass as a function of the stau masses. The region violating the naive vacuum stability bound $m_{R,\tilde{\tau}}^2 + m_{L,\tilde{\tau}}^2 > |y_\tau \mu|^2/2$ is hashed. However, the whole region shown is at least metastable and long-lived according to Section 2.5. The white region does not yield a physical mass spectrum, and the dashed line corresponds to the physical tau mass $m_\tau = 1.777\,\text{GeV}$.

anomalies in the $b \to sll$ transition are relaxed would then be in direct contradiction to the bounds coming from neutral B_s meson mixing.

2.7. Summary

Finally, we summarise the main results of this chapter.

- We showed that it is possible to generate large contributions of $\mathcal{O}(1)$ to the Wilson coefficients C_9 and C_{10} as it is needed to explain the anomalies in the $b \to sll$ transition for $\tan \beta \to \infty$.

- Remarkably, the same parameter space needed to resolve the anomalies in $b \to sll$, explains the long-standing deviation in $(g-2)_\mu$.

This scenario entails a distinctive phenomenology:

- The higgsino and right-handed squark fields are necessarily at $\sim 1\,\text{TeV}$.

- There has to be sub-TeV sleptons, a solution to the anomalies implies left-handed stau and sneutrino fields below $\sim 500\,\text{GeV}$.

- On the other hand, the masses of the heavy Higgs fields are $\mathcal{O}(10\,\text{TeV})$ and therefore nearly degenerate $m_{H^0} \approx m_{A^0} \approx m_{H^\pm}$.

- In contrast to the muon sector the contributions to the transition $b \to s\tau\tau$ are $C_{9,\tau}^{\text{NP}} \approx C_{10,\tau}^{\text{NP}}$.

- As a consequence of the inverted hierarchy in the stau sector compared to the smuons, there is at most an $\mathcal{O}(1)$ enhancement in $b \to s\tau\tau$ processes compared to $b \to s\mu\mu$.

- $B_s \to \tau\tau$: here even a suppression of $C_{S(P),\tau}/C_{S(P),\mu} \sim 1/2$ is possible compared to the decay into muons.

New Physics in the Transition $b \to dll$?

The recent anomalous measurements of the $b \to sll$ transition [2,5] immediately raise the question whether similar anomalies are also present in $b \to dll$ processes. A priori there is no reason for the yet unknown New Physics not to couple to the down quark, more particularly since the $b \to sll$ measurements as well favour a coupling to the first generation lepton [14,67,68]. Yet there are only two observations involving this transition: the decay $B^+ \to \pi^+ \mu\mu$ [111,112], and $\Lambda_b^0 \to p\pi^- \mu\mu$ [113] all performed by LHCb. The reason is the additional CKM suppression by $|V_{td}/V_{ts}|$ compared to the transition $b \to sll$ rendering the measurements even more difficult to perform. However, in the context of the planned LHCb upgrades, significant experimental improvements are expected allowing measurements at the few percent level [114]. For this reason, precise theoretical calculations are essential to enable a comparison with the experiments.

Calculations of the decay $B^+ \to \pi^+ \mu\mu$ in the low q^2 region, i.e. below the charm quark resonances J/ψ are performed in the naive factorisation approach in Reference [115]. While the vector form factor $f_+^{B\pi}$ can be extracted precisely from experimental data, heretofore, lattice data on the tensor form factor $f_T^{B\pi}$ was only sparse. For that reason the tensor form factor $f_T^{B\pi}$ is calculated from the analogous form factor in the $b \to sll$ transition, f_T^{BK}, with the help of an $SU(3)_F$ symmetry ansatz. A similar calculation is performed in Reference [116] within the QCD factorisation (QCDF) approach which is an adaption of the analogous QCDF calculation of the decay $B \to K^* ll$ in Reference [117]. However, instead of an $SU(3)_F$ ansatz, the form factors are taken from a previous light-cone sum rule (LCSR) calculation [118]. The LCSR approach is also used in Reference [119] to determine the non-local contributions to $B \to \pi ll$ in the low q^2 regime. There, this approach is combined with QCDF and an operator product expansion (OPE) at $q^2 < 0, |q|^2 \gg \Lambda_{\text{QCD}}$—a prior developed method to calculate the charm quark effects in $B \to K^{(*)} ll$ [120]. Furthermore, in Reference [121] the decay width is calculated in the whole q^2 range in the relativistic quark model.

For the low recoil region, i.e. above the resonances J/ψ and ψ', an OPE for large q^2—first discussed to some extent in References [122,123] for the $b \to sll$ transition and further systemised in References [124,125]—can be applied, as briefly done in Reference [126].

In this chapter, we will go beyond these available analyses for the decay of B mesons into pseudoscalars P, $B \to Pll$[1]: We combine several approaches by applying the $1/q^2$-OPE for the up quark contribution below the charm resonances where q^2 is still large enough for an expansion in $1/q^2$ and far away from the up quark resonances $q^2 \gg m_{\rho,\omega,\phi}^2$. At the same time, we use QCDF for the charm quark contribution and compare the result with an experimental extraction of the very same contribution from the anomalous $b \to sll$ data. The latter further enables a prediction in the region between the charm quark resonances, i.e. $m_{J/\psi}^2 < q^2 < m_{\psi'}^2$. Next, we analyse the effect of New Physics on processes involving the $b \to dll$ transition in Section 3.2. While the rare $b \to dll$ processes are known to be sensitive to New Physics due to their strong suppression in the Standard Model, we examine in particular the mixing-induced CP violation. Here a large cancellation of theoretical uncertainties is expected, and thus, yielding an even higher sensitivity to physics beyond the Standard Model.

3.1. Semileptonic B Meson Decays into Pseudoscalars

Unless noted otherwise, we follow the convention of Reference [125], and the notation of References [119, 125]. The effective Hamiltonian for $b \to dll$ reads [125]

$$\mathcal{H}_{\text{eff}} = \frac{G_F}{\sqrt{2}} \sum_{p=u,c} \lambda_p \left[C_1 Q_1^p + C_2 Q_2^p + \sum_{i=3}^{10} C_i Q_i \right], \tag{3.1}$$

with $\lambda_p = V_{pd}^* V_{pb}$ and [125]

$$Q_1^p = (\bar{p}b)_{V-A}(\bar{s}p)_{V-A},$$
$$Q_3 = (\bar{s}b)_{V-A} \sum_q (\bar{q}q)_{V-A},$$
$$Q_5 = (\bar{s}b)_{V-A} \sum_q (\bar{q}q)_{V+A},$$
$$Q_7 = \frac{e}{8\pi^2} m_b \bar{s}\sigma_{\mu\nu}(1+\gamma_5)F^{\mu\nu}b,$$
$$Q_9 = \frac{\alpha}{2\pi}(\bar{s}b)_{V-A}(\bar{l}\gamma_\mu l)$$

$$Q_2^p = (\bar{p}_i b_j)_{V-A}(\bar{s}_j p_i)_{V-A},$$
$$Q_4 = (\bar{s}_i b_j)_{V-A} \sum_q (\bar{q}_j q_i)_{V-A},$$
$$Q_6 = (\bar{s}_i b_j)_{V-A} \sum_q (\bar{q}_j q_i)_{V+A},$$
$$Q_8 = \frac{g}{8\pi^2} m_b \bar{s}\sigma_{\mu\nu}(1+\gamma_5)G^{\mu\nu}b,$$
$$Q_{10} = \frac{\alpha}{2\pi}(\bar{s}b)_{V-A}(\bar{l}\gamma_\mu \gamma_5 l), \tag{3.2}$$

where $V \pm A$ denotes $\gamma^\mu(1 \pm \gamma^5)$. Using the unitarity of the CKM matrix $\lambda_u + \lambda_c = -\lambda_t$, Equation (3.1) can be written as

$$\mathcal{H}_{\text{eff}} = \frac{G_F}{\sqrt{2}} \sum_{p=u,c} \lambda_p \left[C_1 Q_1^p + C_2 Q_2^p + \sum_{i=3\dots6,8} C_i Q_i \right] - \frac{G_F}{\sqrt{2}} \lambda_t \sum_{i=7,9,10} C_i Q_i$$

$$\equiv \frac{G_F}{\sqrt{2}} \left[\lambda_u H^u + \lambda_c H^c - \lambda_t \sum_{i=7,9,10} C_i Q_i \right]. \tag{3.3}$$

The decay amplitude for the process $B \to Pll$ is then given by sandwiching the effective Hamiltonian between the initial and final state. The resulting matrix elements of the operators Q_7, Q_9 and Q_{10} are given by the vector, f_+^{BP} and f_-^{BP}, and tensor f_T^{BP} form factors defined through [119, 125]

$$\langle P(p)|\bar{d}\gamma^\mu b|B(p+q)\rangle = 2f_+^{BP}(q^2)p^\mu + \left[f_+^{BP}(q^2) + f_-^{BP}(q^2) \right]q^\mu,$$

---

[1]Note that from now on we drop the meson charges, i.e. $B \equiv B^\pm$ is implicitly understood. Neutral B mesons are written as B_q with the down-type valence quark q. The final state will only be denoted as $P = \pi$ or $P = K$, the exact quark content and the charge immediately follow from the initial state as we only consider $b \to dll$ transitions. In case the final state P is not further specified then $B \equiv B^\pm, B_q$

$$\langle P(p)|\, \bar{d}\sigma^{\mu\nu}q_{\nu}b\,|B(p+q)\rangle = \frac{if_T^{B\pi}(q^2)}{m_B+m_P}\,q^2\,\left[2p^{\mu}+\left(1-\frac{m_B^2-m_P^2}{q^2}\right)q^{\mu}\right]\,, \tag{3.4}$$

with the lepton-pair momentum q^2. Note that the form factor $f_-(q^2)$ from Reference [125] is related to $f^0(q^2)$ from Reference [119] by

$$f_-(q^2) = \frac{m_B^2-m_P^2}{q^2}\left[f^0(q^2)-f_+(q^2)\right]\,. \tag{3.5}$$

In any case, q^{μ} is contracted with the lepton bilinear terms in such a way that after applying the equation of motion,

$$q^{\mu}\bar{l}\gamma_{\mu}P_L l = -m_l\bar{l}P_L l + m_l\bar{l}P_R l = m_l\bar{l}\gamma_5 l\,, \tag{3.6}$$

these terms will be proportional to the lepton masses, and thus, negligible for electrons and muons.

The actual difficulty lies in evaluating the hadronic matrix elements of the Hamiltonians H^{u} and H^{c} introduced in Equation (3.3). Their contribution reads [119,125]

$$\frac{8\pi^2}{q^2}i\int \mathrm{d}^4x\,e^{iq\cdot x}\,\langle P(p)|\,\mathrm{T}j^{\mu}(x)H^{u(c)}(0)\,|B(p+q)\rangle \equiv \langle P(p)|\,\mathcal{K}^{\mu}_{H^{u(c)}}(q^2)\,|B(p+q)\rangle\,, \tag{3.7}$$

with the electromagnetic current $j^{\mu} = Q_q\,\bar{q}\gamma^{\mu}q$. Notice the different sign convention compared to Reference [125]. Altogether the decay amplitude for $b \to dll$ can be written as

$$A(B \to Pll) = -\frac{G_F}{\sqrt{2}}\frac{\alpha}{2\pi}\lambda_t\left[\left(A_9^{\mu}+\frac{\lambda_c}{\lambda_t}A_c^{\mu}+\frac{\lambda_u}{\lambda_t}A_u^{\mu}\right)\bar{u}\gamma_{\mu}v + A_{10}^{\mu}\,\bar{u}\gamma_{\mu}\gamma_5 v\right]\,, \tag{3.8}$$

with

$$A_9^{\mu} = C_9\,\langle P|\,\bar{d}\gamma^{\mu}(1-\gamma^5)b\,|B\rangle + C_7\frac{2im_b}{q^2}q_{\lambda}\,\langle P|\,\bar{d}\sigma^{\lambda\mu}(1+\gamma^5)b\,|B\rangle$$

$$= C_9\,2f_+^{BP}(q^2)p^{\mu} + C_7\frac{2m_b}{m_B+m_P}2f_T^{BP}(q^2)p^{\mu}\,,$$

$$A_{10}^{\mu} = C_{10}\,\langle P|\,\bar{d}\gamma^{\mu}(1-\gamma^5)b\,|B\rangle = C_{10}\,2f_+^{BP}(q^2)p^{\mu}\,,$$

$$A_P^{\mu} = \langle P|\,\mathcal{K}^{\mu}_{H^P}(q^2)\,|B\rangle\,, \tag{3.9}$$

In the following, we briefly describe two methods commonly applied to evaluate the correlator in Equation (3.7) in the high $q^2 \gtrsim m_{\psi(2s)}^2$ and low $q^2 \lesssim m_{J/\psi}^2$ region, respectively. Even though we discuss both regions separately for pedagogical reasons, we bear in mind that for the up quark contribution H^{u}, we want to apply the OPE below the charm quark resonances $q^2 \lesssim m_{J/\psi}^2$ and $q^2 \gg m_{\rho,\omega,\phi}^2, \Lambda_{\mathrm{QCD}}^2$. In the following, we will highlight the differences regarding the calculation of the up quark contribution. For a detailed discussion of the technicalities see References [117,125].

High q^2 Region

In the low recoil region there is a large momentum $q^2 \sim m_b^2$ running through the quark loop. Integrating out this hard quark loop results in an OPE [125]

$$\mathcal{K}^{\mu}_{H^P} = \sum_{d,n}C_{d,n}(q^2)O^{\mu}_{d,n} \equiv \sum_d K^{\mu}_{H^P,d}\,, \tag{3.10}$$
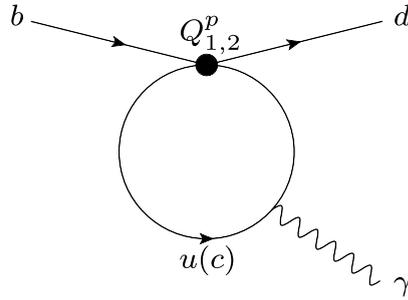
Figure 3.1.: Dimension-3 contributions to the high-q^2 OPE resulting from the insertion of $Q^p_{1,2}$ with $p = u, c$.

with the perturbatively calculable Wilson coefficients $C_{d,n}$ and local operators $O_{d,n}$. Here d denotes the dimension of the operators while n runs over the different operators of the same dimension d. Note that compared to an effective Hamiltonian we integrate out a hard momentum scale instead of a large mass.

The first terms of the OPE are worked out in Reference [125] and read

$$K^\mu_{H^p} = K^\mu_{H^p,3} + K^\mu_{H^p,5} + K^\mu_{H^p,6} + \mathcal{O}\left(\alpha_s, (\Lambda/m_b)^3, m_d/m_b\right), \tag{3.11}$$

up to relative $\mathcal{O}(\alpha_s)$ corrections. Notice however, that we will include the relative α_s corrections to the dimension-3 contributions.

DIMENSION-3   As it was shown in Reference [125], there are only two operators at leading order [125]

$$O^\mu_{3,1} = \left(g^{\mu\nu} - \frac{q^\mu q^\nu}{q^2}\right)\bar{d}\gamma_\nu(1 - \gamma_5)b, \qquad O^\mu_{3,2} = \frac{im_b}{q^2}q_\lambda\,\bar{d}\sigma^{\lambda\mu}(1 + \gamma_5)b. \tag{3.12}$$

Note that $q_\mu O^\mu_{d,n} = 0$ as required by the Ward identity. The corresponding Wilson coefficients are the perturbatively calculated one-loop insertions of the four-quark operators in H^p, see Figure 3.1. The charm quark contribution can be found for example in References [125, 127]. The corresponding contributions for the up quark is obtained by taking the limit $m_c \to 0$. The dominant contributions come from the operators Q^p_1 and Q^p_2 due to the small Wilson coefficients of the QCD penguin operators.

Similarly, the α_s correction is obtained by calculating the two-loop matrix elements of Q^p_1 and Q^p_2 which was done for $b \to dll$ in Reference [128] for the first time. However, there the expansion is performed for low q^2. For this reason we use the result of Reference [129] for the $b \to sll$ transition. Since no expansion in inverse powers of the charm quark mass is performed, we can safely take the limit $m_c \to 0$ to obtain the α_s correction for the up quark loop. Due to the structure of the operators in Equation (3.12), the corresponding coefficients are often absorbed into C_9 and C_7, usually denoted as C_9^{eff} and C_7^{eff}, respectively. Note that for a complete next-to-next-to-leading order (NNLO) evaluation one additionally needs C_9 to two-loop accuracy and the running at three-loop, both available for a long time, see Reference [130] and Reference [131], respectively.[1]

DIMENSION-5   Operators with a gluon field strength tensor $G_{\mu\nu}$ start to contribute at dimension-5 [125]. They read [125]

$$O^\mu_{5,n} = \bar{d}\left(gG\Gamma_n\right)^\mu b, \tag{3.13}$$

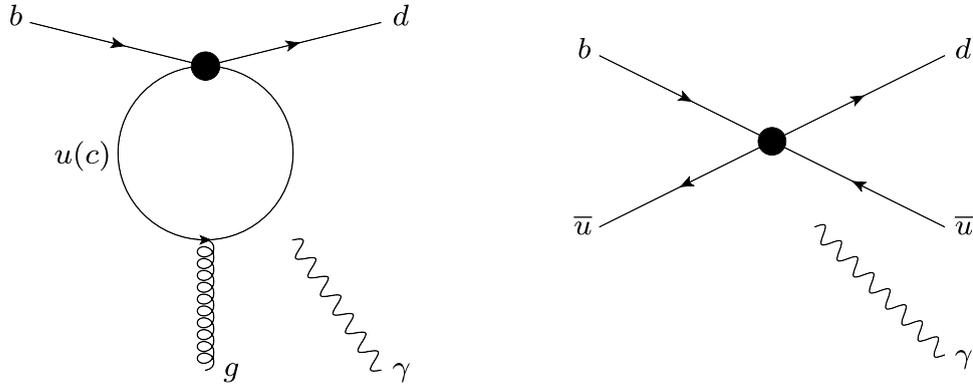[1]Notice that the operator basis differs in some references.

Figure 3.2.: *Left*: Dimension-5 contribution resulting from the expansion of this diagram in $1/q^2$. The photon is attached left and right from the gluon, respectively. The black dots correspond to the insertions of operators from Equation (3.2). *Right*: Dimension-6 contribution resulting from the attachment of the photon to any of the external lines.

with the Dirac and Lorentz structure Γ_n. Such contributions emerge for instance from interactions shown in Figure 3.2, first observed in the context of the transition $b \to s\gamma$ [132]. Since q^2 is large, the gluon momentum r^2 is small, and the corresponding diagrams can be expanded for $q^2 \gg r^2 \sim \Lambda_{\mathrm{QCD}}^2$ which yields a series of local operators [122].

For example, the leading order contribution [122, 125]

$$\mathcal{K}_{H^P,5}^\mu \propto \bar{d}\gamma_\lambda(1-\gamma_5)G_{\alpha\rho}b \left[\epsilon^{\alpha\beta\lambda\rho}\frac{q_\beta q^\mu}{q^2} + \epsilon^{\beta\mu\lambda\rho}\frac{q_\beta q^\alpha}{q^2} - \epsilon^{\alpha\mu\lambda\rho} \right], \tag{3.14}$$

is obtained by expanding the left diagram in Figure 3.2 for $r^2 = 0$ to first order in $1/q^2$. However, all matrix elements of the operators O^μ arising at a higher order $n > 1$ are currently unknown, they contain contributions like

$$O^\mu \sim \bar{s}\gamma_\lambda(1-\gamma_5)\left(\frac{iq\cdot D}{q^2}\right)^n G_{\alpha\rho}b\,\epsilon^{\alpha\mu\lambda\rho}, \tag{3.15}$$

which scales as $\sim q\cdot r/q^2 \sim \Lambda_{\mathrm{QCD}}/\sqrt{q^2}$ for $q^2 \gg r^2$. In the case of the up quark loop, we have a region where $q^2 \gg m_{u\bar{u}}^2$ and $q^2 \lesssim m_{c\bar{c}}^2$ are satisfied, and thus, this OPE is valid below the charm quark resonances [122].

Notice that Reference [125] uses as a transition point from QCDF to OPE the value $q^2 \approx 15\,\mathrm{GeV}^2 \gtrsim m_{c\bar{c}}^2$. This estimate is only based on the dimension-5 power corrections. However, these contributions enter in a suppressed way, and thus, we expect the expansion to be still valid below $15\,\mathrm{GeV}^2$. For this reason we include the error estimate based on dimensional analysis explicitly in the formulae to quantify the error of the OPE since we want to apply it for q^2 as small as possible.

For this, we briefly discuss the terms entering for $r^2 \neq 0$ before turning to the dominant dimension-6 contribution. Beside the interaction of soft gluons with the spectator cloud, the contributions from hard-collinear gluons might be important. This is because for the decay into a light meson the momentum configuration where each of both valence quarks carries half of the momentum is preferred. This can be explicitly seen by inspecting the light-cone distribution amplitudes of light mesons. If we parametrise the kinematics as

$$p_B = \left(m_B, \vec{0}\right)^T, \qquad p_P = (E_P, -\vec{p}_{\mathrm{cm}})^T \approx p_{\mathrm{cm}}n_-, \qquad q = (E_q, \vec{p}_{\mathrm{cm}})^T, \tag{3.16}$$

with

$$p_{\rm cm} = \frac{m_B^2 + m_P^2 - q^2}{2m_B} \approx \frac{m_B^2 - q^2}{2m_B}, \qquad\qquad n_- = (1,0,0,-1)^T, \qquad (3.17)$$

the hard-collinear gluon then carries

$$r \sim \frac{p_{\rm cm}}{2}n_-, \qquad\qquad r^2 \sim \frac{p_{\rm cm}}{2}\Lambda_{\rm QCD}. \qquad (3.18)$$

Compared to the contribution coming from the next order in $1/q^2$ for $r^2 = 0$ which scales as $q \cdot r \sim m_B p_{\rm cm}/2$[1] for this momentum configuration, the hard-collinear gluon contribution is relatively suppressed by $\Lambda_{\rm QCD}/m_B$. The error due to these higher order terms is now estimated by explicitly expanding the left diagram in Figure 3.2. The dominant terms in the expansion are summed coherently since the matrix elements are unknown. The matrix elements are then replaced by the values obtained by dimensional analysis as just discussed. This approach is similar to the one done in Reference [122].

DIMENSION-6   The dominant dimension-6 contribution is given by the weak annihilation operators, see Figure 3.2. Unlike in the transition $b \to sll$, these contributions are not negligible for $B \to \pi$. In the former case the up quark loop can be neglected due to the strong CKM suppression $\alpha|V_{us}^* V_{ub}/(V_{ts}^* V_{tb})|$. However, in the latter case, the large Wilson coefficients C_1 and C_2 enter through the matrix elements of Q_1^u and Q_2^u, respectively. Additionally, these contributions introduce isospin breaking effects through the spectator interaction. The charm quark result [125] can be adapted to the up quark case by adding these missing contributions. At this stage one has to evaluate the matrix elements of four-quark operators. For this we use the same approach as in Reference [125]: Since the recoil E_P of the pseudoscalar P is $\Lambda_{\rm QCD} \ll E_P \ll m_B$, we evaluate the matrix elements to leading order in QCDF which coincides with naive factorisation. This permits the evaluation of the matrix elements in terms of the decay constants f_B and f_P. Of course this introduces an uncertainty, which we parametrise according to dimensional analysis as $\Lambda_{\rm QCD}/E_P$.

Low q^2 Region

To evaluate the matrix element in this region we resort to the QCDF approach. In the low q^2 regime, the large recoil energy of the light meson $E_P \gg \Lambda_{\rm QCD}$ separates the hard scale from the soft gluon interaction, and thus, permits an expansion in $\Lambda_{\rm QCD}/\{E_P, m_b\}$. This translates schematically into the following factorisation formula [117]

$$\langle l^+ l^- P | \mathcal{H}_{\rm eff} | B \rangle = C_P \xi_P + \Phi_B \otimes T_P \otimes \Phi_P + \mathcal{O}\left(\frac{1}{m_b}\right), \qquad (3.19)$$

where Φ_M denotes the light-cone distribution amplitude (LCDA), ξ_P the form factor containing the soft contributions, and $\otimes$ the convolution of the hard scattering kernel T_P with the LCDAs. This hard scattering kernel T_P and the coefficient C_P are perturbatively calculable. The former contains the hard gluon-spectator interaction which compared to high q^2 is now a leading power effect [125]. Both coefficients are usually decomposed into factorisable and non-factorisable contributions. The non-factorisable contributions arise from the insertion of the four-quark operators and chromomagnetic dipole operator. In the large recoil limit, the form factors are related by symmetry relations. Radiative corrections to these relations arise through the factorisable contributions. However, we

---

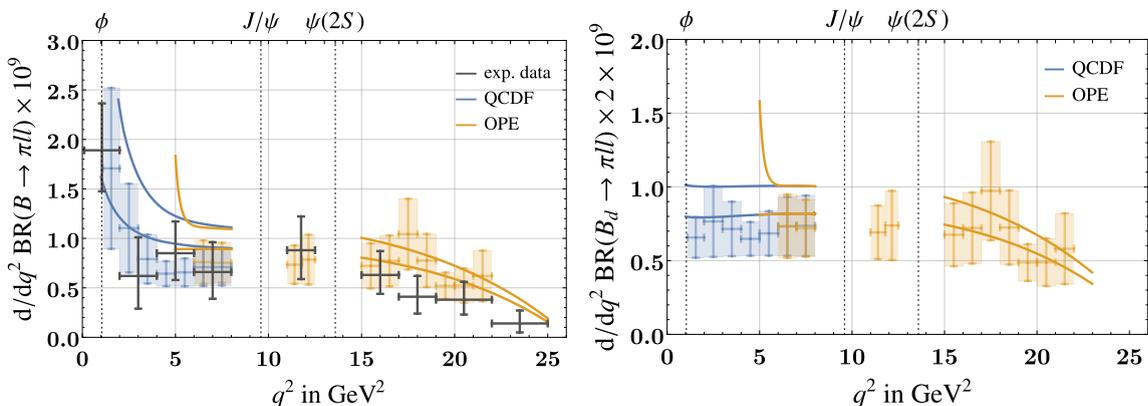[1]The corresponding operator is dimension-6.

Figure 3.3.: Theoretical predictions of the differential branching ratios for the charged (left) and neutral (right) mode, the upper and lower limits of the predictions are shown as solid lines. The OPE is in orange, the bins contain experimental information and are only valid for $l = \mu$, see text. Below the J/ψ resonance, the OPE is combined with QCDF for the charm contribution while blue is based on QCDF for both, the up and charm contribution. The experimental measurements are shown in dark grey.

use the full form factors from LCSR and lattice calculations, and for this reason we drop these factorisable corrections. Therefore we can compactly write

$$\langle P| \mathcal{K}_{H^P}^{\mu} |B\rangle = \langle P| \mathcal{K}_{H^P,3}^{\mu} |B\rangle + \mathcal{I}_P^{(nf)} \,, \tag{3.20}$$

where $\mathcal{I}_P^{(nf)}$ denotes the non-factorisable spectator interactions for the decay into the pseudoscalar meson P. These contributions can be inferred from the decay into longitudinally polarised vector mesons determined in Reference [117]. Note that similarly to the high q^2 case, one has to include the additional weak annihilation contributions from Q_1^u and Q_2^u.

As in the high q^2 region, we estimate the uncertainty by dimensional analysis. Thus we explicitly vary a term of $\mathcal{O}(\Lambda/m_b)$ with a free strong phase, analogously to Reference [133].

Result

Now we are ready to give our predictions for the hadronic $b \to dll$ transitions. The input parameters are listed in Appendix C. We consider the decay of B mesons into charged and neutral pions, as well as into neutral kaons. Before discussing the results, we briefly comment on the experimental perspective. As afore-mentioned the decay into the charged pion has already been observed at the LHCb, and further measurements are planned allowing for a precision better than 2 % for the full 300 fb^{-1} dataset [114]. On the other hand the decay into neutral pions can be well measured at Belle II since the photons from the neutral pion decay can be efficiently reconstructed due to the clean environment. The decay into neutral kaons with a $b \to dll$ transition, however, requires a B_s meson, and unless Belle II runs at the $\Upsilon(5S)$ resonance, it can only be measured at LHCb. Moreover, B_s mesons oscillate much faster than B_d mesons, and thus, LHCb profits from the highly boosted B mesons in CP asymmetry measurements.

Now we turn to the theoretical predictions. The differential branching ratio for $B \to Pll$ processes reads [125, 134]

$$\frac{\mathrm{d}}{\mathrm{d}q^2}\mathrm{BR}(B \to Pll) = \tau_B \frac{G_F^2 \alpha^2}{1536\pi^5 m_B^3 S_P}|V_{ts}^* V_{tb}|^2 \lambda^{3/2}(m_B^2, m_P^2, q^2) f_+^{BP}(q^2)$$
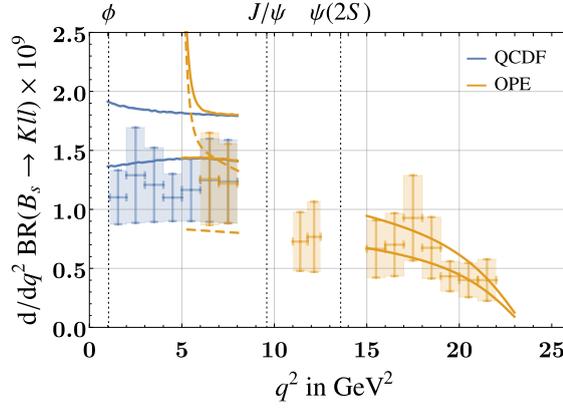
Figure 3.4.: Theoretical predictions of the differential branching ratios, the upper and lower limits of the predictions are shown as solid lines. The OPE is in orange, the bins contain experimental information and are only valid for $l = \mu$, see text. Below the J/ψ resonance, the OPE is combined with QCDF for the charm contribution while blue is based on QCDF for both, the up and charm contribution. The dashed line uses the lattice form factors below the J/ψ resonance, see text.

$$\times \left[\left| C_9 + \Delta C_9 + \frac{2m_b}{m_B + m_P} C_7 \frac{f_T^{BP}(q^2)}{f_+^{BP}(q^2)} \right|^2 + |C_{10}|^2 \right] , \qquad (3.21)$$

for $m_l^2/q^2 \approx 0$, $S_P = 2$ for neutral pions and $S_P = 1$ otherwise, with the B meson lifetime τ_B, and with

$$\Delta C_9 \left(p^\mu - \frac{p \cdot q}{q^2} q^\mu \right) = \frac{\lambda_u/\lambda_t \langle P(p)| \mathcal{K}_{H^u}^\mu |B(p+q)\rangle + \lambda_c/\lambda_t \langle P(p)| \mathcal{K}_{H^c}^\mu |B(p+q)\rangle}{2 f_+^{BP}(q^2)}$$

$$= (\Delta C_{9,u} + \Delta C_{9,c}) \left(p^\mu - \frac{p \cdot q}{q^2} q^\mu \right) ,$$

$$\lambda(m_B^2, m_P^2, q^2) = m_B^4 + m_P^4 + q^4 - 2(m_B^2 m_P^2 + m_B^2 q^2 + m_P^2 q^2) . \qquad (3.22)$$

We vary all input parameters within their quoted errors, cf. Appendix C. We do not add theoretical uncertainties, cf. Appendix D, in quadrature since they are not of statistical nature. The renormalisation scale is varied between 2.5 GeV and 10 GeV. The breakdown of the total uncertainty is shown in Appendix D. From now on, all branching ratios we refer to are CP averaged. The results are shown in Figure 3.3 and 3.4.

Above the J/ψ resonance, an OPE for the up and charm quark loop is performed. In this region, the most precise form factors come from the latest lattice calculations [126, 135–137]. Only the tensor form factor $f_T^{B_s K}$ is not available, for which we therefore use the latest result of a LCSR calculation [138]. For the vector form factor $f_+^{B\pi}$, we make use of the more precise result from a combined fit of LCSR, lattice and experimental data [139].

In the low q^2 region, $m_\phi^2 < q^2 \lesssim m_{J/\psi}^2$, we perform a QCDF for the up and charm quark contributions and use the form factors from the LCSR calculation [138]. These are the most precise results for the low q^2 region except for the vector form factors of $B_s \to K$ and $B \to \pi$. For $f_+^{B\pi}$, we use again the combined fit [139]. For $B_s \to Kll$ in the region $6 \, \text{GeV}^2 \lesssim q^2 \lesssim m_{J/\psi}^2$, the lattice calculation yields for $f_+^{B_s K}$ similar uncertainties but the results are not compatible within the error bands, cf. Reference [138]. Thus, in this
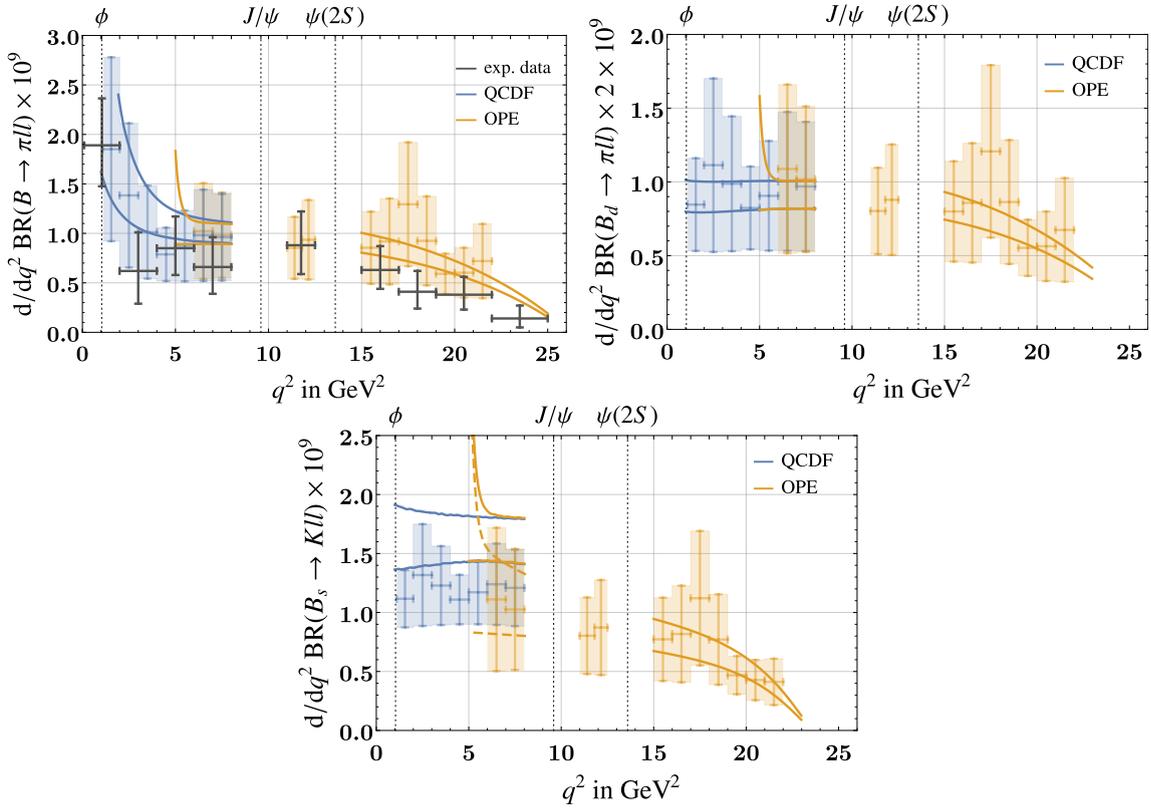
Figure 3.5.: As in Figure 3.3 and 3.4 but with the extraction of the charm contribution after absorbing the form factor dependence into $\Delta C_{9,c}$.

transition region, we use both form factors for the decay $B_s \to K$, see Figure 3.4, and we also apply an OPE for the up quark contribution and a QCDF for the charm quark contribution for all hadronic transition we are considering.

Further, the bins in Figures 3.3–3.5 contain the charm contribution as extracted from the experimental measurements of $B \to K\mu^+\mu^-$ [140]. Since we can extract only the absolute value of this contribution, we vary the strong phase which enters in the interference of the charm and up contributions. This might introduce a large uncertainty, however, this is reduced by CP averaging the branching ratios. Furthermore, this enables a prediction between the charm resonances. To extract this contribution, one has to perform the q^2 integration since the experimental measurements are binned. For this we discretise the q^2 dependence in $\Delta C_{9,c}$ as

$$\Delta C_{9,c}(q^2) = \sum_i \Delta C_{9,c}^i \, \theta \left(q^2 - q_i^2 \right) \theta \left(q_{i+1}^2 - q^2 \right) , \tag{3.23}$$

with $|q_{i+1}^2 - q_i^2| = 1 \, \text{GeV}^2$ outside the charm resonances, and $|q_{i+1}^2 - q_i^2| < 1 \, \text{GeV}^2$ between the charm resonances. Lastly, for the decay of the charged B meson, we overlay the available experimental data, see Figure 3.3 left. Additionally, one can extract the charm contribution $\Delta C_{9,c}$ after absorbing the form factor dependence into $\Delta C_{9,c}$. The result is then independent of the form factors entering in the matrix element of H^c. However, this introduces an additional uncertainty of $\mathcal{O}(30 \, \%)$ due to $SU(3)_F$ breaking. This is large compared to Equation (3.23), where the additional uncertainty is $f_T/f_+ \sim \mathcal{O}(\Lambda_{\text{QCD}}/m_B)$ [141] assuming that the charm contribution can be calculated according to Section 3.1, which is questionable for q^2 close to the charm resonances. Moreover, this reduces the correlation

Table 3.1.: Theoretical predictions of the branching ratios $BR(B \to Pll)$. The error inside the parentheses comes only from the uncertainties of the CKM matrix, while the first error includes all uncertainties.

decay	$[1,6]\,\mathrm{GeV}^2$	$[17,22]\,\mathrm{GeV}^2$
$BR(B \to \pi ll) \times 10^9$	$6.63^{+2.43}_{-1.36}\,(0.32)$	$5.05^{+1.00}_{-0.74}\,(0.32)$
$BR(B_d \to \pi ll) \times 10^9$	$4.47^{+0.78}_{-0.67}\,(0.28)$	$4.69^{+0.94}_{-0.69}\,(0.30)$
$BR(B_s \to Kll) \times 10^9$	$8.03^{+1.63}_{-1.38}\,(0.51)$	$4.20^{+1.12}_{-0.83}\,(0.27)$

Table 3.2.: Theoretical predictions of $BR(B \to P\mu^+\mu^-)$ with experimental input from $BR(B \to K\mu^+\mu^-)$. The error inside the parentheses comes only from the uncertainties of the CKM matrix, while the first error includes all uncertainties.

decay	$[11,11.8]\,\mathrm{GeV}^2$	$[11.8,12.5]\,\mathrm{GeV}^2$
$BR(B \to \pi\mu^+\mu^-) \times 10^9$	$5.86 \pm 1.81\,(0.30)$	$5.48 \pm 1.97\,(0.31)$
$BR(B_d \to \pi\mu^+\mu^-) \times 10^9$	$5.52 \pm 1.69\,(0.30)$	$5.15 \pm 1.85\,(0.30)$
$BR(B_s \to K\mu^+\mu^-) \times 10^9$	$5.83 \pm 2.24\,(0.33)$	$5.37 \pm 2.29\,(0.31)$

between all parameters yielding overall larger uncertainties on the extracted values, see Figure 3.5 in the $SU(3)_F$-limit.

Finally, the theory-only predictions are given in Table 3.1 while the predictions between the charm resonances with experimental input are given in Table 3.2. Note that the $SU(3)_F$ method applied for the latter leads to the predictions in Table 3.2 if the New Physics entering $B \to Kll$ is minimally flavour violating.

Next, we take a look at the CP asymmetries.

3.2. New Physics: CP Asymmetries

In this section, we consider the effect of New Physics on the transition $b \to dll$. This is done in a model-independent way, that is we parametrise the New Physics in terms of the complex Wilson coefficient C_9^{NP}

$$\frac{\mathrm{d}}{\mathrm{d}q^2}BR(B \to Pll) \propto \left| \tilde{C}_9 + \Delta C_9 + C_9^{\mathrm{NP}} \right|^2 + |C_{10}|^2 \,, \tag{3.24}$$

with $\tilde{C}_9 = C_9 + 2m_b/(m_B + m_P)C_7 f_T^{BP}/f_+^{BP}$. First, we briefly discuss the direct CP asymmetries after which we turn to the mixing-induced CP violation.

Direct CP Asymmetry

The direct CP violation in the decay $B \to Pll$ is given by

$$a_{CP}^{\mathrm{dir}}(q^2) = \frac{\frac{\mathrm{d}}{\mathrm{d}q^2}BR(B \to Pll) - \frac{\mathrm{d}}{\mathrm{d}q^2}BR(\overline{B} \to \overline{P}ll)}{\frac{\mathrm{d}}{\mathrm{d}q^2}BR(B \to Pll) + \frac{\mathrm{d}}{\mathrm{d}q^2}BR(\overline{B} \to \overline{P}ll)}\,, \tag{3.25}$$
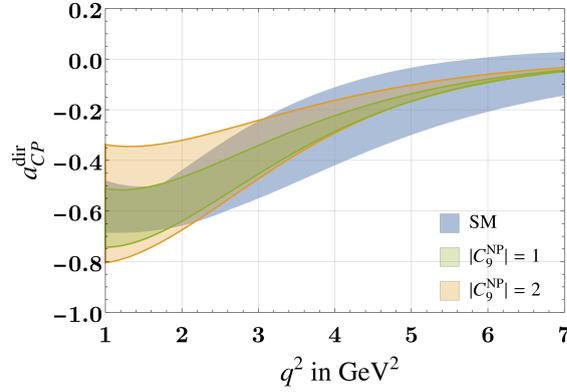
Figure 3.6.: Direct *CP* violation in the Standard Model and beyond. To obtain the New Physics prediction for a_{CP}^{dir}, we use only the central values of all parameters, i.e. no variation of input parameters is performed.

and thus

$$a_{CP}^{\mathrm{dir}} = \frac{2r_q \sin\delta_q \left(\mathrm{Im}(C_9^{\mathrm{NP}})\cos\phi_q - [\tilde{C}_9 + \mathrm{Re}(C_9^{\mathrm{NP}})]\sin\phi_q\right)}{|\tilde{C}_9 + C_9^{\mathrm{NP}}|^2 + r_q^2 + 2r_q \cos\delta_q([\tilde{C}_9 + \mathrm{Re}(C_9^{\mathrm{NP}})]\cos\phi_q + \mathrm{Im}(C_9^{\mathrm{NP}})\sin\phi_q)}, \qquad (3.26)$$

with $\Delta C_9 = r_q e^{i\delta_q} e^{i\phi_q}$, where δ_q and ϕ_q denote the strong and weak phases, respectively. In the Standard Model a_{CP}^{dir} is very small $a_{CP}^{\mathrm{dir}} \sim 10^{-3}$–$10^{-2}$ in the high q^2 bins, and thus, one might expect the direct CP violation to have a high New Physics sensitivity. However, not only is the uncertainty large but also the amplitude r_q is small in the Standard Model $r_q \ll 1$ for $q^2 \gtrsim 15\,\mathrm{GeV}^2$. Since the New Physics contribution only has weak phases, the Wilson coefficient C_9^{NP} in the numerator of Equation (3.26) interferes just with the strong phase δ_q and amplitude r_q. Hence, the New Physics effect will be suppressed just as the Standard Model contribution, cf. Equation (3.26). This is, however, different in the low q^2 bins where there might be large contributions coming from weak annihilation contributions in the hadronic $B \to \pi$ transition yielding a large strong phase. For this reason, we show the direct CP violation, a_{CP}^{dir}, together with the effect of New Physics in Figure 3.6 and Figure 3.7. And indeed, the low q^2 bins are sensitive to New Physics. Interestingly, for large Wilson coefficients $|C_9^{\mathrm{NP}}| > 1$, the preferred value for the direct CP asymmetry lies outside the range of the Standard Model prediction. Now we turn our attention to the mixing-induced CP violation.

Mixing-Induced CP Asymmetry

Mixing-induced CP violation is present in the decays of the neutral B mesons. Since here all final state mesons P are CP eigenstates, we can write the time-dependent CP asymmetry as [142]

$$\begin{aligned} a_{CP}(t) &= \frac{\Gamma(\overline{B}_q(t) \to P) - \Gamma(B_q(t) \to P)}{\Gamma(\overline{B}_q(t) \to P) + \Gamma(B_q(t) \to P)} \\ &= -\frac{A_{CP}^{\mathrm{dir}}\cos(\Delta M t) + A_{CP}^{\mathrm{mix}}\sin(\Delta M t)}{\cosh(\Delta\Gamma t/2) + A_{\Delta\Gamma}\sinh(\Delta\Gamma t/2)} + \mathcal{O}\left(1 - \left|\frac{q}{p}\right|^2\right), \qquad (3.27) \end{aligned}$$
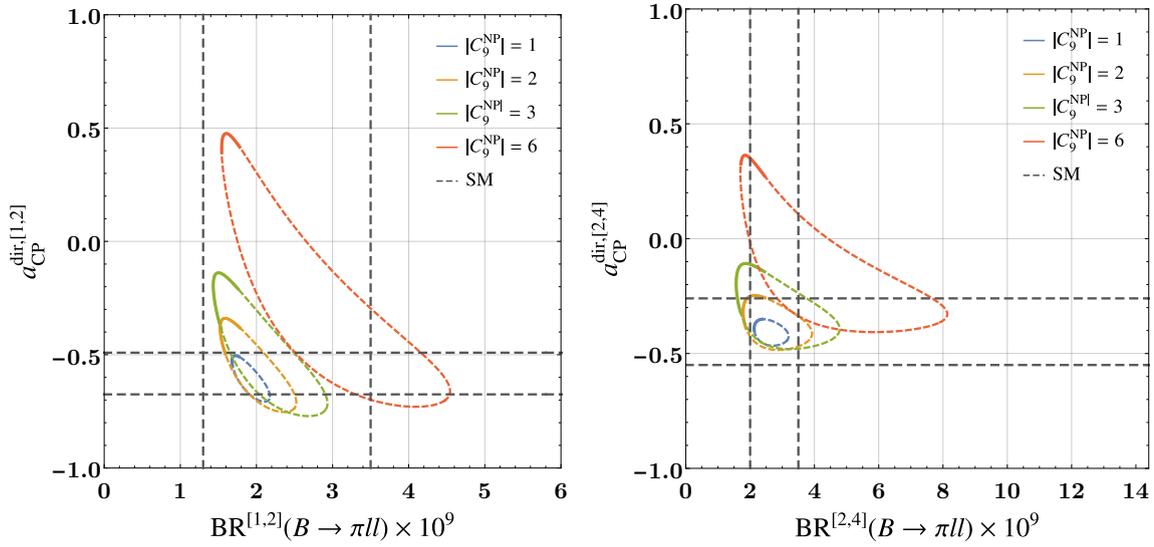
Figure 3.7.: Direct CP violation in the low q^2 bins for different values of $|C_9^{\text{NP}}|$. The range of the Standard Model prediction is dashed in gray. The solid lines show New Physics contributions as favoured by the measurement of $\text{BR}(B \to \pi ll)$ in the bins $[1,6]\,\text{GeV}^2$ and $[17,22]\,\text{GeV}^2$ at $1\,\sigma$. For the predictions in the bin $[2,4]\,\text{GeV}^2$, the x-axis covers the $2\,\sigma$ range of the corresponding experimental measurement.
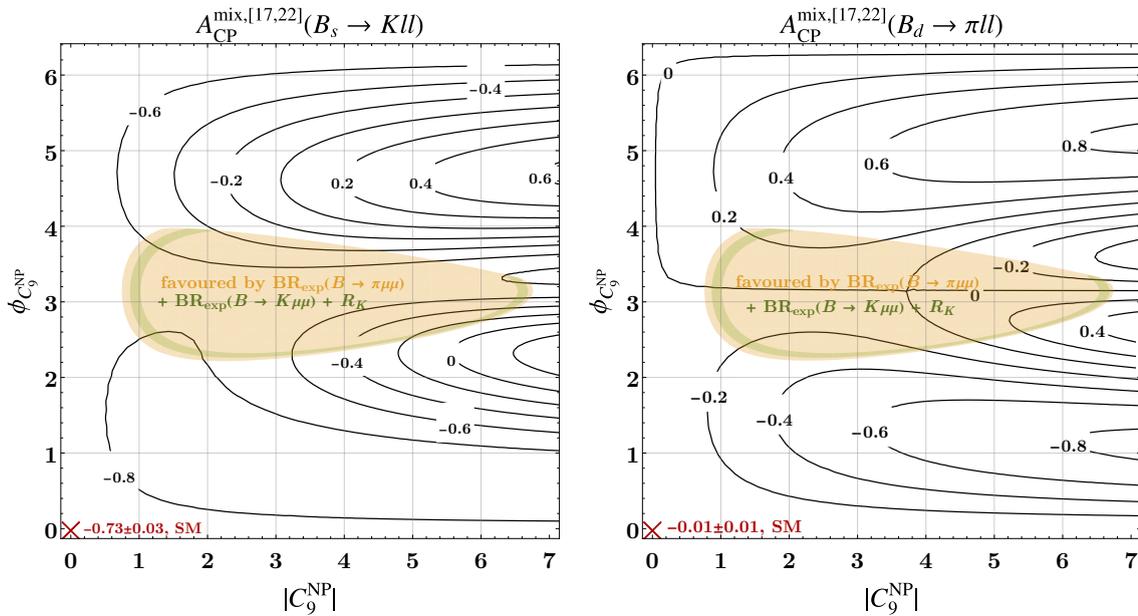
Figure 3.8.: Mixing-induced CP violation for $B_s \to Kll$ (left) and $B_d \to \pi ll$ (right). The coloured regions are favoured for $l = \mu$ by $\text{BR}(B \to \pi \mu^+ \mu^-)$ only (orange) and by the combination with the corresponding decay in kaons and R_K (green) at $1\,\sigma$.

where Γ denotes the partial decay width, and ΔM and $\Delta \Gamma$ denote the mass and width difference, respectively. Further

$$A_{CP}^{\text{dir}} = \frac{1 - |\lambda_P|^2}{1 + |\lambda_P|^2}, \qquad A_{CP}^{\text{mix}} = -\frac{2\,\text{Im}\,(\lambda_P)}{1 + |\lambda_P|^2}, \qquad A_{\Delta\Gamma} = -\frac{2\,\text{Re}\,(\lambda_P)}{1 + |\lambda_P|^2}, \qquad (3.28)$$

where the interference is encoded in the variable [142]

$$\lambda_P = \frac{q}{p} \frac{A(\overline{B}_q \to P)}{A(B_q \to P)},$$
(3.29)

with the amplitude $A(B_q \to P)$, and the B_q meson mixing parameters p and q. The effects of New Physics on the mixing-induced CP violation A_{CP}^{mix} are shown in Figure 3.8. The plots in the high and low q^2 region differ just slightly, so we only show the ones in the high q^2 region. We overlay the contours with the regions favoured by the experimental measurements of $\mathrm{BR}(B \to \pi\mu^+\mu^-)$ [112], $\mathrm{BR}(B \to K\mu^+\mu^-)$ [140], and R_K [2] at 1σ. Of course the New Physics contribution entering $B \to K\mu^+\mu^-$ couples to the strange quarks, and thus, does not have to be the same as in the transition $b \to dll$ that we are considering. For this reason, we show both regions separately. Compared to the direct CP asymmetry, even smaller New Physics contributions to the Wilson coefficients $|C_9^{\mathrm{NP}}| < 1$ have measurable effects on the mixing-induced CP violation.

CHAPTER 4

Conclusion

We have first discussed the *R*-parity conserving MSSM with non-holomorphic couplings in context of the $b \rightarrow sll$ anomalies. This framework allows us to generate the lepton and down-type quark masses radiatively in the limit where only the up-type Higgs doublet has a non-vanishing vev. This renders the lepton and down-type quark Yukawa couplings into nearly free parameters bounded by perturbativity. Large Yukawa couplings together with non-holomorphic couplings make the radiative generation of the masses possible while permitting large contributions to the anomalous $b \rightarrow sll$ processes through higgsino box diagrams. Taking into account experimental and theoretical constraints, we have shown that a parameter space exists that resolves the tensions in the $b \rightarrow sll$ transition. This has been shown explicitly for $R_{K^{(*)}}$ and implicitly for the other anomalous measurements with the help of the global fit results. As a by-product the long-standing deviation in $(g - 2)_\mu$ is resolved. The hierarchy between the muon and tau mass, which have to be generated radiatively in our framework, implies together with the experimental and theoretical constraints a distinctive phenomenology in collider and flavour physics. In particular the sub-TeV sleptons and an $\mathcal{O}(1)$ enhancement and suppression in the transitions $b \rightarrow s\tau\tau$ and $B_s \rightarrow \tau\tau$, respectively, compared to the final states with muons stand out. Interestingly, one additionally needs $\text{sign}(y_\tau y_\mu) = -1$ in order to generate the respective lepton masses while complying with theoretical and experimental constraints.

Furthermore, we have analysed the hadronic transition $B \rightarrow Pll$ with pseudoscalar final states P within and beyond the Standard Model. The branching ratio was calculated by combining different approaches and utilising experimental information. In particular the latter allows for a prediction of the branching ratio between the charm resonances. Finally, the effect of New Physics in terms of a complex Wilson coefficient C_9^{NP} has been analysed in context of the CP asymmetries. In particular the mixing-induced CP is sensitive to smaller New Physics contributions compared to the direct CP violation. The latter only shows a New Physics sensitivity in the low q^2 bins.

Excluding Spontaneous CP Violation with Searches for Charged Higgs Bosons

In this part, we first analyse the most general two-Higgs-doublet model with spontaneous CP violation in Chapter 5. We summarise the model, and determine upper limits on the masses of the heavy Higgs bosons which is made possible through the absence of a decoupling limit. Further, we derive a remarkable sum rule using only experimentally strongly motivated assumptions. The consequences of this sum rule on collider searches are then discussed in Chapter 6. Finally, this part is concluded in Chapter 7.

General Two-Higgs-Doublet Model with Spontaneous CP Violation

This chapter is based on Reference [143].

In the Standard Model CP violation manifests itself through complex Yukawa couplings. Here three fermion generations ensure that one complex phase in the Yukawa sector remains physical. This so-called Kobayashi–Maskawa (KM) mechanism was first proposed in Reference [144] to explain the observed CP violation in the weak interaction and served as a prediction for a third fermion generation. While in this approach CP is broken explicitly by the complex Yukawa couplings, another paper [145] showed soon after that the introduction of a second scalar doublet allows for a spontaneous breaking of CP. Even though a third fermion generation was observed and the KM mechanism is now firmly established, it does not rule out that CP might still be broken spontaneously.

The prime objective of this work is to pave the way for excluding spontaneous CP violation. This is possible, due to two main reasons: Firstly, the additional Higgs fields do not decouple in a spontaneous CP violating scenario. This has also been observed in Reference [146], however, this reference is predated by our previous work in Reference [1]. This non-decoupling behaviour will be briefly reiterated below. Similar non-decoupling scenarios have been observed in the context of a minimal left-right symmetric model [147], and in models based on the Gildener-Weinberg mechanism of scale symmetry [148, 149]. Secondly, flavour violation beyond the one present in the Standard Model has to exist in order to induce a physical KM phase. The main difficulty of this work is the huge parameter space. This is why previous analyses in the literature have only studied special simplified cases of the 2HDM as for example in References [150, 151]. And indeed, this question is already tackled in Reference [1], however, there only a benchmark scenario has been studied which naively is least constrained by flavour and CP violating observables. This is achieved by fixing all but one of the free complex phases. The main result of that study is that with current collider and precision observables spontaneous CP violation is still allowed!

We go beyond Reference [1] by analysing the most general case, and determining new upper limits on the Higgs masses by requiring perturbative unitarity at next-to-leading order (NLO). This is done in Section 5.1. Next, in Section 5.2, we provide a clear path on excluding or verifying spontaneous CP violation as the primary source of CP violation, which is made possible through a remarkable sum rule for the charged-Higgs couplings to bottom quarks.

5.1. Higgs and Yukawa Sector

First we review the model and briefly discuss general features of the Higgs and Yukawa sectors. Since no decoupling of the additional Higgs fields is possible—as it is shown below—their masses are fixed by the quartic couplings in the scalar potential, and thus, we determine stringent upper bounds on these masses by demanding NLO perturbative unitarity as defined below.

Higgs Sector

The most general renormalisable scalar potential with two Higgs doublets $\phi_i = (\phi^0, \phi_i^+)^T$, $i = 1, 2$ reads [152]

$$
\begin{aligned}
V = {} & m_{11}^2 \phi_1^\dagger \phi_1 + m_{22}^2 \phi_2^\dagger \phi_2 - (m_{12}^2 \phi_1^\dagger \phi_2 + \text{h.c.}) \\
& + \frac{\lambda_1}{2} (\phi_1^\dagger \phi_1)^2 + \frac{\lambda_2}{2} (\phi_2^\dagger \phi_2)^2 + \lambda_3 (\phi_1^\dagger \phi_1)(\phi_2^\dagger \phi_2) + \lambda_4 (\phi_1^\dagger \phi_2)(\phi_2^\dagger \phi_1) \\
& + \left[\phi_1^\dagger \phi_2 \left(\frac{\lambda_5}{2} \phi_1^\dagger \phi_2 + \lambda_6 (\phi_1^\dagger \phi_1) + \lambda_7 (\phi_2^\dagger \phi_2) \right) + \text{h.c.} \right] ,
\end{aligned} \tag{5.1}
$$

where in the CP *conserving* case all parameters are real given that the canonical CP transformation rules $CP\phi_i(x^\mu) = \phi_i^*(x^\mu)$ are adopted. In order to spontaneously break CP, the parameters in Equation (5.1) have to be chosen in such a way that the potential develops a minimum for

$$
\langle \phi_1 \rangle = \begin{pmatrix} 0 \\ vc_\beta \end{pmatrix} , \qquad\qquad \langle \phi_2 \rangle = \begin{pmatrix} 0 \\ vs_\beta e^{i\xi} \end{pmatrix} , \tag{5.2}
$$

with the vev $v = 174\,\text{GeV}$ and the complex phase ξ. Note that in this case the minimum is already the global one [153]. Moreover, one has to assure that the potential (5.1) is bounded from below. For a detailed discussion see Reference [152] and in particular Reference [1], here we focus only on the main features of spontaneous CP violation. As usual one can solve the vacuum conditions for the mass parameters m_{ij}^2 in terms of the vevs. In case of spontaneous CP violation one has three minimisation conditions:

$$
\text{Re}\left(\left. \frac{\partial V}{\partial \phi_1} \right|_{\phi_i = \langle \phi_i \rangle} \right) = 0 , \quad \text{Im}\left(\left. \frac{\partial V}{\partial \phi_1} \right|_{\phi_i = \langle \phi_i \rangle} \right) = 0 , \quad \text{Re}\left(\left. \frac{\partial V}{\partial \phi_2} \right|_{\phi_i = \langle \phi_i \rangle} \right) = 0 . \tag{5.3}
$$

Note that the imaginary part of $\partial V / \partial \phi_2$ does not yield an additional minimisation condition. This condition is linearly dependent on the ones in Equation (5.3) since we only have three independent parameters, v, β, and ξ. As a result, one can write all three mass parameters m_{11}^2, m_{22}^2, and m_{12}^2 as a function of v, β, and ξ. Hence, no free mass parameters are left, and thus, *all* Higgs masses are fixed to be around the electroweak scale. We stress, that even in the limit of a vanishing CP violating phase $\xi \to 0$ the Higgs fields do not decouple. The limit $\xi \to 0$ does not yield the general CP conserving case. The transition from CP violation to CP conservation is discontinuous since the latter involves one vacuum condition less; conversely the presence of the tiniest CP violating phase ξ immediately fixes all mass parameters to be of $\mathcal{O}(v^2)$.

Changing to the Higgs basis

$$
\begin{pmatrix} \Phi_1 \\ \Phi_2 \end{pmatrix} = \begin{pmatrix} c_\beta & s_\beta \\ -s_\beta & c_\beta \end{pmatrix} \begin{pmatrix} \phi_1 \\ \phi_2 \end{pmatrix} , \tag{5.4}
$$

directly yields the charged Higgs boson mass [1]

$$m_{H^\pm} = v\sqrt{\lambda_5 - \lambda_4}\,,\tag{5.5}$$

and the sum of the neutral Higgs masses [1]

$$\frac{1}{2v^2}\sum_{i=1}^{3} m^2_{H_i^0} = s_{2\beta}c_\xi\,(\lambda_6 + \lambda_7) + \lambda_2 s_\beta^2 + \lambda_1 c_\beta^2 + \lambda_5\,,\tag{5.6}$$

where the non-decoupling is apparent. Requiring unitarity for the $2 \to 2$ scalar scattering matrix $S^\dagger S = \mathbb{1}$, one now obtains inequalities which have to be satisfied by the quartic couplings. This translates into upper limits on the very same couplings which in turn yields upper bounds for the Higgs masses. Moreover, requiring the NLO contribution to be smaller than the leading order one, i.e. convergence of the perturbative series, strengthens these bounds further. For the combination of those two constraints, we use the term *perturbative unitarity*. Note that this is not always done in the literature, and both terms are often used interchangeably. The unitarity bounds at NLO for renormalisable scalar sectors can be found in Reference [154] while the required β-functions can be found in Reference [152]. In our case this translates into the following upper bounds on the masses of the Higgs fields

$$m_{H^\pm} \lesssim 445\,\text{GeV}\,,\quad m_{H_2^0} \lesssim 545\,\text{GeV}\,,\quad m_{H_3^0} \lesssim 570\,\text{GeV}\,,\quad \sum_{i=1}^{3} m_{H_i^0} \lesssim 1.1\,\text{TeV}\,.\tag{5.7}$$

The correlation of the heavy neutral Higgs bosons, assuming the lightest field H_1^0 to be Standard Model like, is shown in Figure 5.1. Inspecting the determinant of the neutral Higgs mass matrix M_H^2

$$\det M_H^2 = m^2_{H_1^0}\,m^2_{H_2^0}\,m^2_{H_3^0} \propto s_\xi\,s_{2\beta}^2\,,\tag{5.8}$$

it is apparent that identifying the lightest Higgs boson with the Standard Model Higgs field also yields, together with the upper limits on the Higgs masses, an allowed region for the vacuum phases β and ξ, see Figure 5.1

$$0.22 \lesssim \tan\beta \lesssim 4.5\,,\qquad\qquad |\sin\xi| \gtrsim 0.42\,.\tag{5.9}$$

Finally, the neutral Higgs mass basis is defined by

$$O^T M_H^2 O = \text{diag}\left(m_{H_1^0}, m_{H_2^0}, m_{H_3^0}\right)\,,\tag{5.10}$$

with the orthogonal matrix O.

Yukawa Sector

The quark Yukawa Lagrangian reads

$$\mathcal{L}_\text{yuk} = -\overline{Q}_L\left(Y_{u1}\tilde\phi_1 + Y_{u2}\tilde\phi_2\right) u_R - \overline{Q}_L\left(Y_{d1}\phi_1 + Y_{d2}\phi_2\right) d_R + \text{h.c.}\,,\tag{5.11}$$

with $\tilde\phi_i = \epsilon_{ij}\phi_j^*$ where $\epsilon_{12} = 1$. We work in a basis where the 3×3 Yukawa matrices Y_{qi} are real without loss of generality since CP is broken spontaneously. Thus, after electroweak symmetry breaking the quark mass matrices are given by

$$\frac{M_u}{v} = Y_{u1}c_\beta + Y_{u2}e^{-i\xi}s_\beta\,,\qquad\qquad \frac{M_d}{v} = Y_{d1}c_\beta + Y_{d2}e^{i\xi}s_\beta\,.\tag{5.12}$$
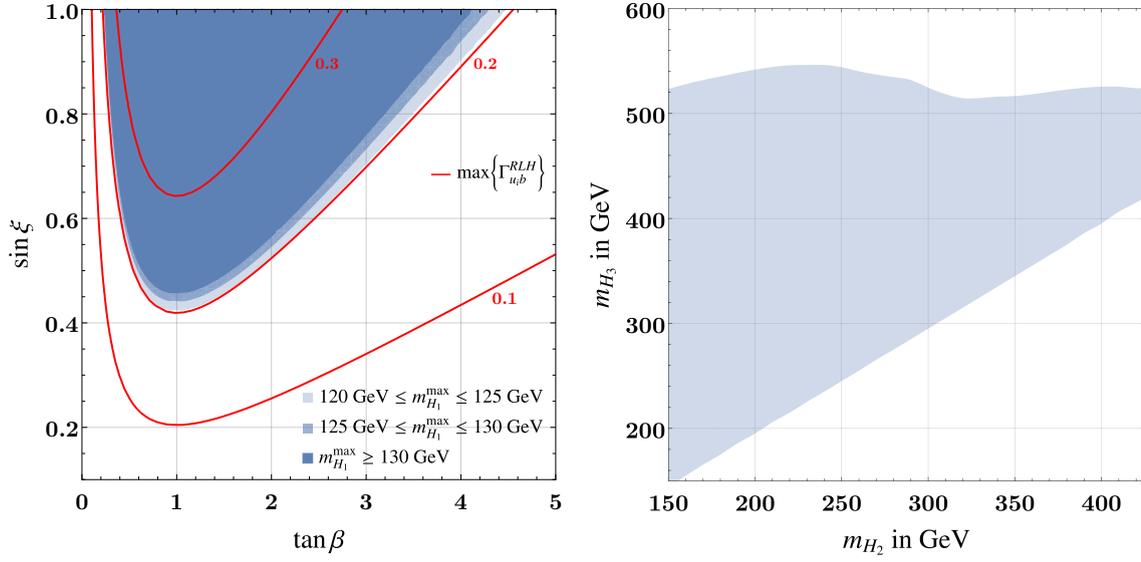
Figure 5.1.: *Left*: Allowed region on the $\tan\beta$–$\sin\xi$ plane where the maximal possible
value for the lightest Higgs mass is shown in different shades blue. In red we
show contours of the lower bound on the largest charged-Higgs coupling to
bottom quarks.
Right: Allowed region on the heavy Higgs mass plane as allowed by NLO
perturbative unitarity assuming a lightest Higgs field with mass $120\,\text{GeV} <
m_{H_1} < 130\,\text{GeV}$.

As discussed in Reference [1], the KM phase can only be induced if the CP violating
vacuum phase ξ remains physical, in other words the Yukawa matrices of either the down
or up quark sector must not be diagonal in the same flavour basis. Thus, not only are the
Higgs masses bounded from above but also there has to be additional flavour violation
at tree-level. Hence, neither a decoupling limit nor a limit where the flavour violation is
aligned to the Standard Model exist. Since flavour violating couplings in the down sector
are strongly constrained by experiment, we work with down quark Yukawa matrices Y_{di}
that are diagonal in the same flavour basis, i.e. no flavour changing neutral currents at
tree-level in the down quark sector.[1] In this case the down quark mass matrix is obtained
through a singular value decomposition with an orthogonal left-handed rotation V_{dL} and
a diagonal phase matrix times an orthogonal right-handed rotation PV_{dR}. Extending V_{dL}
to be an $SU(2)_L$ invariant transformation it can be absorbed into the real Yukawa matrices
Y_{ui}. Thus, the up-type quark mass matrix is diagonalised by $M_u = V^\dagger m_u^{\text{diag}} V_R^\dagger$ with the
CKM matrix V and a free unitary matrix V_R. Finally, the charged-Higgs couplings to the
quarks read

$$\mathcal{L}_{\text{H}} \supset \overline{d}_{L,i} H^- \Gamma^{LRH}_{d_i u_j} u_{R,j} + \overline{u}_{L,i} H^+ \Gamma^{LRH}_{u_i d_j} d_{R,j} + \text{h.c.} , \tag{5.13}$$

with

$$\Gamma^{LRH}_{d_i u_j} = V^*_{ki} \left[\delta_{kj} c_\beta - \frac{\tilde{\epsilon}^u_{kj}}{c_\beta} \right] \frac{m_{u_j}}{v s_\beta} \qquad\qquad \Gamma^{LRH}_{u_i d_j} = V_{ik} \left[\delta_{kj} s_\beta - \frac{\tilde{\epsilon}^d_{kj}}{s_\beta} \right] \frac{m_{d_j}}{v c_\beta} ,$$

$$\tilde{\epsilon}^u_{ij} = (V Y_{u1} V_R)_{ij} \frac{v c_\beta}{m_{u_j}} , \qquad\qquad\qquad \tilde{\epsilon}^d_{ij} = (V^\dagger_{dL} Y_{d2} e^{i\xi} P V_{dR})_{ij} \frac{v s_\beta}{m_{d_j}} , \tag{5.14}$$

---

[1]Note this choice is only broken by tiny radiative corrections $\delta Y_2 \propto Y_{u1} Y^T_{u2} Y_{d1} / (16\pi^2)$.

Notice that $\tilde{\epsilon}^d$ is a diagonal matrix as afore-mentioned. Further, one can solve for Y_{u1} using Equation (5.12)

$$Y_{u1} = \frac{1}{vc_\beta} \left(\mathrm{Re} + \frac{c_\xi}{s_\xi}\mathrm{Im} \right) \left[V^\dagger m_u^{\mathrm{diag}} V_R^\dagger \right] , \qquad (5.15)$$

which yields

$$\tilde{\epsilon}^u_{ij} = \frac{t_\xi - i}{2\, t_\xi}\delta_{ij} + \frac{t_\xi + i}{2\, t_\xi} \left(VV^T m_u V_R^T V_R m_u^{-1} \right)_{ij} , \qquad (5.16)$$

with $t_\xi \equiv \tan\xi$. Up until now V denotes the CKM matrix in any phase convention. Since we are working with real Yukawa matrices which are determined as functions of the CKM matrix, the re-phasing freedom of the CKM matrix can yield physically inequivalent sets of real Yukawa matrices. This can be made explicit, for example, by fixing the phases in the CKM matrix V to the standard parametrisation $V \to V_{\mathrm{PDG}}$ in Equation (5.13). In this case one has to replace V by $V \to V_{\mathrm{PDG}}P$ with a free diagonal phase matrix P in Equation (5.16). Altogether the flavour violation in the up sector is fixed by 11 free real parameters, both vacuum phases, the CKM matrix, and the up quark masses. Interestingly, the V_R dependence of flavour violating couplings at tree-level enters only through the symmetric unitary matrix $V_R^T V_R$.

5.2. Charged-Higgs Couplings to Bottom Quarks: Sum Rule

Here we analyse the flavour violating couplings $\tilde{\epsilon}^u$. Inspecting Equation (5.16), the third row of the couplings matrix ϵ^u is given by

$$
\begin{aligned}
\tilde{\epsilon}^u_{33} &= \frac{t_\xi - i}{2\, t_\xi}\delta_{ij} + \frac{t_\xi + i}{2\, t_\xi} \left(V_{\mathrm{PDG}}\tilde{P}V_{\mathrm{PDG}}^T m_u \tilde{V}_R m_u^{-1} \right)_{33} \\
&= \frac{t_\xi - i}{2\, t_\xi} + \frac{t_\xi + i}{2\, t_\xi} \tilde{P}_{33}\tilde{V}_{R,33} + \mathcal{O}\left(V_{\mathrm{PDG},32}^2 \right) , \\
\tilde{\epsilon}^u_{32} &= \frac{t_\xi + i}{2\, t_\xi} \tilde{P}_{33}\tilde{V}_{R,32} \frac{m_t}{m_c} + \mathcal{O}\left(V_{\mathrm{PDG},32}^2 \right) , \\
\tilde{\epsilon}^u_{31} &= \frac{t_\xi + i}{2\, t_\xi} \tilde{P}_{33}\tilde{V}_{R,31} \frac{m_t}{m_u} + \mathcal{O}\left(V_{\mathrm{PDG},32}^2 \right) ,
\end{aligned}
\qquad (5.17)
$$

with the diagonal phase matrix $\tilde{P} = P^2 = PP^T$, and the unitary matrix $\tilde{V}_R = V_R^T V_R$. The contributions of $\mathcal{O}(V_{\mathrm{PDG},32}^2)$ are negligible yielding only a correction of $\lesssim 0.2\,\%$, and thus, we drop them from now on. Plugging the couplings $\tilde{\epsilon}^u_{3i}$ from Equation (5.17) into the vertices $\Gamma_{qq'}^{LRH} = (\Gamma_{q'q}^{RLH})^*$ from Equation (5.14) yields for the charged-Higgs couplings to light quarks

$$\left| \Gamma_{cb}^{RLH} \right|^2 + \left| \Gamma_{ub}^{RLH} \right|^2 = \left(\frac{m_t}{2vs_\beta c_\beta s_\xi} \right)^2 \left(1 - |\tilde{V}_{R,33}|^2 \right) , \qquad (5.18)$$

while the coupling to top and bottom quarks reads

$$\left| \Gamma_{tb}^{RLH} \right|^2 = \left(\frac{m_t}{2vc_\beta s_\beta} \right)^2 \left| 2c_\beta^2 - \frac{t_\xi + i}{t_\xi} - \frac{t_\xi - i}{t_\xi}\tilde{P}_{33}^* \tilde{V}_{R,33}^* \right|^2 . \qquad (5.19)$$

Adding Equation (5.18) and (5.19), one gets

$$\sum_{i=u,c,t} \left| \Gamma_{u_i b}^{RLH} \right|^2 = \left(\frac{m_t}{2 v s_\beta c_\beta t_\xi} \right)^2 \left[1 + \frac{1}{c_\xi^2} + c_{2\beta}^2 t_\xi^2 + 2 \left| \tilde{V}_{R,33} \right| \left(2 s_\phi t_\xi s_\beta^2 - c_\phi (c_{2\beta} t_\xi^2 + 1) \right) \right],$$
(5.20)

with the free parameters $|\tilde{V}_{R,33}| < 1$, and $0 < \phi < 2\pi$. This equation can be rewritten and brought into a more compact form by solving Equation (5.19) for the entry $\tilde{V}_{R,33}$ and re-inserting it into Equation (5.18) or (5.20). Rearranging these terms leads then to:

$$\boxed{\sum_{i=u,c,t} \left| \Gamma_{ib}^{RLH} \right|^2 = \frac{m_t^2}{v^2} + \frac{2m_t}{v s_{2\beta}} \left(c_{2\beta} \mathrm{Re}\, \Gamma_{tb}^{RLH} - \frac{\mathrm{Im}\, \Gamma_{tb}^{RLH}}{t_\xi} \right),}$$
(5.21)

which does not depend on any free parameters except the vacuum phases! Note that this equation follows solely from spontaneous CP violation, and the experimentally strongly motivated assumption of the down quark Yukawa matrices Y_{di} being approximately diagonal in the same flavour basis. Since the right-hand side of Equation (5.21) is constrained by $\mathrm{Re}\left(\Gamma_{tb}^{RLH} \right)^2 + \mathrm{Im}\left(\Gamma_{tb}^{RLH} \right)^2 = \left| \Gamma_{tb}^{RLH} \right|^2$, one can now determine a lower bound on the couplings [143]

$$\max \left\{ \left| \Gamma_{ub}^{RLH} \right|, \left| \Gamma_{cb}^{RLH} \right|, \left| \Gamma_{tb}^{RLH} \right| \right\} \geq \frac{A}{3} \frac{m_t}{v} \left(\sqrt{1 + 3\kappa} - 1 \right),$$
(5.22)

with

$$A = \frac{\sqrt{c_{2\beta}^2 + 1/t_\xi^2}}{s_{2\beta}}, \qquad\qquad \kappa = \frac{s_{2\beta}^2 t_\xi^2}{1 + c_{2\beta}^2 t_\xi^2}.$$
(5.23)

Identifying the lightest Higgs with the Standard Model Higgs field, and requiring NLO perturbative unitarity for the scalar sector yields

$$\max \left\{ \left| \Gamma_{ub}^{RLH} \right|, \left| \Gamma_{cb}^{RLH} \right|, \left| \Gamma_{tb}^{RLH} \right| \right\} \gtrsim 0.2,$$
(5.24)

see Figure 5.1. There we plot the contours of the lower bound of this maximum as a function of $\tan \beta$ and $\sin \xi$ superimposed with the allowed region on the $\tan \beta$–$\sin \xi$ plane as a function of the lightest Higgs mass. Interestingly, the lightest Higgs mass has a similar dependence on the vacuum angles as this lower bound. For this reason the boundary of the allowed region and the contours of the coupling are approximately parallel.

One might wonder if a sum rule is also present in the neutral Higgs sector, and indeed, there exists such a sum rule. However, since all three neutral Higgs fields mix, the sum rule is quite involved and does not provide much insight. It only simplifies very close to the alignment limit beyond the reach of the High-Luminosity Large Hadron Collider (HL-LHC), and thus, we omit it.

The lower bounds in Equation (5.24) together with the upper bounds on the Higgs masses strongly motivate charged Higgs searches in the low–intermediate mass regime with $pp \to qbH^\pm (\to q'b)$ with all possible combinations of the up-type quarks $q, q' = u, c, t$. A non-observation rules out spontaneous CP violation as the primary source of the KM phase, while an observation, on the other hand, can support this idea by the experimentally accessible sum rule in Equation (5.21). Unfortunately, the only standard search channel, i.e. extensively analysed by the experimental collaborations, is the case $q = q' = t$. For this reason, we scrutinise these channels in the next chapter.

Direct Searches: Standard and Non-Standard Signatures

As we have seen in Chapter 5, the search for the collider signatures $pp \to qH^{\pm}(\to q'b)$ with $q, q' = u, c, t$ is highly motivated. Large couplings to bottom quarks arise naturally within spontaneous CP violation once the flavour violation in the down sector is negligible.

On the one hand, the experimental searches focus mainly on the associated production of a charged Higgs boson with a top quark, and the subsequent decay of that Higgs into top and bottom quarks [155–160]. Usually this is rather well motivated since in typical 2HDMs the third generation couplings dominate. Similarly, the signature probed below the top quark mass threshold is the top decay into a charged Higgs boson and a bottom quark, with the subsequent decay of the Higgs into charm and bottom quarks [161]. For the same reason the other signatures did not gain much impetus.

On the other hand, there is slightly more progress on the theory side, in particular for the signatures with $q = c$. In Reference [162], the authors show that stringent lower bounds on the heavy Higgs masses can be evaded by the introduction of additional flavour violation. The same finding was already illustrated before in Reference [1]. For this reason, they introduce the coupling $\tilde{\epsilon}^u_{32}$ in our notation. While it is done ad-hoc in Reference [162], we have provided strong motivation [143], cf. Chapter 5. Moreover, the charged Higgs field in Reference [162] couples to charm and bottom quarks, and thus cg fusion dominates the production mode. However, it is not apparent if the authors consider this, or only examine the gluon fusion production mode. The authors of Reference [163] come to the same conclusion, and thus, they propose a dedicated analysis for the cg fusion channel.

Nevertheless, those analyses do not cover all relevant possibilities. Therefore, we will systematically discuss all possible combinations of the relevant couplings. We perform the analyses in a model-independent way, i.e. we consider the Lagrangian

$$\mathcal{L} = \sum_i g_{u_i b} \left(H^+ \overline{u}_{R,i} b_L + H^- \overline{b}_L u_{i,R} \right) - m^2_{H^{\pm}} H^+ H^- \,, \tag{6.1}$$

with the real couplings $g_{u_i b}$, $i = 1, 2, 3$. From now on q denotes the light quarks, i.e. $q = u, c$. Depending on the hierarchy of the couplings present in Equation (6.1) different collider signatures might be important. This is summarised in Table 6.1. Additionally, to get a feeling of the order of magnitude of the hierarchy, we show the dominant signature

Table 6.1.: Relevant signatures in the presence of any combination of the charged-Higgs couplings g_{qb} $(q = u, c)$ and g_{tb}. The size of the couplings is such that they either dominate the production or decay. The parentheses around b imply two signatures: one signature without and the other with an associated b quark. $t \to bH^{\pm}$ denotes top quark decays via top quarks produced through $pp \to t\bar{t}$.

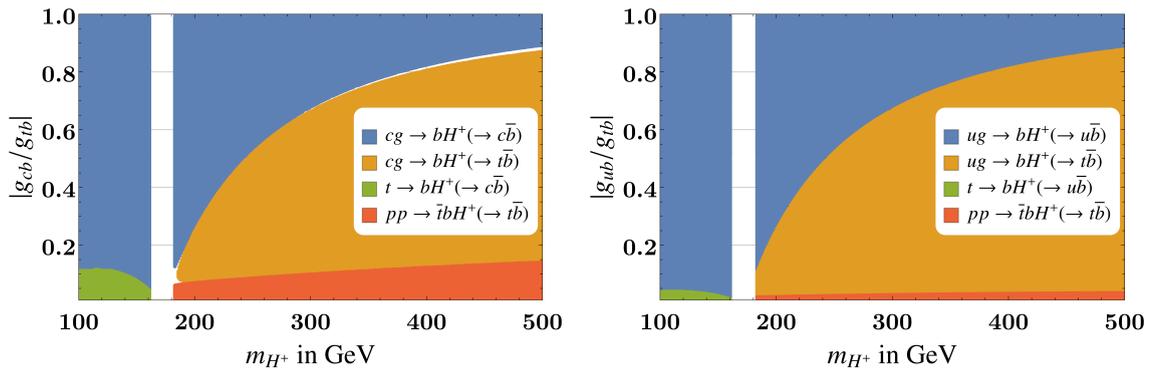| production dominated by	decay dominated by	
	g_{qb}	g_{tb}
g_{qb}	$pp \to (b)H^{\pm}(\to qb)$	$pp \to (b)H^{\pm}(\to tb)$
g_{tb}	$t \to bH^{\pm}(\to qb)$	$pp \to tbH^{\pm}(\to tb)$

Figure 6.1.: Dominant signatures in the presence of g_{tb}, = and g_{cb} (left) or g_{ub} (right) coupling as a function of the charged Higgs mass m_{H^+} and ratio g_{qb}/g_{tb}. The mass window $m_t \pm 10\,\text{GeV}$ is excluded because off-shell effects might become important here. The difference between the plots is due to the larger parton luminosity function of the up quark.

as a function of the charged Higgs mass and the ratio g_{qb}/g_{tb} in Figure 6.1. Our goal is to study the reach of the experiments in constraining the corresponding couplings.

First, we briefly analyse the flavour constraints in Section 6.1. Starting from Section 6.2, we discuss the different collider signatures.

6.1. Flavour Constraints

The most relevant constraint comes from charged Higgs contributions to $\overline{D}$–D mixing. The corresponding box diagrams constrain the combination $g_{ub}g_{cb}$. Another constraint might come from the decay $t \to u(c)\gamma$ which constrains the product $g_{tb}g_{u(c)b}$. This will be analysed in the following.

Neutral D meson mixing

The dominant contribution to D–$\overline{D}$ mixing comes from the charged Higgs box diagram contribution to O_1'. The New Physics contribution to the off-diagonal elements of the D–$\overline{D}$ mixing matrix reads [1]

$$M_{12}^{\text{NP}} = \frac{1}{2M_D} \langle D| H^{\text{NP},|\Delta C|=2} |\overline{D}\rangle = \frac{\eta}{128\pi^2} g_{cb}^2 g_{ub}^{*2} D_2(m_b^2, m_b^2, m_{H^{\pm}}^2, m_{H^{\pm}}^2) \,\text{GeV}^3, \quad (6.2)$$
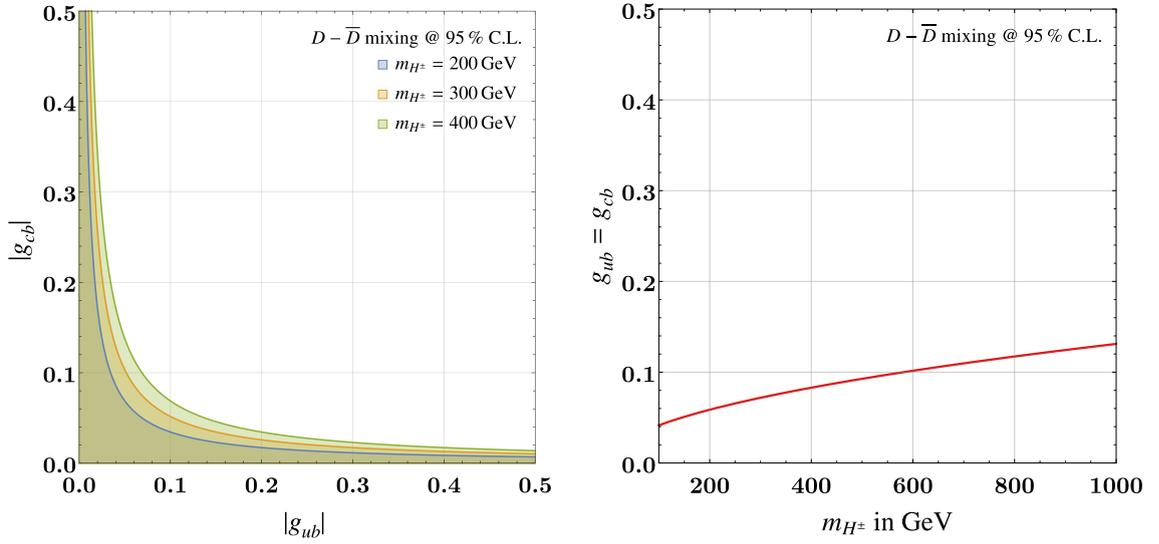
Figure 6.2.: *Left*: Allowed region on the g_{ub}–g_{cb} plane at 95 % C.L. for various Higgs masses taking into account the D meson mixing constraint.
Right: Upper limit @ 95 % C.L. on the couplings $g_{ub} = g_{cb}$ as a function of the charged Higgs mass.

where $\eta \approx 0.021$ includes the hadronic quantities and the QCD running of the Wilson coefficients. The loop function D_2 can be found in Appendix B.

Since the Standard Model contribution is dominated by long-distance effects and no reliable estimates are available, we constrain the product $g_{ub}g_{cb}$ by demanding the New Physics contribution in Equation (6.2) to lie below the experimental value at 95 % C.L., which is taken from the online update of the UTfit collaboration [164]. The allowed region on the coupling plane is shown in Figure 6.2. We also show in the right plot of the very same figure the upper limit on the couplings $g_{ub} = g_{cb}$ as a function of the charged Higgs mass. This corresponds to the intersection of the diagonal $|g_{ub}| = |g_{cb}|$ in the left plot of Figure 6.2 with the upper contours of the allowed regions for different charged-Higgs masses.

Rare Top Decays

The charged Higgs contribution to the rare top decays $t \to u(c)\gamma$ gives a constraint on the combination $g_{tb}g_{u(c)b}$. The current experimental upper limits at 95 % C.L. are [165]

$$\text{BR}_{\text{exp}}(t \to u\gamma) < 6.1 \times 10^{-5},$$
$$\text{BR}_{\text{exp}}(t \to c\gamma) < 1.8 \times 10^{-4}. \tag{6.3}$$

The charged Higgs contribution can be adapted from Reference [98]

$$\text{BR}(t \to q\gamma) = \frac{m_t^5}{4\pi\Gamma_t} \left(\frac{5e}{1152\pi^2 m_{H^\pm}^2} \right)^2 \left| g_{tb}g_{qb}^* \right|^2, \tag{6.4}$$

where $\text{BR}(t \to q\gamma) \sim 10^{-6}$ for a charged Higgs mass as light as $100\,\text{GeV}$ and $\mathcal{O}(1)$ couplings. Therefore, these decay channels do not provide any relevant constraints yet, however, this might change in near future.
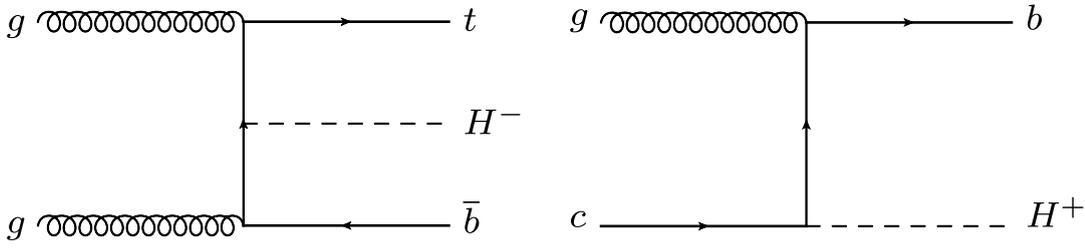
Figure 6.3.: One diagram contributing to the associated production of a charged Higgs with top and bottom quarks (left), and production through quark gluon fusion, here cg fusion as an example, yielding a charged Higgs associated with a bottom quark (right).

Precisely measured meson decays that can be utilised to constrain New Physics involve leptons in the final state, and thus, are not relevant in our case. As we have just seen, the relevant flavour observables only constrain a product of couplings. In this sense, the direct searches at colliders are crucial as they provide the possibility to constrain single couplings.

6.2. Associated Production with tb: $pp \to tbH^\pm(\to tb)$

The associated production of a charged Higgs boson with a top and bottom quark, see left diagram in Figure 6.3, is extensively studied by experimental collaborations. The main reason is that for the usual 2HDMs, for instance type-II, the couplings to the third generation fermions dominate. Thus, for charged Higgs bosons above the top quark mass, this is expected to be the dominant production and decay channel at a hadron collider. However, this is not necessarily true in a general 2HDM. Nonetheless, this signature is relevant for us.

This channel has been analysed by both ATLAS [155–157] and CMS [158–160]. However, CMS has not provided an update with the full Run 2 dataset of 139 fb^{-1}, so we only use the recent result of ATLAS [157]. The upper limit is given in terms of cross section times branching ratio which we recast in a limit on the charged-Higgs coupling g_{tb}. For this we generate the cross section in `MadGraph5_aMC@NLO` [166] using the 2HDM model file [167] at leading order. To save computation time, we refrain from generating the process at NLO, and instead, we use the K factor from Reference [168]. The result is shown in Figure 6.4. As we can see the constraint is still above our lower limit $g_{tb} > 0.2$. However, this might look different with the full 3000 fb^{-1} dataset that is expected to be collected at the HL-LHC [169]. A naive rescaling of the limits suggests that an upper limit of $g_{tb} \gtrsim 0.3$ is to be expected, close to our lower limit from Section 5.2.

6.3. Top Quark Decay: $t \to bH^\pm(\to qb)$

Below the top quark mass m_t, the decay $H^\pm \to tb$ is kinematically forbidden, and thus, $pp \to tbH^\pm(\to tb)$ does not provide a constraint on the coupling g_{tb}. However, if the coupling g_{tb} dominates the production, this means $g_{tb} \gg g_{qb}$ due to the large parton luminosity functions of c and in particular u, the charged Higgs boson is predominantly produced via top quark decays. In this case the relevant signature is $t \to bH^\pm(\to qb)$.

Unfortunately, only one analysis has been performed by the experimental collaborations. In Reference [161] upper limits on the decay $H^\pm \to cb$ for BR($H^\pm \to cb$) = 1, and BR($t \to bH^\pm$) + BR($t \to Wb$) = 1 are provided using the 19.7 fb^{-1} dataset from Run 1.
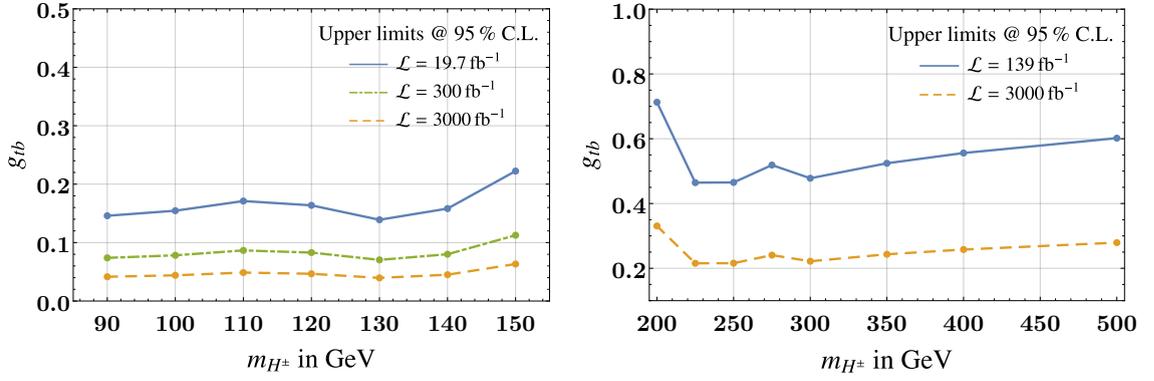
Figure 6.4.: Upper limits at 95 % C.L. on the coupling g_{tb} for $g_{tb} \gg g_{qb}$ above (right) and below (left) the top mass threshold. The upper limits for $\mathcal{L} = 139\,\text{fb}^{-1}$ are recast from Reference [157] and [161], respectively. The projection for $\mathcal{L} = 300\,\text{fb}^{-1}$ and $\mathcal{L} = 3000\,\text{fb}^{-1}$ is obtained by naive rescaling assuming that the significance $\sim S/\sqrt{B}$ grows with $\sqrt{\mathcal{L}}$.

We recast the upper limits in terms of the coupling g_{tb}, see Figure 6.4. As one can see, the search provides a stringent constraint on the couplings g_{tb} in the mass regime $m_{H^\pm} < m_t$ as long as $g_{tb} \gg g_{qb}$. Since the search has been performed for the decay $H^\pm \to cb$, we still have to analyse the case $H^\pm \to ub$. At first sight, it seems that there is no difference between the signatures $H^\pm \to cb$ and $H^\pm \to ub$ since the analysis does not utilise charm tagging techniques. Though, the b jets are tagged, and charm jets have a much higher mistagging rate, $\mathcal{O}(10\,\%)$, than up quark jets $\lesssim 1\,\%$. However, the experimental analysis performs a kinematical fit to identify the pair of jets that are least likely originating from the b quarks of the top decay [161]. Thus, the same bounds should not only apply for $H^\pm \to ub$, but also they are expected to be even more stringent. Since the upper limits in Figure 6.4 for g_{tb} are already below the lower limit of $g_{tb} \gtrsim 0.2$, no further recasting is necessary.

These results have crucial implications for the model considered in Reference [143]: The parameter space where $g_{tb} \gg g_{qb}$ is excluded for $m_{H^\pm} < m_t$.

6.4. Associated Production with b: $pp \to bH^\pm(\to tb)$

Until now, we have considered the hierarchy $g_{tb} \gg g_{qb}$. However, if g_{tb} is not much larger than g_{qb}, i.e. $g_{qb}/g_{tb} \gtrsim 0.1$ for $q = c$, the production is dominated by g_{qb} due to the large parton luminosity functions. Again, we first focus on the charm quark, and consider the case $m_{H^\pm} > m_t$. Further $g_{qb}/g_{tb} \lesssim 1$, otherwise the decay into qb dominates. In this case the relevant production mode is given by quark gluon fusion, and thus, the charged Higgs is associated with one b quark, see Figure 6.3 right. The signature without an associated b quark is only present in the five-flavour scheme, however, to reduce the background we require an additional b jet in the final state, thus, we focus on $pp \to bH^\pm(\to tb)$.

Unfortunately, the associated production of a charged Higgs with a single b quark with the subsequent decay $H^\pm \to tb$ has not been considered in experimental analyses at all. For this reason, Reference [163] proposes a search with at least three b tagged jets and one lepton (e or μ) with transverse momenta of $p_T^b > 25\,\text{GeV}$ and $p_T^l > 35\,\text{GeV}$, respectively. The b jets stem from the associated production, the decay of the charged Higgs into top
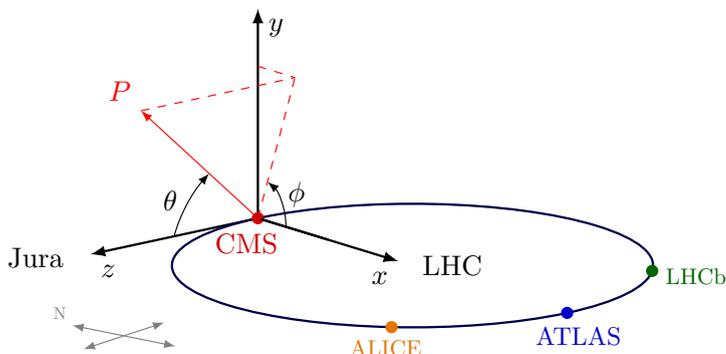
Figure 6.5.: Illustration [170] of the coordinate system as it used by ATLAS [171] and CMS. The red point—corresponding to the origin of the coordinate system—denotes the interaction point in the centre of the detector [171]. The pseudorapidity is defined as $\eta = -\ln\tan(\theta/2)$ with the polar angle θ [171].

and bottom, and the subsequent decay of the top quark into a W and b. The lepton stems from the subsequent decay $W \to l\nu$. For this reason, events are further required to have missing energy of $E_T^{\mathrm{miss}} > 35\,\mathrm{GeV}$. The angular separation ΔR, defined as

$$\Delta R = \sqrt{(\Delta\eta)^2 + (\Delta\phi)^2}\,, \tag{6.5}$$

between any b jets, and between b jet and lepton should satisfy $\Delta R > 0.4$. For the definition of the coordinate system see Figure 6.5. Further $|\eta| < 2.5$ for the lepton and all b jets. Finally, the sum of the three leading b jet transverse momenta and the lepton momentum H_T should be $H_T > 350\,\mathrm{GeV}$. Reference [163] provides only two (promising) benchmark points, and for this reason we perform this analysis ourselves.

The dominant background is $t\bar{t}$ production, which is simulated in `MadGraph5_aMC@NLO` with up to two additional jets in the five-flavour scheme. The resulting Les Houches Event (LHE) file is fed into a `PYTHIA 8.2` [172, 173] standalone version. Jets are matched using the MLM jet matching algorithm [174–176]. The jet finding is performed with `FastJet` [177, 178] using the anti-k_T algorithm with a radius parameter of $R = 0.6$. The K factor is determined by dividing the NNLO cross section, see Reference [179] and references therein, by the leading order cross section *after* jet merging. This yields $K \approx 1.6$.

The analysis is also performed in `PYTHIA 8.2`, for this, we implement the b-tagging as follows: The closest jet axis within a cone of $\Delta R = 0.5$ around the b quark from the hard subprocess is tagged as a b jet. Since this yields a b jet identification and efficiency rate of 100 %, we use the p_T dependent b-tagging efficiency and misidentification rates from the `DELPHES 3.4.2` ATLAS card based on Reference [180]. This corresponds to a working point with an approximately 80 % b-tagging efficiency. In order to apply the different misidentification rates for c and light jets, we internally tag the c jets in the same way as the b jets. The remaining internally untagged jets are treated as light jets. In case of a second lepton with $p_T > 10\,\mathrm{GeV}$, and a separation of $\Delta R > 0.4$ to all b jets, the event is vetoed as in Reference [163]. The missing energy E_T^{miss} is calculated by summing the momenta of all visible final state particles within the detector acceptance and with $p_T > 0.5\,\mathrm{GeV}$.

The signal $pp \to bH^\pm(\to tb)$ is generated at leading order in `MadGraph5_aMC@NLO` using the 2HDM model file [167]. The LHE file is fed into `PYTHIA 8.2` and the same self-written code applied for the background analysis is used.
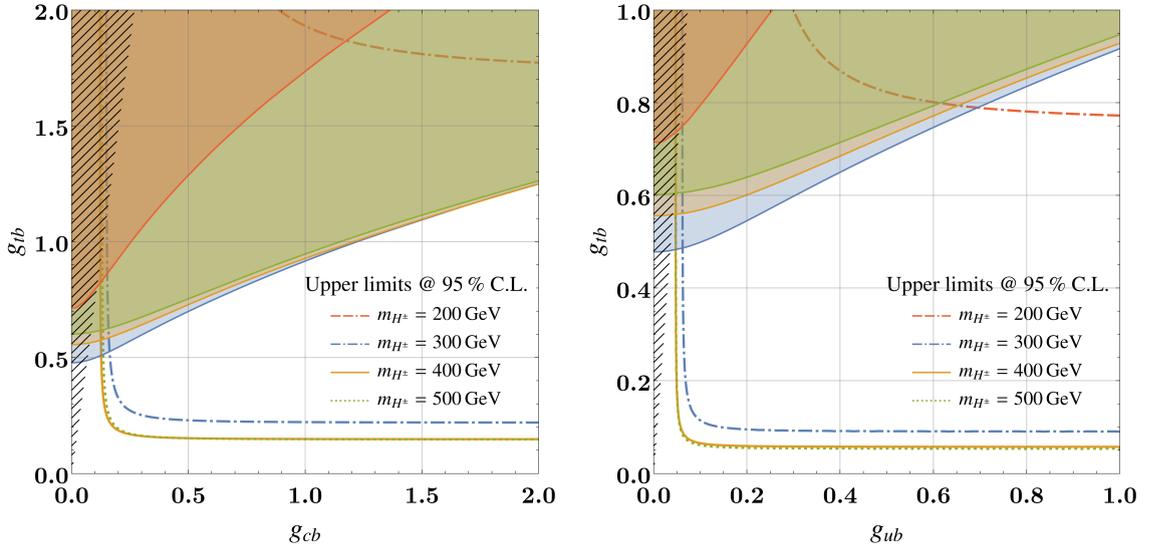
Figure 6.6.: Upper limits at 95 % C.L. are shown as contours on the couplings planes for $\sqrt{s} = 14\,\text{TeV}$[1] and $\mathcal{L} = 139\,\text{fb}^{-1}$. The region where the associated production with top and bottom makes up more than 10 % of the production cross section is hashed. The coloured regions, where the same colour code as for the contour lines has been used, are excluded by the signature from Section 6.2 for $\sqrt{s} = 13\,\text{TeV}$ and $\mathcal{L} = 139\,\text{fb}^{-1}$.

We perform a cut and count analysis, and calculate the significance σ according to the formula [163, 181]

$$\sigma = \sqrt{2\left[(S+B)\log\left(1+\frac{S}{B}\right) - S\right]} \overset{B \gg S}{\approx} \frac{S}{\sqrt{B}}, \qquad (6.6)$$

with the number of signal S and background events B.

The signal analysis is performed once for each charged Higgs mass point. The number of signal events as a function of the couplings is obtained by rescaling. The exclusion limits at 95 % C.L. are shown in Figure 6.6. In case of the up quark gluon fusion production channel, we expect stronger limits due to the larger parton luminosity functions compared to the charm quark. And indeed, this is what we see in Figure 6.6. Note that for large g_{tb} contamination from the associated production with top quarks is not negligible anymore, and constraints therefor become important, cf. Section 6.2. The region where the associated production with top and bottom quarks makes up more than 10 % is hashed in the plots of Figure 6.6. The resulting constraints are overlaid with the exclusion limits obtained in Section 6.2 due to the presence of a g_{tb} coupling. We also provide the constraints in terms of cross section times branching ratio in Figure 6.7.

6.5. Resonant Production: $pp \to H^\pm(\to qb)$

Dedicated searches of a charged Higgs boson that is entirely produced via, and that decays into, light quarks have not been performed by the experimental collaborations. However,

---

[1]While available searches are done at $\sqrt{s} = 13\,\text{TeV}$, we perform the ones not analysed by the experimental collaborations for $\sqrt{s} = 14\,\text{TeV}$.
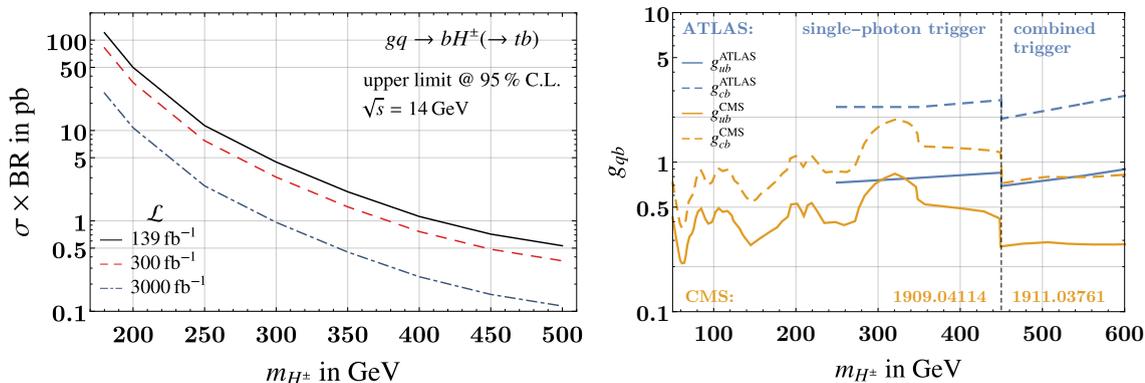
Figure 6.7.: *Left*: Upper limits at 95 % C.L. on the cross section times branching ratio $\sigma \times$ BR. The projection for $\mathcal{L} = 300\,\text{fb}^{-1}$ and $\mathcal{L} = 3000\,\text{fb}^{-1}$ is obtained by rescaling the result obtained for $\mathcal{L} = 139\,\text{fb}^{-1}$.
Right: Upper limits at 95 % C.L. on the couplings g_{ub} (solid blue) and g_{cb} (dashed blue) as a function of the charged Higgs mass $m_{H^\pm}$ from recasting Reference [171]. Below resonance masses of 450 GeV the single-photon trigger has been used, above 450 GeV the combined trigger. The rescaling of the CMS results by the parton luminosity functions as in Reference [182] for the large-radius jet and a jet from initial state radiation (1909.04114) [183] is shown for masses below 450 GeV for the coupling g_{ub} (solid orange) and g_{cb} (dashed orange). For masses above 450 GeV the results from the CMS search (1911.03761) with an initial state radiated jet [184] has been rescaled [182].

since the signature of this channel is a dijet resonance, one can put limits on the couplings by recasting other searches.

At the LHC, searches for dijet resonances below 1 TeV are involved since the high rate of the multi-jet background would saturate the trigger if all event information is collected [171]. If only partial event information is collected, these searches can be extended down to $\approx 500\,\text{GeV}$ [171, 185, 186]. For masses below $\approx 500\,\text{GeV}$ the events can be efficiently recorded by requiring a high-p_T photon [171] or jet [184] in the final state stemming from an initial state radiation, though, this comes at the cost of a reduced signal acceptance [171, 187, 188]. For even lower masses, i.e. $\lesssim 200$–$350\,\text{GeV}$ [171], the two jets stemming from the resonant decay are collimated and they form a large-radius jet. Searches for this signatures together with jet substructure variables, chosen in such a way to optimise the signal significance [189], allow to put exclusion limits for dijet resonances as light as $50\,\text{GeV}$ [183, 189–191]. The recast of the latter search, i.e. the signature with a large-radius jet and a photon from initial state radiation will be done elsewhere. Here, we focus on the former search, which was performed by the ATLAS collaboration in Reference [171], namely the search for initial state radiation with two well separated jets.

In Reference [171] the search was done for the signature $pp \to Z' \to q\bar{q}$ with a radiated photon. The selected events had been divided into two categories, one where both jets from the resonant decay are b-tagged, and the other without b-tagging. Since the resonance does not decay into two b jets in our case, we focus on the analysis performed for the latter category. Moreover, two different triggers have been used depending on the resonance masses and differing by the transverse energy cut on the photon $E^{\gamma}_{T,\text{trig}}$, and the p_T cut on the jets. The single-photon trigger, used for resonance masses below 450 GeV, requires only a single photon with transverse energy $E^{\gamma}_{T,\text{trig}} > 150\,\text{GeV}$. Above

Table 6.2.: Selection criteria of Reference [171]. y_1 and y_2 denote the rapidities of the p_T-leading and -subleading jet. See text for the other definitions. Table adapted from Reference [171].

Criterion	Single-photon trigger	Combined trigger
Number of jets	$n_{\text{jets}} \geq 2$	
Number of photons	$n_\gamma \geq 1$	
Leading photon	$E_T^\gamma > 150\,\text{GeV}$	$E_T^\gamma > 95\ \text{GeV}$
Leading, subleading jet	$p_T^{\text{jet}} > 25\,\text{GeV}$	$p_T^{\text{jet}} > 65\,\text{GeV}$
Centrality	$|y^*| = |y_1 - y_2|/2 < 0.75$	
Invariant mass	$m_{jj} > 169\,\text{GeV}$	$m_{jj} > 335\,\text{GeV}$
Jet $|\eta|$	$|\eta^{\text{jet}}| < 2.8$	

450 GeV, the combined trigger is used allowing for a lower transverse energy cut on the photon $E_{T,\text{trig}}^\gamma > 75\ (85)\,\text{GeV}$ for the 2016 (2017) datasets by additionally requiring two jet candidates with each $p_{T,\text{trig}}^{\text{jet}} > 50\,\text{GeV}$. Photons are collected in the region $|\eta| < 2.37$ excluding $1.37 < |\eta| < 1.52$. The selection criteria are listed in Table 6.2. Additionally, if a reconstructed jet is not well separated from the isolated high-p_T photon, i.e. an angular separation of $\Delta R < 0.4$, the jet candidate is removed.

To set the limits on the charged-Higgs couplings, we calculate the local significance σ around the resonance, using the observed data from Reference [171] provided in the online repository HEPData, using $\sigma \approx S/\sqrt{B} \approx S/\sqrt{S+B}$.

Thus, the only missing ingredients are the signal events. We generate $pp \to \gamma H^\pm(\to qb)$ data in `MadGraph5_aMC@NLO` at leading order using the 2HDM model file [167]. To populate the phase space with sufficient events satisfying the E_T^γ cut on the photons, the events are generated with a p_T^γ cut of $p_T^\gamma > 100\ (50)\,\text{GeV}$ for the single-photon (combined) trigger.

The analysis is performed in `PYTHIA 8.2`. Photons from the hard subprocess or initial state radiation are identified internally via the status code and are traced to the final state. We neglect possible photon conversion. The photon isolation is then checked by summing the transverse energy of all visible final state particles, excluding the photon candidate itself, within a cone with $\Delta R = 0.4$ around the photon candidate. Using the tight isolation requirement of ATLAS based on calorimeter information only, the transverse energy of the photon E_T^γ is required to satisfy [192]

$$E_T^{\text{cone}} < 0.022 E_T^\gamma + 2.45\,, \tag{6.7}$$

where E_T^{cone} denoted the transverse energy of the cone around the photon.

Jets are reconstructed using `FastJet` with the anti-k_T algorithm with a radius parameter of $R = 0.4$, similarly to the experimental analysis [171].

The code and analysis procedure are checked and compared to the experimental analysis by applying it to the signature $pp \to \gamma Z'(\to q\bar{q})$. This enables a direct comparison with the experimental analysis, see Appendix E. The resulting upper limits on the charged-Higgs couplings at 95 % C.L. are shown in Figure 6.7. Let us compare this to existing bounds from other searches in this mass region. As afore-mentioned, searches for one

large-radius jet with hard photons or jets from initial state radiations are performed down to even lower resonance masses [183, 189–191]. The recasting of this search with a hard photon [189] will be done elsewhere. Limits from searches tailored to Z' models where the photon is replaced by a jet can be estimated by rescaling the upper limits obtained by the experimental analysis with the parton luminosity functions. This is for example done in Reference [182], and the result is overlaid in the right-hand plot of Figure 6.7. Although, the recasted search with a hard photon and two separated jets is expected to have a higher sensitivity than the large-radius jet searches for masses $\gtrsim 300\,\text{GeV}$ [183], we hardly observe this. The reason is the cancellation between the diagrams with a photon radiated from the initial states which is not present in the analysed Z' models.

COMMENT ON POSSIBLE OPTIMISATIONS   Since the dominant couplings of the charged Higgs boson are the ones to bottom quarks, the background can be reduced further by requiring a single b-tagged jet in the final state. Alternatively or even additionally one can require a b-tagged jet not stemming from the resonance produced via associated production with the charged Higgs boson. The latter corresponds to the signature $pp \rightarrow bH^{\pm}(\rightarrow qb)$ with photon or jet radiation. However, since no such analyses exist, we have to perform the background simulation ourselves, and hence, it is done elsewhere.

Conclusion

In this part, we have first analysed the most general 2HDM with spontaneous CP violation. In such a scenario all mass scales are set by the electroweak scale up to quartic couplings. This fact has been exploited to determine stringent upper limits on the masses of the additional Higgs bosons using NLO perturbative unitarity for the very same couplings. Moreoever, the flavour structure cannot be aligned to the Standard Model, since otherwise the KM phase would be zero, in contradiction to experimental observations. However, flavour violation in the down quark sector is strongly constrained by experiment. Necessarily, the dominant flavour violation has to be present in the up quark sector. We have shown that this in turn yields a sum rule for the charged-Higgs couplings to bottom quarks. The latter implies in particular lower limits on those couplings.

The interplay between the upper limits on the Higgs masses and lower limits on the charged-Higgs couplings, makes it possible to determine the origin of CKM CP violation in Nature. Furthermore, the sum rule illustrates the importance of collider signatures that are not yet analysed by the experiments. And thus, in Chapter 6 we first analysed the flavour constraints, where we have seen that the only relevant constraint is currently given by neutral D meson mixing. Albeit, this only constrains the product of the couplings $g_{cb}g_{ub}$. In future, the rare top decays $t \to q\gamma$ with $q = u, c$ might also become important which will then constrain the product $g_{tb}g_{qb}$ with $q = u, c$. In this respect, collider searches are crucial since they allow to put limits on a single coupling at a time. Consequently, we determined current and future limits on the charged-Higgs couplings using available and new collider searches. A large part of the parameter space has already been ruled out, however, without additional experimental optimisation, the model remains on the edge of exclusion. Thus, we further proposed the new searches $pp \to (b)H^{\pm}(\to qb)$ with initial jet or photon radiation which might increase the current reach of the experiment. Together with the better experimental performance, for instance the improved b tagging or jet substructure analyses, expected in the upcoming (HL-)LHC runs, this provides a clear path on excluding or verifying spontaneous CP violation.

New Physics Effects in Hydrogen Isotopologues

In this part we provide the first extensive study of New Physics effects on the ro-vibrational spectrum of molecules. For this, we first review the theoretical and experimental status of molecular spectroscopy in Chapter 8. This serves as a foundation for Chapter 9 where we analyse the effect of a plethora of New Physics models on the molecular spectra of hydrogen isotopologues. Finally, we conclude in Chapter 10.

Ro-Vibrational Spectroscopy of Hydrogen Isotopologues

Up to this point, we have discussed New Physics around and beyond the electroweak scale motivated by the hints and evidences of physics beyond the Standard Model observed at the LHC. Nonetheless, no heavy particles beyond the ones present in the Standard Model have been discovered. In light of the fact that new particles might as well arise at much lower energies, we turn our attention to light New Physics. Light particles below the GeV scale arise in many models, for instance the axion in models to solve the strong CP puzzle [194], as dark matter candidates [195–197], or as a light mediator to a hidden sector [198,199].

The low energy region can be probed for instance in molecular spectroscopy. Molecular hydrogen and its isotopologues are particularly favourable since precise theoretical calculations and experimental measurements are available. This enables a thorough examination of possible New Physics effects. As the typical bond length is $\sim 1\,\text{Å}$, one expects to be sensitive to particle masses of $\mathcal{O}(\text{keV})$. However, this region is already being probed by other experiments, for example in QED precision tests with atomic spectroscopy [200–203], or from astrophysics [204–206] and cosmology [207]. While the former might even yield slightly better constraints, nuclei-nuclei interactions are absent and can only be probed in molecules. The latter yields strong *indirect* constraints below a few MeV, and in this sense, molecular spectroscopy is important as a *direct* and complementary test in the laboratory.

In the literature, the effect of New Physics is analysed as a *fifth force*. The New Physics contribution is parametrised in terms of a Yukawa type potential

$$V_Y(r) \propto \frac{g_{\text{NP}}}{r} e^{-mr}\,, \tag{8.1}$$

with the mass m and coupling g_{NP} of the new mediator. Such forces are also probed in gravitational interactions [208–211]. The absence of any deviation from the known interaction puts strong limits on the New Physics coupling, $g_{\text{NP}} \lesssim 10^{-34}$. However, the bounds only apply to mediator masses up to $\mathcal{O}(\text{meV})$. Similarly, one can derive constraints on the couplings of keV-scale mediators by measuring the electromagnetic forces in atomic and molecular spectroscopy which is done for example in References [212,213] for the Yukawa type potential. However, in general the New Physics contribution does not need to arise from a scalar interaction, and the description by the Yukawa type potential in
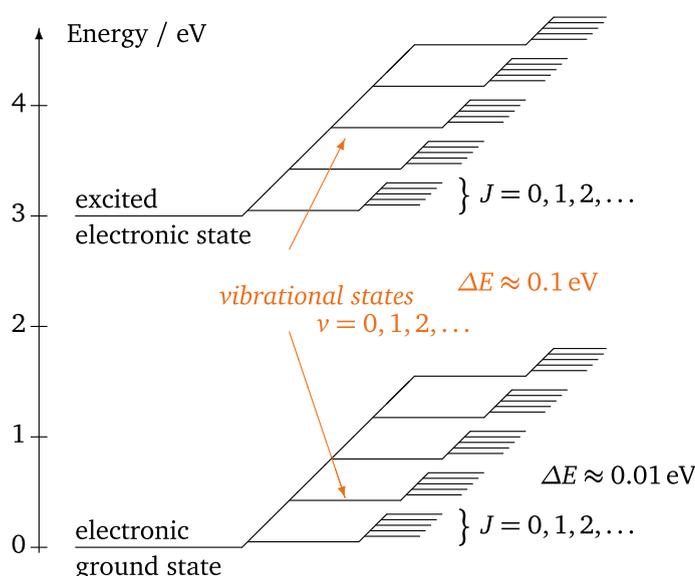
Figure 8.1.: Schematic energy level diagram of a molecular spectrum adapted from Reference [214]. The vibrational quantum number is denoted by v, and the rotational quantum number by J. The splitting between the vibrational and rotational lines within one electronic state is smaller than the splitting between the electronic states. Hence, molecular spectra are sensitive to smaller energy scales.

Equation (8.1) is not necessarily complete. But before we devote ourselves to the New Physics analysis, which will be done in Chapter 9, we first lay the foundations.

In order to perform such an analysis, a thorough understanding of theory and experiment is necessary. Thus, in Section 8.1 and 8.2, we review the theoretical and experimental status of molecular spectroscopy, respectively.

8.1. Theoretical Status

The treatment of molecules in quantum mechanics is intrinsically difficult. Even the simplest molecule, the dihydrogen cation H_2^+ cannot be solved analytically. Thus, the hydrogen molecule is even more involved. Although a theoretical description is challenging, a precise solution is rewarding as molecular spectra are much richer than atomic spectra. As a result of the second nucleus, there are not only electronic excitations, but also rotational and vibrational transitions, see Figure 8.1. Hence, each electronic spectral line is split further into many lines corresponding to the ro-vibrational transitions. The separation between the transitions within this band is much smaller than the electronic transitions, and hence, molecules are sensitive to effects at lower energies.

First solutions to the hydrogen molecule started in 1927, where Heitler and London [215], and Born and Oppenheimer [216] independently presented two approaches. Both approaches rely on the fact that the nuclei are much heavier than the electrons, i.e. $m_N \gg m_e$. For this reason Heitler and London neglected the motions of the nuclei. Born and Oppenheimer, on the other hand, performed an expansion in the small mass ratio $\sqrt[4]{m_e/m_N}$. However, it was clear that for a reliable and precise calculation one cannot rely on this so-called adiabatic approximation [217]. Instead, it has been proposed in Reference [217] to start with the exact Schrödinger equation, as it is done in the very same reference.

Hitherto, no reliable estimates of numerical uncertainties has been made for such direct approaches [218]. And thus, in Reference [218] a systematic perturbative expansion has been developed to take the non-adiabatic corrections into account. Beyond those non-relativistic contributions, one has to include the relativistic and QED corrections, which are calculated in the framework of non-relativistic QED (NRQED). Altogether, this yields the total energy in terms of an expansion in the fine structure constant α and the ratio of the electron mass over the reduced nuclear mass m_e/μ_n

$$
\begin{aligned}
E = \alpha^2 & \left(E^{(2,0)} + E^{(2,1)} + E^{(2,2)} + \dots \right) \\
& + \alpha^4 \left(E^{(4,0)} + E^{(4,1)} + \dots \right) + \alpha^5 \left(E^{(5,0)} + \dots \right) + \dots ,
\end{aligned}
\tag{8.2}
$$

with $E^{(n,m+1)}/E^{(n,m)} \sim m_e/\mu_n$. Beside the terms shown in Equation (8.2), the leading correction of $\mathcal{O}(\alpha^6)$ is fully known, and the correction of $\mathcal{O}(\alpha^7)$ is partially known [219–226]. At this level of accuracy one also has to take the finite nuclear size effect into account. All these results have recently been made publicly available through the computer program H2spectre [227, 228]. In the following, we briefly outline the main steps on how to include corrections to leading order in $\sim m_e/\mu_n$, for a nice and more complete review see Reference [229].

The full non-relativistic Hamiltonian of a heteronuclear molecule with two electrons reads

$$
H = \frac{\vec{p}_1^2}{2m_e} + \frac{\vec{p}_2^2}{2m_e} + \frac{\vec{p}_A^2}{2m_A} + \frac{\vec{p}_B^2}{2m_B} + \alpha_{\text{em}} \left(\frac{1}{r_{12}} + \frac{1}{r_{AB}} - \frac{1}{r_{1A}} - \frac{1}{r_{1B}} - \frac{1}{r_{2A}} - \frac{1}{r_{2B}} \right) ,
\tag{8.3}
$$

where r_{12} and r_{AB} denote the distances between electron 1 and 2, and between the nuclei A and B, respectively. Similarly r_{iX} denotes the distances between electron $i = 1, 2$ and nucleus $X = A, B$. As it turns out, the most convenient reference frame is obtained by separating the centre of mass of the system and taking the positions relative to the geometric centre of the nuclei. Then, the Hamiltonian H can be written as a sum of a purely electronic Hamiltonian including the nuclear repulsion, H_{el}, and a nuclear Hamiltonian H_n including the nuclear motion and kinetic interactions [229]

$$
\begin{aligned}
H &= H_{\text{el}} + H_n \\
H_{\text{el}} &= \frac{\vec{p}_1^2}{2m_e} + \frac{\vec{p}_2^2}{2m_e} + \alpha_{\text{em}} \left(\frac{1}{r_{12}} + \frac{1}{r_{AB}} - \frac{1}{r_{1A}} - \frac{1}{r_{1B}} - \frac{1}{r_{2A}} - \frac{1}{r_{2B}} \right) , \\
H_n &= -\frac{1}{2\mu_n} \left[\vec{\nabla}_R^2 + \left(\frac{\vec{\nabla}_1 + \vec{\nabla}_2}{2} \right)^2 \right] + \left(\frac{1}{M_A} - \frac{1}{M_B} \right)^2 \vec{\nabla}_R \cdot \frac{\vec{\nabla}_1 + \vec{\nabla}_2}{2} .
\end{aligned}
\tag{8.4}
$$

Here, μ_n denotes the reduced mass $\mu_n = M_A M_B/(M_A + M_B)$ of the nuclei A and B, and $R = |\vec{R}| = |\vec{r}_{ab}|$ denotes their separation. We closely follow the notation of Reference [229].

Neglecting for now the non-adiabatic effects means one can write the total wave function as

$$
\Phi(\vec{r}_1, \vec{r}_2, \vec{R}) = \psi_{\text{el}}(\vec{r}_1, \vec{r}_2; \vec{R}) \chi(\vec{R}) ,
\tag{8.5}
$$

where ψ_{el} solves the Schrödinger equation of the clamped nuclei Hamiltonian H_{el}

$$
H_{\text{el}} \psi_{\text{el}} = \mathcal{E}^{(2,0)}(R) \psi_{\text{el}} ,
\tag{8.6}
$$

for fixed nuclear distances R. The resulting effective potential $\mathcal{E}(R) \equiv \mathcal{E}^{(2,0)}(R)$ enters the one dimensional Schrödinger equation for the nuclear wave function $\chi(\vec{R})$

$$\left[-\frac{\vec{\nabla}_R^2}{2\mu_n} + \mathcal{E}^{(2,0)}(R) \right] \chi(\vec{R}) = E^{(2,0)}\chi(\vec{R}) \,, \tag{8.7}$$

yielding the Born–Oppenheimer contribution $E^{(2,0)}$, which is treated as the leading order energy of the full system. Further, the nuclear wave function can be written as

$$\chi(\vec{R}) = \frac{\chi(R)}{R} Y_{Jm}(\hat{\vec{r}}) \,, \tag{8.8}$$

with the radial wave function $\chi(R)$ and the spherical harmonics $Y_{Jm}(\hat{\vec{R}})$. Thus, the eigenvalues and wave function $\chi(\vec{R})$ are characterised by the angular momentum quantum number J, and the vibrational quantum numbers ν, both non-negative integers.

All neglected contributions which are present in Equation (8.4), as well as higher order contributions are now perturbatively included. For example, the first order correction to the Born–Oppenheimer energy is given by the adiabatic contribution [224]

$$E^{(2,1)} = \langle\chi| \langle\psi_{\mathrm{el}}| H_n |\psi_{\mathrm{el}}\rangle |\chi\rangle \,. \tag{8.9}$$

Alternatively, one could have included, from the beginning, $\mathcal{E}^{(2,1)} = \langle\psi_{\mathrm{el}}| H_n |\psi_{\mathrm{el}}\rangle$ in the nuclear Schrödinger equation (8.7). The resulting effective potential $\mathcal{E}^{(2,0)}(R) + \mathcal{E}^{(2,1)}(R)$ then yields the adiabatically corrected energy $E_a^{(2)}$ [228, 230]. However, this approach spoils the strict expansion in the ratio m_e/μ_n, see Reference [228].

As mentioned, the non-adiabatic contributions are taken into account in the framework of the non-adiabatic perturbation theory (NAPT) [231]. Here, the total wave function is corrected by a small non-adiabatic term $\delta\phi_{\mathrm{na}}$

$$\Phi(\vec{r}_1, \vec{r}_2, \vec{R}) = \psi_{\mathrm{el}}(\vec{r}_1, \vec{r}_2; \vec{R})\chi(\vec{R}) + \delta\phi_{\mathrm{na}}(\vec{r}_1, \vec{r}_2, \vec{R}) \,, \tag{8.10}$$

with $\langle\delta\phi_{\mathrm{na}}|\psi_{\mathrm{el}}\rangle = 0$. Plugging the corrected wave function into the full Schrödinger equation, one can now perturbatively determine the non-adiabatic corrections. Since we are only interested in the leading New Physics effects, this is of no further relevance for us, and a detailed discussion can be found for instance in Reference [231].

Similarly, the leading order relativistic correction is included via [229]

$$E^{(4,0)} = \langle\chi| \langle\psi_{\mathrm{el}}| H^{(4,0)} |\psi_{\mathrm{el}}\rangle |\chi\rangle \,, \tag{8.11}$$

where $H^{(4,0)}$ denotes the Breit–Pauli Hamiltonian. For consistency $H^{(4,0)}$ should only contain terms to order m_e/μ_n since, again, higher orders in this mass ratio enter through NAPT [229].

Determination of the Born–Oppenheimer Wave Functions

As we are going to include the New Physics contributions in a similar fashion as all higher order corrections, we have to determine the Born–Oppenheimer wave function. The electronic part is obtained by solving the Schrödinger equation (8.6) for fixed nuclear distances R. However, this differential equation does not have an analytical solution, and one has to make use of numerical methods. Usually this is done with the help of

the variational method. This means, the electronic wave function is approximated by an expansion in a basis ϕ_n

$$\psi_{\text{el}} = \sum_n c_n \phi_n(u_1, u_2, \dots) . \tag{8.12}$$

with the coefficients c_n that differ for different variational parameters $u_i, i = 1, 2, \dots$. The latter are chosen such that

$$\frac{\langle \psi_{\text{el}}(u_1, u_2, \dots) | H_{\text{el}} | \psi_{\text{el}}(u_1, u_2, \dots) \rangle}{\langle \psi_{\text{el}}(u_1, u_2, \dots) | \psi_{\text{el}}(u_1, u_2, \dots) \rangle} \geq \mathcal{E}^{(2,0)} , \tag{8.13}$$

is minimal. Plugging the expansion from Equation (8.12) into Equation (8.13) yields a secular equation which determines the energy eigenvalue and the coefficients c_n. For hydrogen isotopologues, the electronic ground state can be precisely estimated for an expansion in the symmetric James–Coolidge basis [232, 233]

$$\psi_{\text{el}}(r_{12}, r_{1A}, r_{1B}, r_{2A}, r_{2B}; R_{AB}; u)$$
$$= \hat{S} \sum_{n_0, n_1, n_2, n_3, n_4} C_{n_0, \dots, n_4} R_{AB}^{-3-n_0-n_1-n_2-n_3-n_4} \, e^{-u(r_{1A}+r_{1B}+r_{2A}+r_{2B})}$$
$$\times r_{12}^{n_0}(r_{1A} - r_{1B})^{n_1}(r_{2A} - r_{2B})^{n_2}(r_{1A} + r_{1B})^{n_3}(r_{2A} + r_{2B})^{n_4} , \tag{8.14}$$

with the variational parameter u, the non-negative integers $n_i, i = 0, 1, \dots 4$, and the symmetrisation operator $\hat{S}$ such that the wave function satisfies the Pauli principle.

Part of the numerical procedure is implemented in `H2SOLV` [234]. There, an expansion in terms of the more general Kołos–Wolniewicz basis is performed, and the secular equation resulting from Equation (8.13) is solved numerically. Thus, we use `H2SOLV` to perform an expansion in the symmetric James–Coolidge basis for a fixed nuclear distance R_{AB}, fixed variational parameter u, and a basis rank of 7. The latter corresponds to a wave function with 228 terms. This returns the minimal energy and the corresponding cofficients $C_{n_0, \dots, n_4}$ on a grid in R and u. The resulting two dimensional potential curve is interpolated with splines of degree two and minimised with respect to u to obtain the effective potential $\mathcal{E}^{(2,0)}(R)$ and the Born–Oppenheimer wave function $\psi_{\text{el}}(\vec{r}_1, \vec{r}_2, \vec{R}) \equiv \psi_{\text{el}}(r_{12}, r_{1A}, r_{1B}, r_{2A}, r_{2B}; R_{AB}; u(R_{AB}))$. The latter is needed to calculate the New Physics contributions later on.

As indicated before, the very same approach can be used to determine the solution of the full non-relativistic Hamiltonian in Equation (8.3). Using a suitable basis directly yields the energy $E^{(2)}$ at α^2 to all orders in m_e/μ_n. For the ground molecular state $\nu = 0, J = 0$, also a direct evaluation of the relativistic and leading QED corrections is available [221, 224, 229]. In the former case the theoretical uncertainty is dominated by the unknown m_e/μ_n correction to the leading QED result. In the latter case the accuracy is limited by the partially known α^7 correction [229]. Remarkably, once the α^7 correction is known, the energy levels can be determined nearly as precisely as the ones of the hydrogen atom [222].[1]

The nuclear Born–Oppenheimer wave function χ can be extracted together with all available Standard Model contributions from the publicly available code `H2spectre` [227].

---

[1]This also means that the Rydberg constant R_∞ can then be determined from hydrogen molecular spectroscopy [222].

8.2. Experimental Status

Ro-vibrational transitions are classified by the change in the angular momentum quantum number ΔJ. A vibrational transition with no change in the angular momentum, $\Delta J = 0$, is called Q branch. Similarly, vibrational transitions involving a change of $\Delta J = -2, -1, 1, 2$ are referred to as O, P, R and S branches, respectively. The molecular spectra of hydrogen isotopologues are nowadays probed up to a relative precision of $\mathcal{O}(10^{-10})$ due to the advances in laser spectroscopy. For example, the most precise measurements of all tritiated hydrogen isotopologues, T_2, DT, and HT were just recently obtained with the help of Coherent Anti-Stokes Raman Scattering Spectroscopy (CARS) with a relative precision of $\mathcal{O}(10^{-10})$ [235–238].

Similar results are obtained for the lightest isotopologues H_2, D_2 and HD using the Doppler-free laser spectroscopy. Here, two counterpropagating waves from the same source illuminate the probe [239]. In this way the Doppler shift effects are cancelled allowing for a precise determination of the spectra, see Reference [239] for a review. For the light isotoplogues a relative precision up to $\mathcal{O}(10^{-10})$ is achieved [240–242].

Less precise results, i.e. a relative precision of $\mathcal{O}(10^{-6})$, for D_2 are obtained with stimulated Raman spectroscopy [243]. Here, one uses two beam sources with different frequencies where one of the frequencies is scanned over. Once the frequency difference matches the energy difference of the transition, a resonant enhancement of the Stokes line is observed, see Reference [243] for a review.

This method is improved further by CARS [235], where the underlying effect was first observed at the Ford Motor Company [244,245]. Compared to Raman spectroscopy, here, the anti-Stokes line is induced. Not only does this reduce the background but also smaller probe volumes are required despite the suppression compared to the Stokes line. This has allowed for a precise determination of the Q branch ($\nu = 0 \to 1$) of all tritiated hydrogen species [235–238].

New Physics Effects in Hydrogen Isotopologues

As of 2019, the calculation of relativistic and QED corrections to the ro-vibrational spectrum of molecular tritium T_2 gave rise to an approximately 3σ deviation in some lines of the Q branch ($\nu = 0 \rightarrow 1$) compared to the experimental measurements [236], see Table 9.1. As we have discussed in Reference [193], it is unlikely that this discrepancy is due to New Physics effects. Not only do the deviations have different signs depending on the transition, but also they are absent in the spectra of H_2 and D_2.

One might deem the variational method as a source of the discrepancy, however, the calculations of the H_2 and D_2 spectra, and some lines in T_2 show a perfect agreement with the experiment. Moreover, current technological advances allow for a precise determination of the Born–Oppenheimer wave function given that the necessary computational resources are available. Already in the past a discrepancy between theory [246] and experiment lead to an experimental reinvestigation that yielded a close agreement with the theory predictions [247]. Corrections are systematically taken into account, such that to current order of precision there is little doubt concerning the accuracy of the theoretical predictions.

And indeed, the measurements have been updated recently [238], and now show a perfect agreement with the theory calculation, see Table 9.1. Hence, these precise measurements can be used to strongly constrain the effect of New Physics. In the mass regime of interest, i.e. $\mathcal{O}(\text{keV})$, there are already strong but only indirect constraints coming from astrophysics and cosmology. In particular, the star cooling constraint coming from the sun and red giants excludes a large part of the parameter space [204–206]. However, there is no consensus on the exact mass range of the new mediator for which these bounds apply. Hence, it is of great interest to have direct and complementary constraints. Moreover, compared to astrophysical and cosmological constraints, atomic and molecular spectroscopy directly probe the single particle interaction. In particular, molecular spectroscopy allows to directly probe all possible combinations of interactions between nuclei and electrons. Given for example a Yukawa interaction induced by a new mediator with mass m, the most general potential reads

$$V_{\text{NP-full}}(\vec{r}_1, \vec{r}_2, \vec{r}_A, \vec{r}_B) = \alpha_{\text{em}} \left\{ \left(-1 + \frac{g_{eN}}{4\pi\alpha_{\text{em}}} e^{-mr_{1A}} \right) \frac{1}{r_{1A}} + \left(-1 + \frac{g_{eN}}{4\pi\alpha_{\text{em}}} e^{-mr_{2B}} \right) \frac{1}{r_{2B}} \right.$$
$$\left. + \left(-1 + \frac{g_{eN}}{4\pi\alpha_{\text{em}}} e^{-mr_{1B}} \right) \frac{1}{r_{1B}} + \left(-1 + \frac{g_{eN}}{4\pi\alpha_{\text{em}}} e^{-mr_{2A}} \right) \frac{1}{r_{2A}} \right.$$

Table 9.1.: Measurement of the fundamental vibrational splittings in the T_2 molecule for the $Q(J)$ band, and for $v = 0 \rightarrow 1$ [236] as well as its update [238]. Note that the latter is not included in our published version of this part [193]. The theory predictions are determined with `H2spectre` [227]. The theoretical uncertainties are added linearly, see text in Section 9.1. Thus the deviation we observe is below 3σ compared to Reference [228]. The numbers are given in cm^{-1}.

Line	experiment	update	theory	$\Delta_{\text{exp–th}}$	$\Delta_{\text{update–th}}$
$Q(0)$	2464.5052(4)	2464.50394(67)	2464.50415(28)	0.0011	-0.00021
$Q(1)$	2463.3494(3)	2463.34817(42)	2463.34836(28)	0.0010	-0.00019
$Q(2)$	2461.0388(4)	2461.03917(42)	2461.03917(28)	-0.0004	0.00000
$Q(3)$	2457.5803(4)	2457.58135(42)	2457.58137(28)	-0.0011	-0.00002
$Q(4)$	2452.9817(4)	2452.98233(42)	2452.98211(28)	-0.0004	0.00022
$Q(5)$	2447.2510(4)	2447.25061(42)	2447.25085(28)	0.0001	-0.00024

$$+ \left(1 + \frac{g_{ee}}{4\pi\alpha_{\text{em}}} e^{-mr_{12}} \right) \frac{1}{r_{12}} + \left(1 + \frac{g_{NN}}{4\pi\alpha_{\text{em}}} e^{-mR_{AB}} \right) \frac{1}{R_{AB}} \Bigg\}$$
$$(9.1)$$

with the New Physics couplings, g_{ee}, g_{NN}, and g_{eN} between electrons, between nuclei, and between electron and nucleus, respectively. In general, the couplings g_{ij} can have both signs, however, g_{ee} and g_{NN} are positive if the couplings g_{ij} are expressed in terms of Yukawa couplings $g_{ij} \sim y_i y_j^*$. This is implicitly assumed from now on. Further, to estimate the maximal reach of the experiments, we consider one coupling at a time. Note that an electron–nucleus coupling g_{eN} implies the presence of an electro–electron and nucleus–nucleus coupling. Nevertheless, their effect is negligible since the electron–nucleus coupling dominates the contribution as it enters four times. Since, however, they depend on the position differently, we numerically checked that the impact of the additional terms indeed affects the results only slightly.

In References [212, 237], only the last term of the potential (9.1) has been analysed. We go beyond those works by analysing all other terms, and by considering other models of New Physics. First, we discuss the implementation of the New Physics contributions. In Section 9.2, we analyse the effects of various New Physics models.

9.1. New Physics: Implementation

Given a New Physics potential $V_{\text{NP}} \equiv V_{\text{NP}}(\vec{r}_1, \vec{r}_2, \vec{r}_A, \vec{r}_B; m, g_{\text{NP}})$ and a ro-vibrational level (v, J), we calculate the leading New Physics correction $\Delta E_{v,J}^{\text{NP}}$ to the Standard Model contribution $E_{v,J}^{\text{SM}}$ to first order in perturbation theory

$$\Delta E_{v,J}^{\text{NP}} = \langle \chi_{v,J} | \langle \psi_{\text{el}} | V_{\text{NP}} | \psi_{\text{el}} \rangle | \chi_{v,J} \rangle .$$
$$(9.2)$$

In this way and to leading order in m_e/μ_n, the New Physics correction enters in the same way as all the Standard Model corrections do, cf. Section 8.1. The total energy $E_{v,J}^{\text{NP}}$ is then given by

$$E_{v,J}^{\text{NP}} = E_{v,J}^{\text{SM}} + \Delta E_{v,J}^{\text{NP}} .$$
$$(9.3)$$

To evaluate Equation (9.2), we use the Born–Oppenheimer wave function ψ_{el} derived as described in Section 8.1. This means, we first evaluate the electronic part

$$\mathcal{E}^{\text{NP}}(R) = \langle \psi_{\text{el}} | \, V_{\text{NP}} \, | \psi_{\text{el}} \rangle \,, \tag{9.4}$$

on a grid for the mediator mass m, and for the nuclear separation R on which the electronic Born–Oppenheimer wave function was determined. This corresponds to a six dimensional integration

$$\mathcal{E}^{\text{NP}}(R) = \int d^3 \vec{r}_1 \int d^3 \vec{r}_2 \, |\psi_{\text{el}}(\vec{r}_1, \vec{r}_2, R)|^2 \, V_{\text{NP}} \,. \tag{9.5}$$

on each grid point, which is performed numerically in C++ using the VEGAS algorithm implemented in the GNU Scientific Library [248]. The dependence of $\mathcal{E}^{\text{NP}}$ on R and m is recovered by an interpolation with splines of degree two.

Next, one has to perform the part of the integration that includes the nuclear wave functions

$$\Delta E_{v,J}^{\text{NP}} = \langle \chi_{v,J} | \, \mathcal{E}^{\text{NP}}(R) \, | \chi_{v,J} \rangle \,, \tag{9.6}$$

with the nuclear Born–Oppenheimer wave function extracted from H2spectre in a discrete value representation (DVR). This means, Equation (9.6) turns into [227, 229]

$$\Delta E_{v,J}^{\text{NP}} = \Delta R \sum_i \chi_{v,J}(R_i) V(R_i) \chi_{v,J}(R_i) \,, \tag{9.7}$$

with the DVR grid points R_i and spacing ΔR.

In general, the potentials might be spin dependent. In case of the electrons, the spin wave function is fixed to be antisymmetric since we are considering the electronic ground state. In case of the nuclei of homonuclear molecules, however, the symmetry of the total spin wave function depends on the angular momentum quantum number J. This leads to a $2l + 1$ fold degeneracy for a total spin of l. Thus, the New Physics correction to the ground state is calculated according to degenerate perturbation theory which amounts to a diagonalisation in the degenerate subspace.

Altogether, the energy of a ro-vibrational transition $(v_1, J_1) \to (v_2, J_2)$ including New Physics effects is then given by

$$E_{(v_1,J_1)\to(v_2,J_2)}^{\text{NP}} = E_{(v_2,J_2)}^{\text{NP}} - E_{(v_1,J_1)}^{\text{NP}} \,. \tag{9.8}$$

As we are using the precise measurement and Standard Model prediction to constrain the effect of New Physics, we can safely assume that the corresponding uncertainty is much smaller than the Standard Model one, $\sigma_{\Delta E_{(v,J)}^{\text{NP}}} \ll \sigma_{E_{(v,J)}^{\text{SM}}}$. The latter can be extracted from H2spectre. Thus, the total theoretical uncertainty of an energy level is given by

$$\sigma_{E^{\text{NP}}} = \sigma_{\Delta E^{\text{NP}}} + \sigma_{E^{\text{SM}}} \approx \sigma_{E^{\text{SM}}} \,, \tag{9.9}$$

where the quantum numbers are suppressed for clarity. The error of a ro-vibrational transition, $\sigma_{E_{(v_1,J_1)\to(v_2,J_2)}^{\text{NP}}}$, is then obtained by linearly adding the uncertainties of the corresponding energy levels. We stress that the theoretical uncertainties are not added in quadrature as they do not have a statistical meaning. Additionally, some systematic uncertainties of the energy levels might cancel in the transition (9.8). However, we stay with our choice of error treatment as it is more conservative.
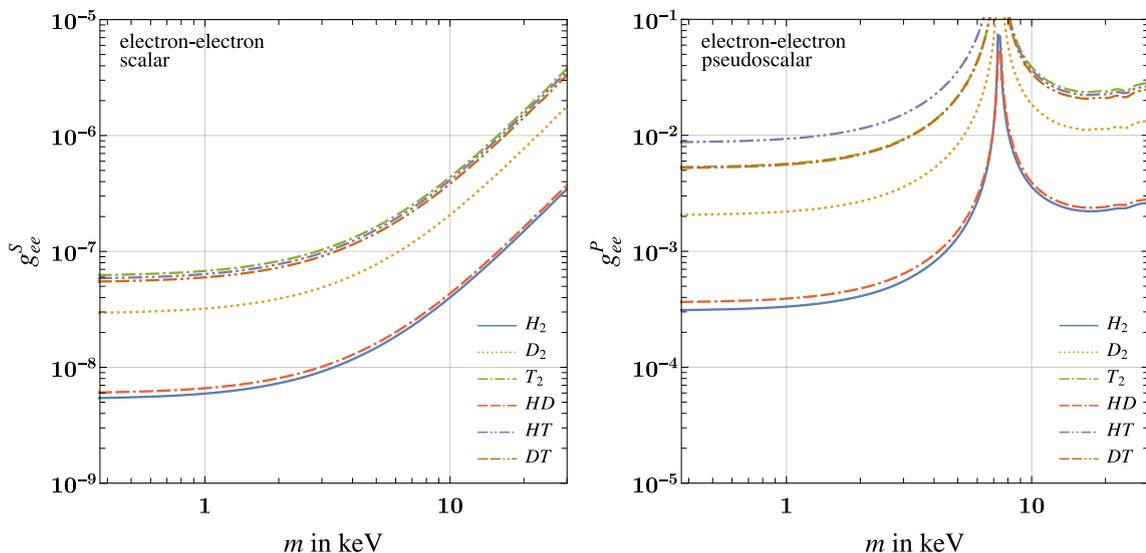
Figure 9.1.: Upper limits at $3\,\sigma$ on the scalar (left) and pseudoscalar (right) electron–electron coupling as a function of the new mediator mass m.

Since we want to determine upper limits on the New Physics couplings at the $3\,\sigma$ level, we demand—given an experimental measurement $E^{\mathrm{exp}}_{(\nu_1, J_1) \to (\nu_2, J_2)}$ of a transition $(\nu_1, J_1) \to (\nu_2, J_2)$ with an uncertainty $\sigma_{E^{\mathrm{exp}}_{(\nu_1, J_1) \to (\nu_2, J_2)}}$ —the total contribution $E^{\mathrm{NP}}_{(\nu_1, J_1) \to (\nu_2, J_2)}$ to lie within the interval

$$E^{\mathrm{exp}} - 3\,\sigma_{E^{\mathrm{exp}}} - \sigma_{E^{\mathrm{NP}}} \leq E^{\mathrm{NP}} \leq E^{\mathrm{exp}} + 3\,\sigma_{E^{\mathrm{exp}}} + \sigma_{E^{\mathrm{NP}}} \,, \tag{9.10}$$

where the quantum numbers are suppressed for clarity. Note that in Equation (9.10), the non-statistical nature of the theoretical uncertainty is made explicit since only the experimental uncertainty is multiplied by a factor of three.

9.2. New Physics: Potentials

In this section, we discuss the effect of various New Physics scenarios. We first discuss the (pseudo)scalar and (axial)vector potentials. Finally, we comment on potentials arising from effective four-particle interactions. The New Physics potentials arising from different interactions are available in the literature, for instance in Reference [249] whose notation we partially follow. Although such bounds are often plotted over several orders of magnitude in the literature, we only discuss the relevant mass scale $\mathcal{O}(\mathrm{keV})$. For higher masses the contribution drops too quickly to have an effect on molecular scales. For lighter masses it seems that the bounds saturate, see for instance Figure 9.1. However, the aforementioned Yukawa term for example cannot be distinguished from a Coulomb potential for masses $m \to 0$ such that it contributes to α_{em} which in turn has to be renormalised accordingly, see Reference [200]. This weakens the bounds for lower masses again.

Scalar and Pseudoscalar Potentials

Forces mediated by scalar (S) and pseudoscalar (P) particles occur in a plethora of New Physics scenarios. There, the new force is mediated for example by an additional Higgs
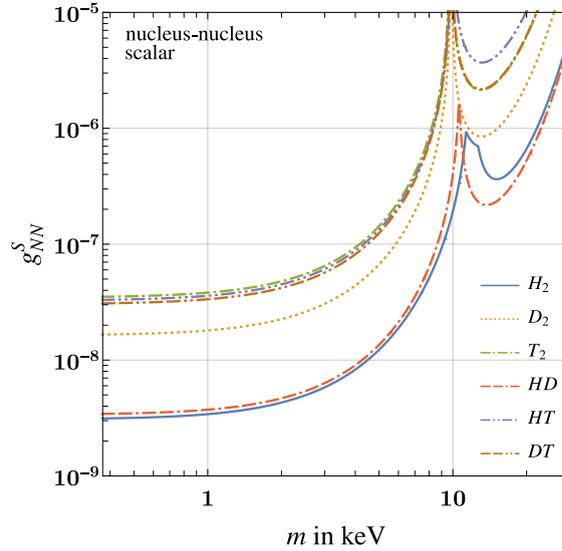
Figure 9.2.: Upper limits at $3\,\sigma$ on the scalar nucleus–nucleus couplings as a function of the new mediator mass m.

boson [199,250], axion [194,251–254], or majoron [255]. The Lagrangian for a new scalar interaction reads

$$\mathcal{L} = \phi\,\overline{\psi}\left(g_\psi^S + i\gamma_5 g_\psi^P\right)\psi\,, \tag{9.11}$$

with the scalar and pseudoscalar coupling g_ψ^S and g_ψ^P, respectively, between the fermion ψ and the new scalar ϕ. Note that at the length scale we are considering $\sim 1\,\text{Å}$, the nuclei can be considered as a fundamental particle. Hence, this interaction is absent for deuterons as they are bosonic. The corresponding non-relativistic potential is obtained by calculating the matrix element of the tree-level ϕ exchange between the fermions ψ. Taking the non-relativistic limit of the occurring spinor bilinears, and performing a subsequent Fourier transformation, one obtains the well-known potentials in position space [249]

$$V_S(\vec{r}) = -g_{ab}^S\,\frac{\mathrm{e}^{-mr}}{4\pi r}\,,$$

$$V_P(\vec{r}) = -g_{ab}^P\,\frac{m^2}{4m_a m_b}\left[(\vec{\sigma}_a\cdot\vec{\sigma}_b)\left(\frac{1}{m^2 r^2} + \frac{1}{mr} + \frac{4\pi r}{3m^2}\delta^{(3)}(\vec{r})\right)\right.$$
$$\left. - (\vec{\sigma}_a\cdot\hat{r})(\vec{\sigma}_b\cdot\hat{r})\left(1 + \frac{3}{m^2 r^2} + \frac{3}{mr}\right)\right]\frac{\mathrm{e}^{-mr}}{4\pi r}\,. \tag{9.12}$$

Here m denotes the mass of the scalar mediating the new force between the fermions a and b with masses m_a and m_b, respectively. Further, the vector $\vec{\sigma}_{a,b}$ contains the Pauli matrices and the unit vector $\hat{r}$ points from fermion b to fermion a. Inspecting the potentials in Equation (9.12), one sees that contributions from V_P are relatively suppressed by $m^2/(m_a m_b)$ compared to the scalar potential V_S. Thus, we expect $m^2/m_e^2 \sim 10^{-6}$ weaker bounds for a keV-scale mediator's coupling to electrons, and $m^2/m_N^2 \sim 10^{-11}$ weaker bounds for the coupling to nuclei.

ELECTRON–ELECTRON INTERACTION   The upper limits on the electron–electron couplings $g_{ee}^{S(P)}$ at $3\,\sigma$ are shown in Figure 9.1. For a scalar coupling g_{ee}^S, the most stringent constraints come from the measurements of H_2 and HD yielding an upper limit of $\mathcal{O}(10^{-8})$.
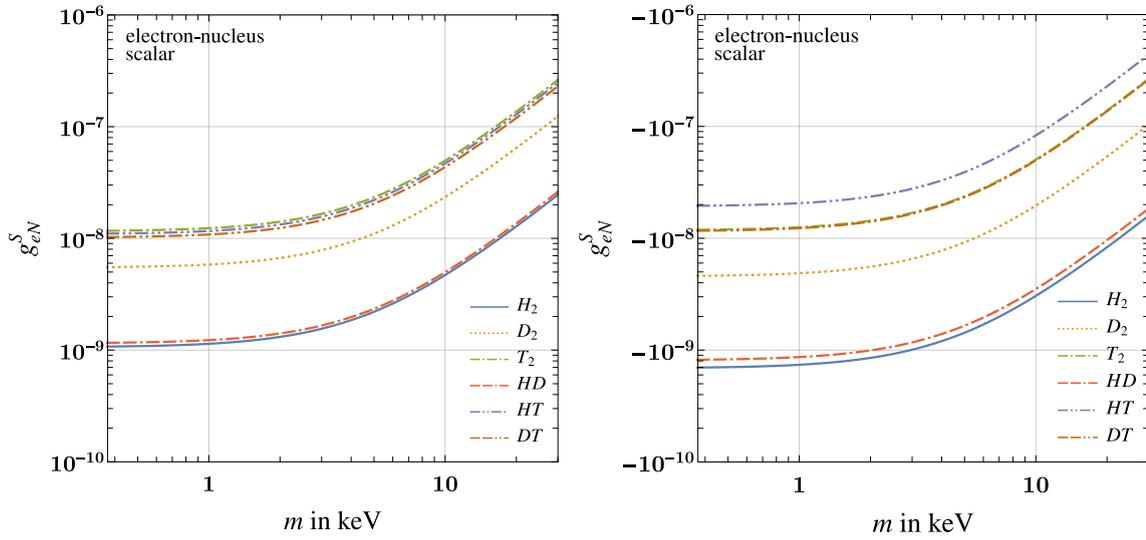
Figure 9.3.: Upper limits at 3σ on the scalar electron–nucleus coupling $g_{eN}^S > 0$ (left) $g_{eN}^S < 0$ (right) as a function of the new mediator mass m.

As expected, the pseudoscalar couplings g_{ee}^P are much weaker constrained, $g_{ee}^P \lesssim 10^{-3}$. Moreover, there is a cancellation between the two spin dependent terms in V_P, cf. Equation (9.12), such that the New Physics contribution drops for increasing masses up to $\approx 7\,\text{keV}$. Eventually, the correction changes its sign and the constraints become stronger again which explains the behaviour of the curves in Figure 9.1 right.

NUCLEUS–NUCLEUS INTERACTION   The upper limits on the nucleus–nucleus couplings g_{NN}^S are shown in Figure 9.2. Similarly to the electron–electron interaction, the most stringent constraint on the scalar coupling comes from H_2 and HD. Slightly above $10\,\text{keV}$, the constraints coming from the D_2 measurements become important. Moreover, for some transitions the New Physics contributions to the involved energy levels cancel around $10\,\text{keV}$ such that the bounds on the coupling weaken before strengthening again, cf. Figure 9.2. This is also the interaction that is usually considered in the literature, for example in References [212,237]. Notice, their $\alpha_5 = g/(4\pi)$ in our notation. The seemingly weaker bounds are owed to the different normalisation and exclusion limits as we are excluding at the more conservative choice of 3σ. We do not consider the case of a pseudoscalar interaction since the bounds are weaker by a factor $m^2/m_N^2 \sim 10^{-11}$.

ELECTRON–NUCLEUS INTERACTION   Finally, the constraints on the electron–nucleus coupling g_{eN}^S are shown in Figure 9.3. The behaviour is similar to the electron–electron case with slightly stronger bounds due to the afore-mentioned additional contributions. Moreover, the case $g_{eN}^S < 0$ yields slightly stronger bounds of $\mathcal{O}(10^{-9})$ compared to the opposite sign. Note that for the pseudoscalar potential, the spin matrix elements vanish for the electronic ground state.

Vector and Axialvector Potentials

New vector and axialvector interactions arise for example from an additional $U(1)$ gauge group usually introduced in models containing a dark photon. The dark photon mixes with the Standard Model photon, and thus, enters the interactions with the Standard Model fermions resulting in a Lagrangian of the type

$$\mathcal{L} = A'_{\mu} \overline{\psi} \gamma^{\mu} \left(g^V_{\psi} + i\gamma_5 g^A_{\psi} \right) \psi . \tag{9.13}$$

Here A'_{μ} denotes the new spin 1 gauge field with the vector and axialvector couplings to the fermion ψ, g^V_{ψ} and g^A_{ψ}, respectively. This interaction Lagrangian results in the following non-relativistic potentials [249]

$$V_V(\vec{r}) = \frac{g^V_{ab}}{4\pi} \frac{e^{-mr}}{r} \Bigg\{ 1 + $$
$$\frac{m^2}{4m_a m_b} \left[\vec{\sigma}_a \cdot \vec{\sigma}_b \left(\frac{1}{m^2 r^2} + \frac{1}{mr} + 1 - \frac{8\pi r}{3m^2} \delta^{(3)}(\vec{r}) \right) \right.$$
$$\left. - (\vec{\sigma}_a \cdot \hat{r})(\vec{\sigma}_b \cdot \hat{r}) \left(\frac{3}{m^2 r^2} + \frac{3}{mr} + 1 \right) \right] \Bigg\}, \tag{9.14}$$

$$V_A(\vec{r}) = -\frac{g^A_{ab}}{4\pi} \frac{e^{-mr}}{r} \Bigg\{ \vec{\sigma}_a \cdot \vec{\sigma}_b \left[1 + \frac{1}{m^2 r^2} + \frac{1}{mr} + \frac{4\pi r}{3m^2} \delta^{(3)}(\vec{r}) \right]$$
$$- (\vec{\sigma}_a \cdot \hat{r})(\vec{\sigma}_b \cdot \hat{r}) \left[1 + \frac{3}{m^2 r^2} + \frac{3}{mr} \right] \Bigg\}. \tag{9.15}$$

with the same definitions as in Equation (9.12). Since $m^2/(m_a m_b) \ll 1$ for keV-scale mediators that couple to electrons and nuclei, the leading contribution to the vector potential is given by the scalar potential up to a relative sign

$$V_V(\vec{r}) = \frac{g^V_{ab}}{4\pi} \frac{e^{-mr}}{r} = -V_S(\vec{r})\big|_{g^V_{ab} \to g^S_{ab}} . \tag{9.16}$$

Moreover, the leading axialvector contribution remains unsuppressed compared to the pseudoscalar contribution, and thus, we also expect strong bounds coming from an axialvector exchange.

ELECTRON–ELECTRON INTERACTION   The bounds on the electron–electron vector interaction are shown in Figure 9.4. As expected, the constraints for a vector electron–electron coupling are very close to the scalar coupling with the strongest bounds coming from H_2 and HD yielding an upper limit of $\mathcal{O}(10^{-8})$. The same lines yield the strongest bounds for the axialvector coupling which is even stronger constrained $g^A_{ee} \lesssim 10^{-11}$.

NUCLEUS–NUCLEUS INTERACTION   The upper limits on the nucleus–nucleus vector couplings are shown in Figure 9.5. The bounds on the coupling g^V_{NN} are similar to the corresponding ones from the scalar coupling while the axialvector coupling g^A_{NN} is most stringently constrained by H_2 yielding an upper bound of $g^A_{NN} \lesssim 10^{-10}$.

ELECTRON–NUCLEUS INTERACTION   The spin matrix elements vanish again for the electronic ground state, thus, the result of the vector potential with $g^V_{eN} > 0$ equals the one of the scalar potential in Figure 9.3 with $g^S_{eN} < 0$ and the other way around. For the same reason, the corrections due to an axialvector interaction vanish as in the pseudoscalar case.
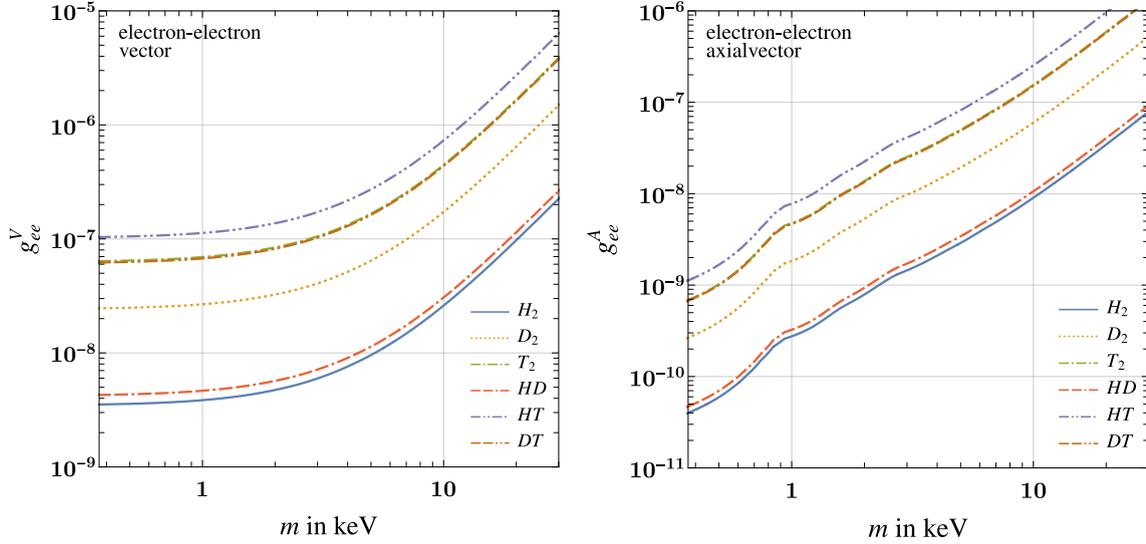
Figure 9.4.: Upper limits at $3\,\sigma$ on the vector (left) and axialvector (right) electron–electron couplings as a function of the new mediator mass m.

Effective Contact Interaction

FERMIONIC EXCHANGE POTENTIAL   In the Standard Model there is a long-range interaction resulting from a double insertion of the effective four-fermion operator, see Figure 9.6, resulting in a two neutrino exchange potential [256, 257]

$$V(r) = \frac{G_F^2}{16\pi^3 r^5} \, , \tag{9.17}$$

with the Fermi constant G_F. We know that neutrinos are not massless, in the case of Majorana and Dirac type neutrinos, the potentials read [258]

$$V_M(r) = \frac{G_{\text{eff}}^2 m_\nu^2}{8\pi^2 r^3} K_2(2m_\nu r) \overset{m_\nu r \gg 1}{\approx} \frac{G_{\text{eff}}}{16\pi^2 r^2} \sqrt{\frac{m_\nu^3}{\pi r^3}} e^{-2m_\nu r} \, ,$$

$$V_D(r) = \frac{G_{\text{eff}}^2 m_\nu^3}{16\pi^3 r^2} K_3(2m_\nu r) \overset{m_\nu r \gg 1}{\approx} \frac{G_{\text{eff}}}{32\pi^2} \sqrt{\frac{m_\nu^5}{\pi r^5}} e^{-2m_\nu r} \, , \tag{9.18}$$

with the neutrino mass m_ν and the modified Bessel functions $K_{2,3}$. G_{eff} denotes the effective coupling, which in the Standard Model corresponds to the Fermi constant G_F. Note that for $m_\nu \to 0$ both potentials in Equation (9.18) yield the one of Equation (9.17).

One might attempt to calculate the effect of these potentials at atomic and molecular scales as for example done in a recent paper [259]. However, the wave functions do not necessarily vanish at the origin $r = 0$, instead the integral exhibits a quadratic divergence which has also been observed in the very same Reference [259]. For instance, in case of the electron–electron interaction this can be seen by introducing spherical coordinates for the relative position of the two electrons r_{12}. In this case the r_{12} integration yields

$$\Delta E^{NP} \sim \int \mathrm{d}^3 \vec{r}_1 \int \mathrm{d}^3 \vec{r}_2 \, |\psi(\vec{r}_1, \vec{r}_2, R)|^2 \, V(r_{12}) \sim \int \mathrm{d}^3 \vec{r} \int \mathrm{d}\Omega \int_\Lambda^\infty \mathrm{d}r_{12} \frac{r_{12}^2}{r_{12}^5} \sim \frac{1}{\Lambda^2} \, . \tag{9.19}$$

In Reference [259] a cutoff at the Z boson mass has been introduced, $\Lambda \sim m_Z$, and stringent bounds for the electron–electron coupling from positronium and muonium spectroscopy
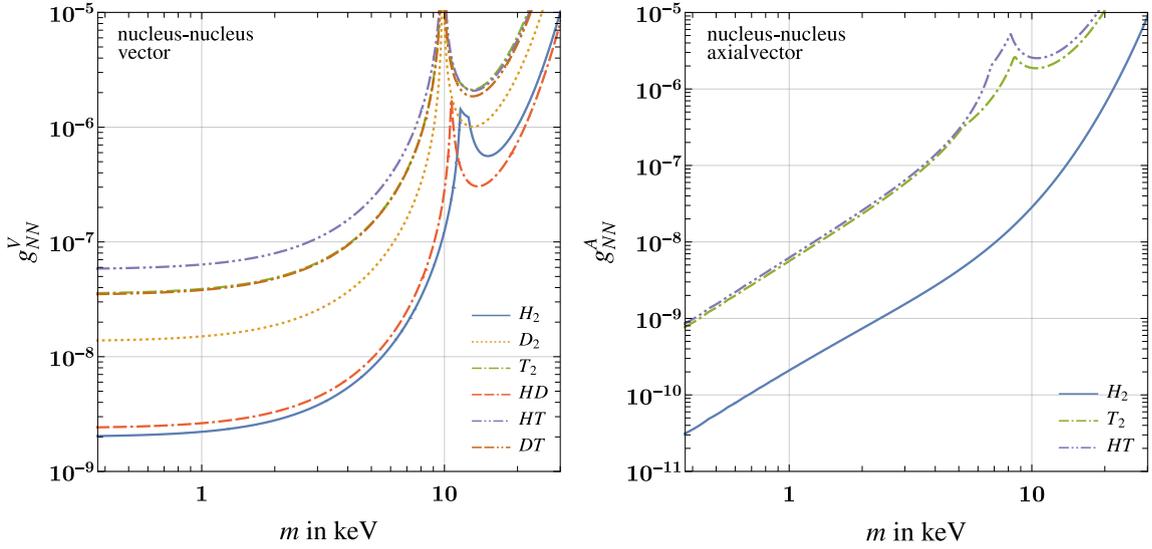
Figure 9.5.: Upper limits at $3\,\sigma$ on the vector (left) and axialvector (right) nucleus–nucleus coupling as a function of the new mediator mass m.

are derived. The authors of Reference [259] conclude that current atomic and molecular spectroscopy are only two orders of magnitude away from being sensitive to Standard Model neutrino effects. However, this is fallacious, as the result strongly depends on the chosen cutoff parameter, which points towards an incorrect treatment of the divergences. And indeed, the non-relativistic description already breaks down far below the Z boson mass. Relativistic effects become important at the electron mass m, or in terms of length, at the Compton wavelength of the electron. However, the momentum of the electrons is $m\alpha$, and thus, it is not clear what should be chosen as a cutoff scale. In any case, the divergence points to missing contributions as in the derivation of the long range potential in Equation (9.17) the hard scale contributions were dropped since they correspond to delta functions in position space. Such contributions, on the other hand, introduce infrared divergences at the hard scale which should cancel the soft scale ultraviolet divergences if all contributions are included, and matched correctly to the non-relativistic quantum field theory. This should be similar to the higher order corrections to helium [260] and positronium [261, 262] where the occurring operators are too singular and the expectation values with the non-relativistic wave functions are divergent [260]. There, dimensional regularisation is applied and one can explicitly see the cancellation of the singularites in the sum of the long and short range contribution [261]. For an illuminating discussion see Reference [260].

The two-neutrino exchange potential has also been analysed in the context of atomic parity violation [263, 264]. There, the appearing wave functions drop quickly for $r \to 0$ and the integrals are finite. However, the effect is, as one intuits, far below the current experimental sensitivity.

BOSONIC EXCHANGE POTENTIAL   Similarly to the two-neutrino exchange potential, a long-range potential arises in the presence of an additional (pseudo)scalar boson a coupling to the Standard Model Higgs boson H[1], see Figure 9.6. The interaction Lagrangian is given by

$$\mathcal{L} = g_{Haa}\, aaH\,, \tag{9.20}$$

---

[1]Or to an additional scalar which couples to the Standard Model fermions.
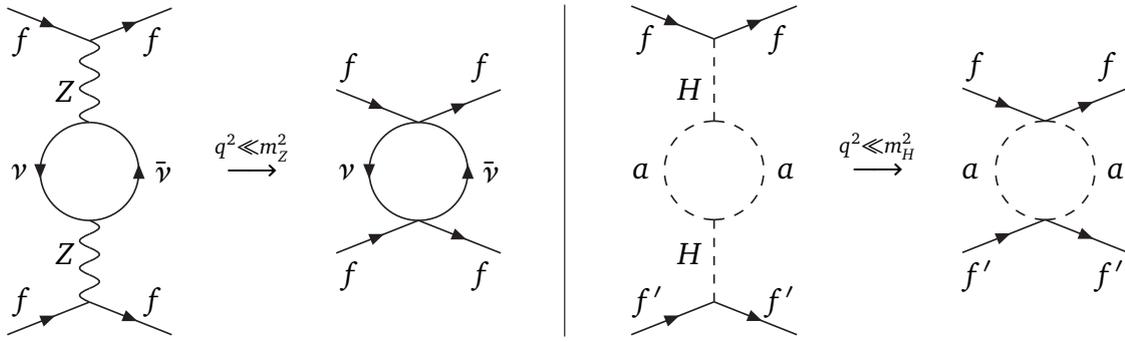
Figure 9.6.: Integrating out the Z (left) or Higgs (right) boson results in an effective four-particle interaction such that a long-range force is mediated by neutrinos ν (left) or additional (pseudo)scalars a (right).

with the New Physics coupling g_{Haa}. This leads to a potential of the form [265]

$$V(r) = -\frac{Gm}{8\pi^3 r^2} K_1(2mr), \tag{9.21}$$

where K_1 denotes the modified Bessel function, and m the mass of the new (pseudo)scalar mediator. The coupling strength G reads

$$G = \frac{g_{Hff}g_{Hf'f'}g_{Haa}^2}{m_H^4} \sim 10^{-19}\,\mathrm{GeV}^{-4}\,g_{Haa}^2, \tag{9.22}$$

in the case of the Standard Model Higgs field. Since this coupling is tiny, no observable effects in atomic and molecular spectroscopy are expected.

CHAPTER 10

Final Remarks

We have performed the first extensive and comprehensive study of New Physics at molecular scales. Using the precise Standard Model predictions available in the literature, we have derived constraints on the new couplings of several New Physics potentials which we have treated in the same manner as the leading order corrections in m_e/μ_n of higher orders in α_{em} in the Standard Model. Compared to the stronger astrophysical and cosmological bounds, these constraints stem from *direct* measurements.

Let us briefly compare our results to existing bounds in the literature. The electron–nucleus coupling is also constrained by atomic spectroscopy which yields up to three orders of magnitude stronger bounds [200]. Similarly, the constraints on new nucleus interactions derived from neutron scattering experiments are up to three orders of magnitude stronger [266]. However, the bounds we derive are on nucleus couplings compared to new couplings to nucleons, in particular neutrons as probed by neutron scattering experiments. For the same reason the bounds derived on the New Physics couplings in Reference [237] from molecular spectroscopy appear to be stronger than the ones from our derivation. There, the coupling between the nucleons has been considered, and thus, considering for example T_2, and assuming coherent effects, this yields a constraint stronger by a combinatorial factor of nine on the nucleon coupling compared to a nucleus–nucleus coupling. However, as we are considering length scales of $\mathcal{O}(\mathring{A})$, we prefer giving the constraints in terms of a nucleus coupling. Lastly, the coupling between electrons is probed by helium spectroscopy [201] and measurements of the anomalous magnetic moment of the electron. While our bounds are competitive with the former, the constraints from the latter are up to two orders of magnitude stronger. Nonetheless, molecular spectroscopy is interesting from a theoretical point of view as it allows to constrain a variety of New Physics interactions between *different* types of particles in one single measurement—in contrast to all the afore-mentioned laboratory measurements.

Effects from long-range potentials mediated by neutrinos are not expected to have a measurable effect on molecular and atomic spectra in the foreseeable future, contrary to recent claims in the literature. These claims are due to the fact that a consistent treatment of this potential from the hard scale down to the soft scale, as needed for atomic and molecular spectroscopy, is missing in the corresponding literature.

Final Conclusion and Outlook

Since the main physical results have been summarised along the way, we return to the big picture. We have first shown that it is possible to solve the b anomalies within the R-parity conserving MSSM despite all the claims in the literature. If the anomalous measurements are further confirmed in the near future, this has crucial implications on the phenomenology of the MSSM since this explanation implies falsifiable predictions. Among those implications are the sub-TeV sleptons. This suggests that a sophisticated collider analysis should be performed in order to confirm or rule out this possibility. Additionally, future measurements in $b \to s\tau\tau$ help to sort this possibility out. Further, measurements of $b \to dll$ processes are important in order to determine the nature of the New Physics. For this reason, we have investigated the decays $B \to Pll$ with the pseudoscalar P. While the experimental uncertainties are going to be reduced to $\mathcal{O}(1\%)$ in the upcoming experiments at LHCb, the theoretical uncertainty is currently dominated by the form factor errors. Nevertheless, the upcoming and ongoing measurements at LHCb and Belle II, will reveal if there is New Physics. In that case, further work to reduce the theoretical uncertainties in hadronic $b \to dll$ is required to unlock the detailed nature of the New Physics.

In Part II, we have inspected the general 2HDM with spontaneous CP violation. Contrary to the claim in the literature that it is difficult to distinguish between explicit and spontaneous CP violation [267], we have presented clear phenomenological differences and provided a sum rule which might help to determine the primary origin of CP violation in Nature. Motivated by this sum rule, we subsequently examined the collider phenomenology. Unfortunately, the searches for the relevant signatures within the context of 2HDMs did not yet gain much impetus from the experimental side. Nevertheless, using and recasting available searches we were able to derive stringent limits on the parameter space. In the light of the upcoming LHC runs, another work regarding the collider signatures is currently underway. However, this still has to be pursued by the experimental collaborations in order to draw a final conclusion regarding the primary origin of CP violation.

Finally, in Part III, a model-independent analysis of light New Physics—as they often arise in models aimed at solving the strong CP puzzle or providing a dark matter candidate— has been performed. For this, the effects of a variety of New Physics potentials on molecular spectra of hydrogen isotopologues are calculated. Even though it has turned

out that single interactions between the constituents are similarly or even stronger constrained by experiments like atomic spectroscopy, neutron scattering or measurements of the anomalous magnetic moments, molecular spectroscopy is interesting since single measurements constrain different interactions between all constituents.

PART IV

Appendices

Mass Matrices

For completeness, we list here the general mass matrices of the Higgs and gaugino sectors.

Higgs Sector

The neutral scalar Higgs mass matrix M_H reads in the general CP conserving case [29]

$$M_H^2 = \begin{pmatrix} -m_{12}^2 \frac{v_u}{v_d} + \frac{e^2 v_d^2}{2s_W^2 c_W^2} & m_{12}^2 - \frac{e^2 v_d v_u}{2s_W^2 c_W^2} \\ m_{12}^2 - \frac{e^2 v_d v_u}{2s_W^2 c_W^2} & -m_{12}^2 \frac{v_d}{v_u} + \frac{e^2 v_u^2}{2s_W^2 c_W^2} \end{pmatrix}, \tag{A.1}$$

and is diagonalised by the rotation Z_R [29]

$$\text{Re}(H_i^i) = \frac{1}{\sqrt{2}} Z_R^{ij} H_j^0 + v_i, \tag{A.2}$$

implying

$$Z_R^T m_H^2 Z_R = \begin{pmatrix} m_{H_1^0}^2 & 0 \\ 0 & m_{H_2^0}^2 \end{pmatrix}, \qquad Z_R = \begin{pmatrix} c_\alpha & -s_\alpha \\ s_\alpha & c_\alpha \end{pmatrix}, \tag{A.3}$$

with $s_\alpha \equiv \sin \alpha$, $c_\alpha \equiv \cos \alpha$, $H_1^1 = H_d^1$ and $H_2^2 = H_u^2$. And indeed, for $v_d \to 0$ we recover Equation (2.18).

Gaugino Sector

Here we consider the chargino and neutralino sector of the MSSM.

Chargino sector

The chargino mixing matrix M_χ is given by [29]

$$M_\chi = \begin{pmatrix} M_2 & \frac{e v_u}{s_W} \\ \frac{e v_d}{s_W} & \mu \end{pmatrix}, \tag{A.4}$$

and is diagonalised by the bi-unitary transformation

$$Z_-^T M_\chi Z_+ = \begin{pmatrix} m_{\chi_1} & 0 \\ 0 & m_{\chi_2} \end{pmatrix}, \qquad m_{\chi_i} > 0, \; i = 1, 2. \qquad (A.5)$$

Z_- and Z_+ can be determined by diagonalising $M_\chi^\dagger M_\chi$ and $M_\chi M_\chi^\dagger$, respectively. A perturbative diagonalisation yields

$$m_{\chi_1}^2 = M_2^2, \qquad m_{\chi_2}^2 = \mu^2, \qquad (A.6)$$

up to $\mathcal{O}(v^2/M_{\text{SUSY}})$ and for real mass parameters.

Neutralino sector

The neutralino mass matrix M_N reads [29]

$$M_N = \begin{pmatrix} M_1 & 0 & \dfrac{-ev_d}{\sqrt{2}c_W} & \dfrac{ev_u}{\sqrt{2}c_W} \\ 0 & M_2 & \dfrac{ev_d}{\sqrt{2}s_W} & \dfrac{-ev_u}{\sqrt{2}s_W} \\ \dfrac{-ev_d}{\sqrt{2}c_W} & \dfrac{ev_d}{2s_W} & 0 & -\mu \\ \dfrac{ev_u}{\sqrt{2}c_W} & \dfrac{-ev_u}{2s_W} & -\mu & 0 \end{pmatrix}, \qquad (A.7)$$

and is diagonalised by the unitary matrix Z_N obtained through Takagi's factorisation

$$Z_N^T M_N Z_N = \text{diag}(m_{\chi_1^0}, m_{\chi_2^0}, m_{\chi_3^0}, m_{\chi_4^0}). \qquad (A.8)$$

The masses read

$$m_{\chi_1^0}^2 = M_1^2, \qquad m_{\chi_2^0}^2 = M_2^2, \qquad m_{\chi_3^0}^2 = \mu^2, \qquad m_{\chi_4^0}^2 = \mu^2, \qquad (A.9)$$

up to $\mathcal{O}(v^2/M_{\text{SUSY}})$ and for real mass parameters.

Loop Functions

Here we list the loop functions used in this work. The two- and four-point functions with vanishing external momenta are defined as [63, 88]

$$
B_0(m_1^2, m_2^2) = (4\pi)^2 \int \frac{\mathrm{d}^d k}{(2\pi)^d} \frac{-i}{(k^2 - m_1^2)(k^2 - m_2^2)},
$$

$$
D_{2n}(m_1^2, m_2^2, m_3^2, m_4^2) = (4\pi)^2 \int \frac{\mathrm{d}^d k}{(2\pi)^d} \frac{i k^{2n}}{\prod_{i=1}^4 (k^2 - m_i^2)}. \tag{B.1}
$$

Notice that we define the two- and four-point function with a relative sign. With these definitions, the two-point function reads [88]

$$
B_0(m_1^2, m_2^2) = 1 + \frac{m_1^2 \log\left(Q^2/m_1^2\right) - m_2^2 \log\left(Q^2/m_2^2\right)}{m_1^2 - m_2^2}, \tag{B.2}
$$

and the four-point functions D_0 and D_2 are given by [63]

$$
\begin{aligned}
D_0(m_1^2, m_2^2, m_3^2, m_4^2) &= \frac{m_2^2 \log\left(m_2^2/m_1^2\right)}{(m_2^2 - m_1^2)(m_2^2 - m_3^2)(m_2^2 - m_4^2)} \\
&+ \frac{m_3^2 \log\left(m_3^2/m_1^2\right)}{(m_3^2 - m_1^2)(m_3^2 - m_2^2)(m_3^2 - m_4^2)} \\
&+ \frac{m_4^2 \log\left(m_4^2/m_1^2\right)}{(m_4^2 - m_1^2)(m_4^2 - m_2^2)(m_4^2 - m_3^2)}, \\
D_2(m_1^2, m_2^2, m_3^2, m_4^2) &= \frac{\left(m_2^2\right)^2 \log\left(m_2^2/m_1^2\right)}{(m_2^2 - m_1^2)(m_2^2 - m_3^2)(m_2^2 - m_4^2)} \\
&+ \frac{\left(m_3^2\right)^2 \log\left(m_3^2/m_1^2\right)}{(m_3^2 - m_1^2)(m_3^2 - m_2^2)(m_3^2 - m_4^2)} \\
&+ \frac{\left(m_4^2\right)^2 \log\left(m_4^2/m_1^2\right)}{(m_4^2 - m_1^2)(m_4^2 - m_2^2)(m_4^2 - m_3^2)}.
\end{aligned} \tag{B.3}
$$

Further, we define

$$
\begin{aligned}
\tilde{B}(m_1^2, m_2^2, m_3^2, m_4^2) &= \left(m_1^2 - m_2^2\right) B_0\left(m_3^2, m_4^2\right) \\
&\quad + \left(m_2^2 - m_3^2\right) B_0\left(m_1^2, m_4^2\right) \\
&\quad + \left(m_3^2 - m_1^2\right) B_0\left(m_2^2, m_4^2\right), \\
D_2^0(m_1^2, m_2^2, m_3^2, m_4^2) &= D_2(m_1^2, m_2^2, m_3^2, m_4^2) + 2m_1 m_2 D_0(m_1^2, m_2^2, m_3^2, m_4^2).
\end{aligned} \tag{B.4}
$$

Input Parameters

Unless noted otherwise, we use the input parameters that are shown in Table C.1. The QCD running of the quark masses and the strong coupling constant is performed in RunDec [268]. The CKM matrix is taken from the summer 2016 results of the UTfit collaboration [269]. For the used form factors see the discussion in Section 3.1 below Equation (3.22).

Table C.1.: Input parameters used in this work.

parameter	value	ref.	parameter	value	ref.
m_W	$80.379(12)\,\text{GeV}$	[83]	$m_{K^\pm}$	$0.494\,\text{GeV}$	[270]
m_Z	$91.1876(21)\,\text{GeV}$	[83]	m_{K^0}	$0.498\,\text{GeV}$	[270]
$m_s(2\,\text{GeV})$	$93^{+11}_{-5}\,\text{MeV}$	[83]	$m_{\pi^\pm}$	$0.13957\,\text{GeV}$	[270]
$m_c(3\,\text{GeV})$	$0.993(8)\,\text{GeV}$	[271]	m_{π^0}	$0.13498\,\text{GeV}$	[270]
$m_b(m_b)$	$4.163(16)\,\text{GeV}$	[272]	f_B	$0.202^{+35}_{-21}\,\text{GeV}$	[138]
$m_{c,\text{pole}}$	$1.67(7)\,\text{GeV}$	[83]	f_{B_s}	$0.222^{+38}_{-24}\,\text{GeV}$	[138]
$m_{b,\text{pole}}$	$4.78(6)\,\text{GeV}$	[83]	f_K	$0.156\,\text{GeV}$	[273]
$m_{t,\text{pole}}$	$173.1(9)\,\text{GeV}$	[270]	f_π	$0.130\,\text{GeV}$	[273]
m_B	$5.279\,\text{GeV}$	[270]	λ_B	$0.46(11)\,\text{GeV}$	[274]
m_{B_d}	$5.280\,\text{GeV}$	[270]	a_1^K	0.0525^{+31}_{-33}	[275]
m_{B_s}	$5.367\,\text{GeV}$	[270]	a_2^K	0.106^{+15}_{-16}	[275]
m_{B^*}	$5.325\,\text{GeV}$	[270]	a_2^π	$0.22\text{–}0.33$	[276]
$m_{B_s^*}$	$5.415\,\text{GeV}$	[270]	a_4^π	$0.12\text{–}0.25$	[276]

Breakdown of the Uncertainties in the $B \to Pll$ Transitions

In this appendix, we break down the uncertainties of the theoretical predictions from Section 3.1. To estimate the error from the different input parameters, we vary the masses, the CKM matrix elements, the form factors and decay constants, the power corrections, the renormalisation scale and the remaining hadronic parameters separately. The results in the low and high q^2 region are shown in Figure D.1. As one can see, the largest uncertainty of all branching ratios comes from the form factors followed by the uncertainties of the CKM matrix elements. The errors shown in the legend are sorted according to their size. We also show the theory prediction of the branching ratios with a quadratic addition of the uncertainties in Table D.1.

Table D.1.: Theoretical predictions of the branching ratios $\mathrm{BR}(B \to Pll)$ adding the different types of uncertainties in quadrature.

decay	$[1,6]\,\mathrm{GeV}^2$	$[17,22]\,\mathrm{GeV}^2$
$\mathrm{BR}(B \to \pi ll) \times 10^9$	6.63 ± 1.29	5.05 ± 0.52
$\mathrm{BR}(B_d \to \pi ll) \times 10^9$	4.47 ± 0.50	4.69 ± 0.48
$\mathrm{BR}(B_s \to Kll) \times 10^9$	8.03 ± 1.03	4.20 ± 0.63

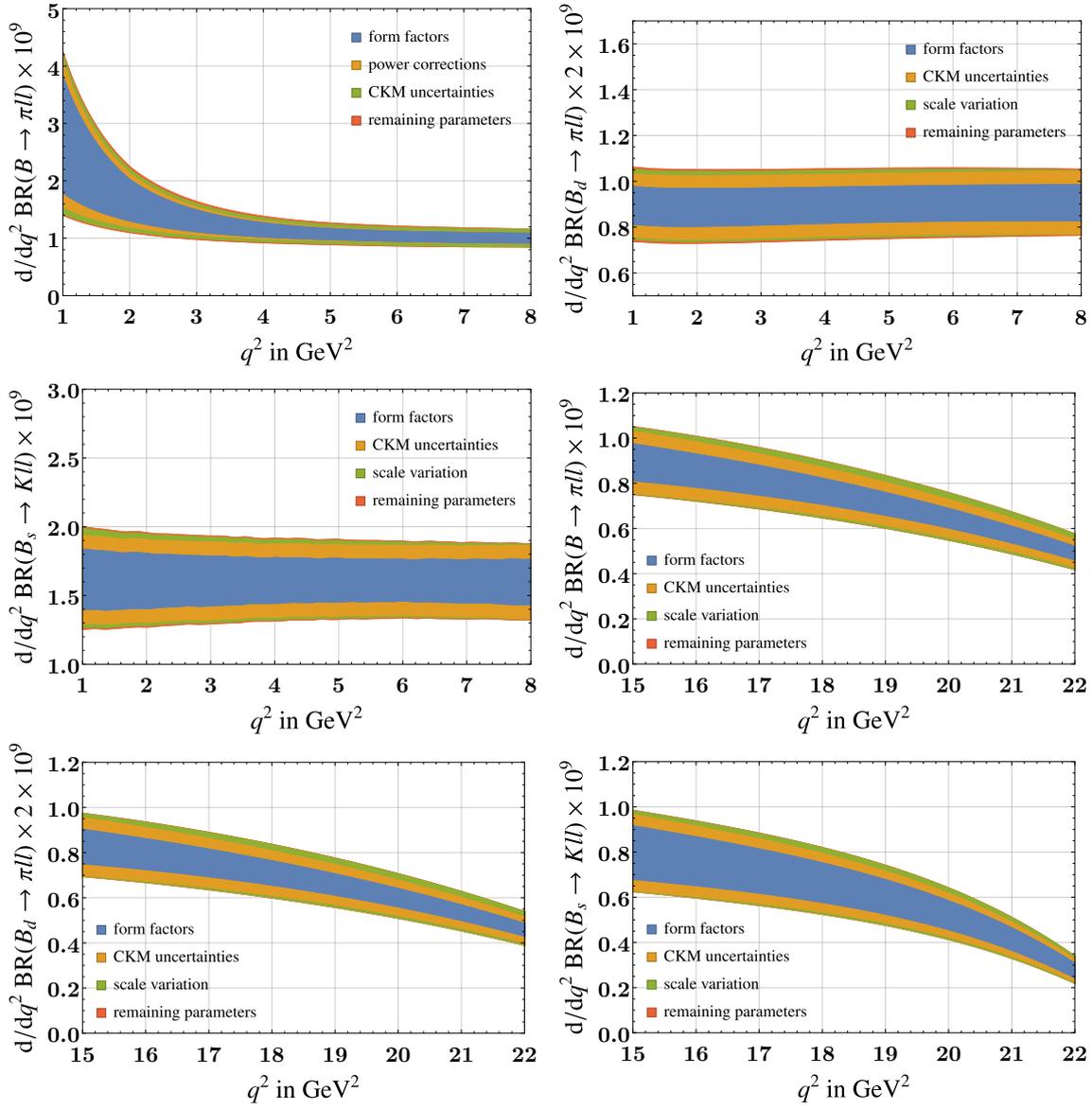**Figure D.1.:** Breakdown of the uncertainties of the differential branching ratios of $B \to \pi ll$, $B_d \to \pi ll$, and $B_s \to K ll$.

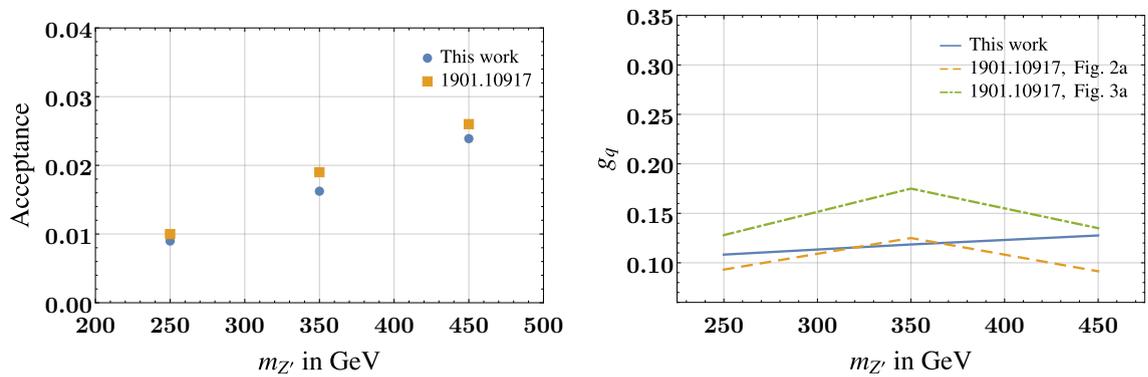## Comparison with the Experimental Analysis

Figure E.1.: Comparison of the acceptance (left) and of the limit on the coupling (right) between our analysis and the experimental analysis from Reference [171] (1901.10917).

Here we cross-check our analysis procedure which we used to recast the results of Reference [171], cf. Section 6.5. For this we apply our code to the Z' model that has been analysed in the very same reference. This enables a direct comparison between our analysis and the experimental one. The data for the process $pp \rightarrow \gamma Z'(\rightarrow jj)$ is generated in `MadGraph5_aMC@NLO` using the vector-leptoquark model file of Reference [277]. The acceptance of our procedure is shown together with the acceptance of the experimental analysis, that can be found in the auxiliary materials of Reference [171], in Figure E.1. Further, we determine the limits on the coupling as described in Section 6.5. The result is shown in Figure E.1 where we overlaid the results of Reference [171]. Both results show a good agreement with the more sophisticated experimental analysis.

Experimental Input for Part III

All experimental measurements used in our analysis in Section 9.2 to constrain New Physics are listed here. Measurements in heteronuclear and homonuclear hydrogen isotopologues are shown in Table F.1 and Table F.2, respectively. Note the updated measurements compared to Reference [193].

Table F.1.: List of all measurements of the transitions $(\nu_1, J_1) \to (\nu_2, J_2)$ used in the analysis in Section 9.2. All numbers are given in cm^{-1}.

molecule	transition	energy	reference
HD	$(1,0) \to (0,0)$	3632.16052(22)	[242]
HD	$(1,1) \to (0,1)$	3628.30450(22)	[242]
HD	$(2,2) \to (0,1)$	7241.84935087(67)	[278]
HD	$(2,3) \to (0,2)$	7306.48322250(93)	[278]
HD	$(2,4) \to (0,3)$	7361.90317335(93)	[278]
DT	$(1,0) \to (0,0)$	2743.34160(42)	[238]
DT	$(1,1) \to (0,1)$	2741.73204(39)	[238]
DT	$(1,2) \to (0,2)$	2738.51662(42)	[238]
DT	$(1,3) \to (0,3)$	2733.70479(42)	[238]
DT	$(1,4) \to (0,4)$	2727.30745(42)	[238]
DT	$(1,5) \to (0,5)$	2719.34221(42)	[238]
HT	$(1,0) \to (0,0)$	3434.81248(53)	[238]
HT	$(1,1) \to (0,1)$	3431.57509(53)	[238]
HT	$(1,2) \to (0,2)$	3425.11265(53)	[238]
HT	$(1,3) \to (0,3)$	3415.45258(53)	[238]

Table F.2.: List of all measurements of the transitions $(v_1, J_1) \rightarrow (v_2, J_2)$ used in the analysis in Section 9.2. All numbers are given in cm^{-1}.

molecule	transition	energy	reference
H_2	$(3,5) \rightarrow (0,3)$	12559.74952(5)	[279]
H_2	$(1,0) \rightarrow (0,0)$	4161.16636(15)	[242]
H_2	$(1,1) \rightarrow (0,1)$	4155.25400(21)	[242]
H_2	$(1,2) \rightarrow (0,2)$	4143.46553(15)	[242]
H_2	$(11,1) \rightarrow (0,0)$	32937.7554(16)	[280]
H_2	$(11,3) \rightarrow (0,0)$	33186.4791(16)	[280]
H_2	$(11,4) \rightarrow (0,0)$	33380.1025(33)	[280]
H_2	$(11,5) \rightarrow (0,0)$	33615.5371(18)	[280]
D_2	$(1,0) \rightarrow (0,0)$	2993.61706(15)	[242]
D_2	$(1,1) \rightarrow (0,1)$	2991.50706(15)	[242]
D_2	$(1,2) \rightarrow (0,2)$	2987.29352(15)	[242]
D_2	$(0,2) \rightarrow (0,0)$	179.068(2)	[281]
D_2	$(0,3) \rightarrow (0,1)$	297.533(3)	[281]
D_2	$(0,4) \rightarrow (0,2)$	414.648(2)	[281]
T_2	$(1,0) \rightarrow (0,0)$	2464.50394(67)	[238]
T_2	$(1,1) \rightarrow (0,1)$	2463.34817(42)	[238]
T_2	$(1,2) \rightarrow (0,2)$	2461.03917(42)	[238]
T_2	$(1,3) \rightarrow (0,3)$	2457.58135(42)	[238]
T_2	$(1,4) \rightarrow (0,4)$	2452.98233(42)	[238]
T_2	$(1,5) \rightarrow (0,5)$	2447.25061(42)	[238]

Bibliography

[1] M. Tabet, *Spontaneous CP-Violation in the Two-Higgs-Doublet Model of Type-III.* Master thesis, KIT, Karlsruhe, February, 2018.

[2] **LHCb** Collaboration, R. Aaij *et al.*, "Test of lepton universality in beauty-quark decays," `arXiv:2103.11769 [hep-ex]`.

[3] M. Bordone, G. Isidori, and A. Pattori, "On the Standard Model predictions for R_K and R_{K^*}," *Eur. Phys. J. C* **76** no. 8, (2016) 440, `arXiv:1605.07633 [hep-ph]`.

[4] **LHCb** Collaboration, R. Aaij *et al.*, "Test of lepton universality using $B^+ \to K^+ \ell^+ \ell^-$ decays," *Phys. Rev. Lett.* **113** (2014) 151601, `arXiv:1406.6482 [hep-ex]`.

[5] **LHCb** Collaboration, R. Aaij *et al.*, "Test of lepton universality with $B^0 \to K^{*0} \ell^+ \ell^-$ decays," *JHEP* **08** (2017) 055, `arXiv:1705.05802 [hep-ex]`.

[6] **BaBar** Collaboration, B. Aubert *et al.*, "Measurements of branching fractions, rate asymmetries, and angular distributions in the rare decays $B \to K\ell^+\ell^-$ and $B \to K^*\ell^+\ell^-$," *Phys. Rev. D* **73** (2006) 092001, `arXiv:hep-ex/0604007`.

[7] **BaBar** Collaboration, J. P. Lees *et al.*, "Measurement of Branching Fractions and Rate Asymmetries in the Rare Decays $B \to K^{(*)}l^+l^-$," *Phys. Rev. D* **86** (2012) 032012, `arXiv:1204.3933 [hep-ex]`.

[8] **Belle** Collaboration, J. T. Wei *et al.*, "Measurement of the Differential Branching Fraction and Forward-Backword Asymmetry for $B \to K^{(*)}\ell^+\ell^-$," *Phys. Rev. Lett.* **103** (2009) 171801, `arXiv:0904.0770 [hep-ex]`.

[9] **Belle** Collaboration, A. Abdesselam *et al.*, "Test of lepton flavor universality in $B \to K^*\ell^+\ell^-$ decays at Belle," `arXiv:1904.02440 [hep-ex]`.

[10] **BELLE** Collaboration, S. Choudhury *et al.*, "Test of lepton flavor universality and search for lepton flavor violation in $B \to K\ell\ell$ decays," *JHEP* **03** (2021) 105, `arXiv:1908.01848 [hep-ex]`.

[11] **LHCb** Collaboration, R. Aaij *et al.*, "Measurement of Form-Factor-Independent Observables in the Decay $B^0 \to K^{*0}\mu^+\mu^-$," *Phys. Rev. Lett.* **111** (2013) 191801, `arXiv:1308.1707 [hep-ex]`.

[12] S. Descotes-Genon, J. Matias, and J. Virto, "Understanding the $B \to K^*\mu^+\mu^-$ Anomaly," *Phys. Rev. D* **88** (2013) 074002, `arXiv:1307.5683 [hep-ph]`.

[13] W. Altmannshofer and D. M. Straub, "New Physics in $B \to K^*\mu\mu$?," *Eur. Phys. J. C* **73** (2013) 2646, `arXiv:1308.1501 [hep-ph]`.

[14] M. Algueró, B. Capdevila, A. Crivellin, S. Descotes-Genon, P. Masjuan, J. Matias, M. Novoa Brunet, and J. Virto, "Emerging patterns of New Physics with and without Lepton Flavour Universal contributions," *Eur. Phys. J. C* **79** no. 8, (2019) 714, `arXiv:1903.09578 [hep-ph]`. [Addendum: Eur.Phys.J.C 80, 511 (2020)].

[15] M. Algueró, B. Capdevila, S. Descotes-Genon, J. Matias, and M. Novoa-Brunet, "$b \to s\ell\ell$ global fits after Moriond 2021 results," in *55th Rencontres de Moriond on QCD and High Energy Interactions*. 4, 2021. `arXiv:2104.08921 [hep-ph]`.

[16] S. Descotes-Genon, L. Hofer, J. Matias, and J. Virto, "Global analysis of $b \to s\ell\ell$ anomalies," *JHEP* **06** (2016) 092, `arXiv:1510.04239 [hep-ph]`.

[17] S. Trifinopoulos, "B -physics anomalies: The bridge between R -parity violating supersymmetry and flavored dark matter," *Phys. Rev. D* **100** no. 11, (2019) 115022, `arXiv:1904.12940 [hep-ph]`.

[18] Q.-Y. Hu and L.-L. Huang, "Explaining $b \to s\ell^+\ell^-$ data by sneutrinos in the R -parity violating MSSM," *Phys. Rev. D* **101** no. 3, (2020) 035030, `arXiv:1912.03676 [hep-ph]`.

[19] Q.-Y. Hu, Y.-D. Yang, and M.-D. Zheng, "Revisiting the *B*-physics anomalies in *R*-parity violating MSSM," *Eur. Phys. J. C* **80** no. 5, (2020) 365, `arXiv:2002.09875 [hep-ph]`.

[20] G. Hiller and M. Schmaltz, "R_K and future $b \to s\ell\ell$ physics beyond the standard model opportunities," *Phys. Rev. D* **90** (2014) 054014, `arXiv:1408.1627 [hep-ph]`.

[21] B. Gripaios, M. Nardecchia, and S. A. Renner, "Composite leptoquarks and anomalies in *B*-meson decays," *JHEP* **05** (2015) 006, `arXiv:1412.1791 [hep-ph]`.

[22] W. Altmannshofer, S. Gori, M. Pospelov, and I. Yavin, "Quark flavor transitions in $L_\mu - L_\tau$ models," *Phys. Rev. D* **89** (2014) 095033, `arXiv:1403.1269 [hep-ph]`.

[23] A. Crivellin, G. D'Ambrosio, and J. Heeck, "Explaining $h \to \mu^\pm \tau^\mp$, $B \to K^* \mu^+ \mu^-$ and $B \to K\mu^+\mu^- / B \to Ke^+e^-$ in a two-Higgs-doublet model with gauged $L_\mu - L_\tau$," *Phys. Rev. Lett.* **114** (2015) 151801, `arXiv:1501.00993 [hep-ph]`.

[24] A. Celis, J. Fuentes-Martin, M. Jung, and H. Serodio, "Family nonuniversal Z' models with protected flavor-changing interactions," *Phys. Rev. D* **92** no. 1, (2015) 015007, `arXiv:1505.03079 [hep-ph]`.

[25] A. Falkowski, M. Nardecchia, and R. Ziegler, "Lepton Flavor Non-Universality in B-meson Decays from a U(2) Flavor Model," *JHEP* **11** (2015) 173, `arXiv:1509.01249 [hep-ph]`.

[26] C. Bobeth, A. J. Buras, A. Celis, and M. Jung, "Patterns of Flavour Violation in Models with Vector-Like Quarks," *JHEP* **04** (2017) 079, `arXiv:1609.04783 [hep-ph]`.

[27] S. Bifani, S. Descotes-Genon, A. Romero Vidal, and M.-H. Schune, "Review of Lepton Universality tests in *B* decays," *J. Phys. G* **46** no. 2, (2019) 023001, `arXiv:1809.06229 [hep-ex]`.

[28] W. Altmannshofer and D. M. Straub, "New physics in $b \to s$ transitions after LHC run 1," *Eur. Phys. J. C* **75** no. 8, (2015) 382, `arXiv:1411.3161 [hep-ph]`.

[29] J. Rosiek, "Complete Set of Feynman Rules for the Minimal Supersymmetric Extension of the Standard Model," *Phys. Rev.* **D41** (1990) 3464. [Complete set of Feynman rules for the MSSM: Erratum: hep-ph/9511250].

[30] S. P. MARTIN, "A supersymmetry primer," *Advanced Series on Directions in High Energy Physics* (Jul, 1998) 198, `hep-ph/9709356`.

[31] H. Dreiner, "An introduction to explicitr-parity violation," *Pramana* **51** no. 1-2, (Jul, 1998) 123133, `hep-ph/9707435`.

[32] H. Pagels and J. R. Primack, "Supersymmetry, Cosmology and New TeV Physics," *Phys. Rev. Lett.* **48** (1982) 223.

[33] H. Goldberg, "Constraint on the Photino Mass from Cosmology," *Phys. Rev. Lett.* **50** (1983) 1419. [Erratum: Phys.Rev.Lett. 103, 099905 (2009)].

[34] J. Edsjo and P. Gondolo, "Neutralino relic density including coannihilations," *Phys. Rev. D* **56** (1997) 1879–1894, `arXiv:hep-ph/9704361`.

[35] J. Beuria and A. Dey, "Exploring Charge and Color Breaking vacuum in Non-Holomorphic MSSM," *JHEP* **10** (2017) 154, `arXiv:1708.08361 [hep-ph]`.

[36] M. Misiak, S. Pokorski, and J. Rosiek, "Supersymmetry and FCNC effects," *Adv. Ser. Direct. High Energy Phys.* **15** (1998) 795–828, `arXiv:hep-ph/9703442`.

[37] L. J. Hall, V. A. Kostelecky, and S. Raby, "New Flavor Violations in Supergravity Models," *Nucl. Phys. B* **267** (1986) 415–432.

[38] F. Gabbiani and A. Masiero, "FCNC in Generalized Supersymmetric Theories," *Nucl. Phys. B* **322** (1989) 235–254.

[39] F. Gabbiani, E. Gabrielli, A. Masiero, and L. Silvestrini, "A Complete analysis of FCNC and CP constraints in general SUSY extensions of the standard model," *Nucl. Phys. B* **477** (1996) 321–352, `arXiv:hep-ph/9604387`.

[40] A. Dedes, M. Paraskevas, J. Rosiek, K. Suxho, and K. Tamvakis, "Mass Insertions vs. Mass Eigenstates calculations in Flavour Physics," *JHEP* **06** (2015) 151, `arXiv:1504.00960 [hep-ph]`.

[41] J. Rosiek, "MassToMI —A Mathematica package for an automatic Mass Insertion expansion," *Comput. Phys. Commun.* **201** (2016) 144–158, `arXiv:1509.05030 [hep-ph]`.

[42] **ATLAS** Collaboration, M. Aaboud *et al.*, "Search for photonic signatures of gauge-mediated supersymmetry in 13 TeV *pp* collisions with the ATLAS detector," *Phys. Rev. D* **97** no. 9, (2018) 092006, `arXiv:1802.03158 [hep-ex]`.

[43] **CMS** Collaboration, A. M. Sirunyan *et al.*, "Search for gauge-mediated supersymmetry in events with at least one photon and missing transverse momentum in pp collisions at $\sqrt{s} = 13$ TeV," *Phys. Lett.* **B780** (2018) 118–143, `arXiv:1711.08008 [hep-ex]`.

[44] **CMS** Collaboration, A. M. Sirunyan *et al.*, "Search for top squarks decaying via four-body or chargino-mediated modes in single-lepton final states in proton-proton collisions at $\sqrt{s} = 13$ TeV," `arXiv:1805.05784 [hep-ex]`.

[45] **CMS** Collaboration, C. Collaboration, "Search for supersymmetry using events with a photon, a lepton, and missing transverse momentum in pp collisions at sqrt(s) = 13 TeV,". `http://cds.cern.ch/record/2628543`.

[46] **CMS** Collaboration, A. M. Sirunyan *et al.*, "Search for supersymmetry in events with a τ lepton pair and missing transverse momentum in proton-proton collisions at $\sqrt{s} = 13$ TeV," `arXiv:1807.02048 [hep-ex]`.

[47] **CMS** Collaboration, A. M. Sirunyan *et al.*, "Search for supersymmetric partners of electrons and muons in proton-proton collisions at $\sqrt{s} = 13$ TeV," *Submitted to: Phys. Lett.* (2018) , `arXiv:1806.05264 [hep-ex]`.

[48] **ATLAS** Collaboration, M. Aaboud *et al.*, "Search for pair production of higgsinos in final states with at least three b-tagged jets in $\sqrt{s} = 13$ TeV pp collisions using the ATLAS detector," *Submitted to: Phys. Rev.* (2018) , `arXiv:1806.04030 [hep-ex]`.

[49] **CMS** Collaboration, S. Chatrchyan *et al.*, "Search for Supersymmetry in pp Collisions at $\sqrt{s} = 7$ TeV in Events with Two Photons and Missing Transverse Energy," *Phys. Rev. Lett.* **106** (2011) 211802, `arXiv:1103.0953 [hep-ex]`.

[50] **ATLAS** Collaboration, G. Aad *et al.*, "Search for squarks and gluinos using final states with jets and missing transverse momentum with the ATLAS detector in $\sqrt{s} = 7$ TeV proton-proton collisions," *Phys. Lett.* **B701** (2011) 186–203, `arXiv:1102.5290 [hep-ex]`.

[51] **ATLAS, CMS** Collaboration, A. Ventura, "Searches for supersymmetry," *Int. J. Mod. Phys. Conf. Ser.* **46** (2018) 1860006, `arXiv:1711.00152 [hep-ex]`.

[52] **ATLAS** Collaboration, G. Aad *et al.*, "Search for squarks and gluinos in final states with one isolated lepton, jets, and missing transverse momentum at $\sqrt{s} = 13$ TeV with the ATLAS detector," `arXiv:2101.01629 [hep-ex]`.

[53] **ATLAS** Collaboration, G. Aad *et al.*, "Search for new phenomena in events with two opposite-charge leptons, jets and missing transverse momentum in pp collisions at $\sqrt{s} = 13$ TeV with the ATLAS detector," `arXiv:2102.01444 [hep-ex]`.

[54] **ATLAS** Collaboration, G. Aad *et al.*, "Search for new phenomena in final states with b-jets and missing transverse momentum in $\sqrt{s} = 13$ TeV pp collisions with the ATLAS detector," `arXiv:2101.12527 [hep-ex]`.

[55] **CMS** Collaboration, A. M. Sirunyan *et al.*, "Search for top squarks in final states with two top quarks and several light-flavor jets in proton-proton collisions at $\sqrt{s} = 13$ TeV," `arXiv:2102.06976 [hep-ex]`.

[56] **CMS** Collaboration, A. M. Sirunyan *et al.*, "Search for top squark production in fully-hadronic final states in proton-proton collisions at $\sqrt{s} = 13$ TeV," `arXiv:2103.01290 [hep-ex]`.

[57] **ATLAS** Collaboration, G. Aad *et al.*, "Search for supersymmetry in events with four or more charged leptons in 139 fb^{-1} of $\sqrt{s} = 13$ TeV pp collisions with the ATLAS detector," `arXiv:2103.11684 [hep-ex]`.

[58] **ATLAS** Collaboration, G. Aad *et al.*, "Search for R-parity violating supersymmetry in a final state containing leptons and many jets with the ATLAS experiment using $\sqrt{s} = 13$ TeV proton-proton collision data," `arXiv:2106.09609 [hep-ex]`.

[59] **ATLAS** Collaboration, "Search for long-lived charginos based on a disappearing-track signature using 136 fb^{-1} of pp collisions at $\sqrt{s} = 13$ TeV with the ATLAS detector,". `http://cds.cern.ch/record/2759676`.

[60] M. S. Chanowitz, M. A. Furman, and I. Hinchliffe, "Weak Interactions of Ultraheavy Fermions. 2.," *Nucl. Phys. B* **153** (1979) 402–430.

[61] M. Gorbahn, S. Jager, U. Nierste, and S. Trine, "The supersymmetric Higgs sector and $B - \bar{B}$ mixing for large tan β," *Phys. Rev. D* **84** (2011) 034030, `arXiv:0901.2065 [hep-ph]`.

[62] **LHCb** Collaboration, K. A. Petridis, "New results on theoretically clean observables in rare B-meson decays from LHCb. 2. Test of Lepton Flavour Universality in $B^+ \to K^+ l^+ l^-$ decays," in *LHC Seminar*. March, 2021. https://indico.cern.ch/event/976688/. Last accessed 26 May 2021.

[63] A. Dedes, J. Rosiek, and P. Tanedo, "Complete One-Loop MSSM Predictions for B −> lepton lepton' at the Tevatron and LHC," *Phys. Rev. D* **79** (2009) 055006, arXiv:0812.4320 [hep-ph].

[64] P. L. Cho, M. Misiak, and D. Wyler, "K(L) —> pi0 e+ e- and b —> X(s) lepton+ lepton- decay in the MSSM," *Phys. Rev. D* **54** (1996) 3329–3344, arXiv:hep-ph/9601360.

[65] C.-S. Huang and X.-H. Wu, "B(s) —> mu+ mu- and B —> X(s) mu+ mu- in MSSM," *Nucl. Phys. B* **657** (2003) 304–332, arXiv:hep-ph/0212220.

[66] B. Capdevila, A. Crivellin, S. Descotes-Genon, J. Matias, and J. Virto, "Patterns of New Physics in $b \to s\ell^+\ell^-$ transitions in the light of recent data," *JHEP* **01** (2018) 093, arXiv:1704.05340 [hep-ph].

[67] J. Aebischer, W. Altmannshofer, D. Guadagnoli, M. Reboud, P. Stangl, and D. M. Straub, "*B*-decay discrepancies after Moriond 2019," *Eur. Phys. J. C* **80** no. 3, (2020) 252, arXiv:1903.10434 [hep-ph].

[68] M. Algueró, B. Capdevila, S. Descotes-Genon, P. Masjuan, and J. Matias, "Are we overlooking lepton flavour universal new physics in $b \to s\ell\ell$?," *Phys. Rev. D* **99** no. 7, (2019) 075017, arXiv:1809.08447 [hep-ph].

[69] E. Lunghi, A. Masiero, I. Scimemi, and L. Silvestrini, "B —> X(s) lepton+ lepton- decays in supersymmetry," *Nucl. Phys. B* **568** (2000) 120–144, arXiv:hep-ph/9906286.

[70] S. Bertolini, F. Borzumati, A. Masiero, and G. Ridolfi, "Effects of supergravity induced electroweak breaking on rare *B* decays and mixings," *Nucl. Phys. B* **353** (1991) 591–649.

[71] J. Foster, K.-i. Okumura, and L. Roszkowski, "Probing the flavor structure of supersymmetry breaking with rare B-processes: A Beyond leading order analysis," *JHEP* **08** (2005) 094, arXiv:hep-ph/0506146.

[72] A. Behring, C. Gross, G. Hiller, and S. Schacht, "Squark Flavor Implications from B −> K* l+ l-," *JHEP* **08** (2012) 152, arXiv:1205.1500 [hep-ph].

[73] M. Tanimoto and K. Yamamoto, "Probing SUSY with 10 TeV stop mass in rare decays and CP violation of kaon," *PTEP* **2016** no. 12, (2016) 123B02, arXiv:1603.07960 [hep-ph].

[74] **Muon g-2** Collaboration, B. Abi *et al.*, "Measurement of the Positive Muon Anomalous Magnetic Moment to 0.46 ppm," *Phys. Rev. Lett.* **126** (2021) 141801, arXiv:2104.03281 [hep-ex].

[75] **Muon g-2** Collaboration, G. W. Bennett *et al.*, "Final Report of the Muon E821 Anomalous Magnetic Moment Measurement at BNL," *Phys. Rev. D* **73** (2006) 072003, arXiv:hep-ex/0602035.

[76] T. Aoyama *et al.*, "The anomalous magnetic moment of the muon in the Standard Model," *Phys. Rept.* **887** (2020) 1–166, arXiv:2006.04822 [hep-ph].

[77] S. P. Martin and J. D. Wells, "Muon Anomalous Magnetic Dipole Moment in Supersymmetric Theories," *Phys. Rev. D* **64** (2001) 035003, `arXiv:hep-ph/0103067`.

[78] M. Bach, J.-h. Park, D. Stöckinger, and H. Stöckinger-Kim, "Large muon $(g-2)$ with TeV-scale SUSY masses for $\tan\beta \to \infty$," *JHEP* **10** (2015) 026, `arXiv:1504.05500 [hep-ph]`.

[79] **UTfit** Collaboration, M. Bona *et al.*, "Constraints on new physics from the quark mixing unitarity triangle," *Phys. Rev. Lett.* **97** (2006) 151803, `arXiv:hep-ph/0605213`.

[80] **UTfit** Collaboration, M. Bona *et al.*, "Model-independent constraints on $\Delta F = 2$ operators and the scale of new physics," *JHEP* **03** (2008) 049, `arXiv:0707.0636 [hep-ph]`.

[81] W. Altmannshofer, A. J. Buras, and D. Guadagnoli, "The MFV limit of the MSSM for low tan(beta): Meson mixings revisited," *JHEP* **11** (2007) 065, `arXiv:hep-ph/0703200`.

[82] A. Crivellin and M. Davidkov, "Do squarks have to be degenerate? Constraining the mass splitting with Kaon and D mixing," *Phys. Rev. D* **81** (2010) 095004, `arXiv:1002.2653 [hep-ph]`.

[83] **Particle Data Group** Collaboration, P. A. Zyla *et al.*, "Review of Particle Physics," *PTEP* **2020** no. 8, (2020) 083C01.

[84] C. Bobeth, M. Gorbahn, T. Hermann, M. Misiak, E. Stamou, and M. Steinhauser, "$B_{s,d} \to l^+l^-$ in the Standard Model with Reduced Theoretical Uncertainty," *Phys. Rev. Lett.* **112** (2014) 101801, `arXiv:1311.0903 [hep-ph]`.

[85] **Belle** Collaboration, A. Abdesselam *et al.*, "Measurement of the inclusive $B \to X_{s+d}\gamma$ branching fraction, photon energy spectrum and HQE parameters," in *38th International Conference on High Energy Physics.* August, 2016. `arXiv:1608.02344 [hep-ex]`.

[86] M. Misiak *et al.*, "Updated NNLO QCD predictions for the weak radiative B-meson decays," *Phys. Rev. Lett.* **114** no. 22, (2015) 221801, `arXiv:1503.01789 [hep-ph]`.

[87] M. Misiak, A. Rehman, and M. Steinhauser, "Towards $\overline{B} \to X_s\gamma$ at the NNLO in QCD without interpolation in m$_c$," *JHEP* **06** (2020) 175, `arXiv:2002.01548 [hep-ph]`.

[88] A. Crivellin, L. Hofer, and J. Rosiek, "Complete resummation of chirally-enhanced loop-effects in the MSSM with non-minimal sources of flavor-violation," *JHEP* **07** (2011) 017, `arXiv:1103.4272 [hep-ph]`.

[89] A. Crivellin, "Effective Higgs Vertices in the generic MSSM," *Phys. Rev. D* **83** (2011) 056001, `arXiv:1012.4840 [hep-ph]`.

[90] J. Girrbach, S. Mertens, U. Nierste, and S. Wiesenfeldt, "Lepton flavour violation in the MSSM," *JHEP* **05** (2010) 026, `arXiv:0910.2663 [hep-ph]`.

[91] M. Drees, M. Gluck, and K. Grassie, "A New Class of False Vacua in Low-energy $N = 1$ Supergravity Theories," *Phys. Lett. B* **157** (1985) 164–168.

[92] N. Polonsky, *Supersymmetry: Structure and phenomena. Extensions of the standard model*, vol. 68. 2001. `arXiv:hep-ph/0108236`.

[93] R. Alonso, B. Grinstein, and J. Martin Camalich, "Lepton universality violation and lepton flavor conservation in *B*-meson decays," *JHEP* **10** (2015) 184, `arXiv:1505.05164 [hep-ph]`.

[94] L. Calibbi, A. Crivellin, and T. Li, "Model of vector leptoquarks in view of the *B*-physics anomalies," *Phys. Rev. D* **98** no. 11, (2018) 115002, `arXiv:1709.00692 [hep-ph]`.

[95] B. Capdevila, A. Crivellin, S. Descotes-Genon, L. Hofer, and J. Matias, "Searching for New Physics with $b \to s\tau^+\tau^-$ processes," *Phys. Rev. Lett.* **120** no. 18, (2018) 181802, `arXiv:1712.01919 [hep-ph]`.

[96] A. Crivellin, D. Müller, and T. Ota, "Simultaneous explanation of R(D$^{(*)}$) and b→sμ^+ μ^-: the last scalar leptoquarks standing," *JHEP* **09** (2017) 040, `arXiv:1703.09226 [hep-ph]`.

[97] S. Kumbhakar and J. Saini, "New physics effects in purely leptonic B_s^* decays," *Eur. Phys. J. C* **79** no. 5, (2019) 394, `arXiv:1807.04055 [hep-ph]`.

[98] A. Crivellin, A. Kokulu, and C. Greub, "Flavor-phenomenology of two-Higgs-doublet models with generic Yukawa structure," *Phys. Rev. D* **87** no. 9, (2013) 094031, `arXiv:1303.5877 [hep-ph]`.

[99] J. C. Alexander and J. A. Yorke, "The Homotopy Continuation Method: Numerically Implementable Topological Procedures," *Transactions of the American Mathematical Society* **242** (1978) 271–284. `http://www.jstor.org/stable/1997737`.

[100] M. Maniatis and D. Mehta, "Minimizing Higgs Potentials via Numerical Polynomial Homotopy Continuation," *Eur. Phys. J. Plus* **127** (2012) 91, `arXiv:1203.0409 [hep-ph]`.

[101] J. E. Camargo-Molina, B. O'Leary, W. Porod, and F. Staub, "**Vevacious**: A Tool For Finding The Global Minima Of One-Loop Effective Potentials With Many Scalars," *Eur. Phys. J. C* **73** no. 10, (2013) 2588, `arXiv:1307.1477 [hep-ph]`.

[102] W. G. Hollik, G. Weiglein, and J. Wittbrodt, "Impact of Vacuum Stability Constraints on the Phenomenology of Supersymmetric Models," *JHEP* **03** (2019) 109, `arXiv:1812.04644 [hep-ph]`.

[103] S. R. Coleman, "The Fate of the False Vacuum. 1. Semiclassical Theory," *Phys. Rev. D* **15** (1977) 2929–2936. [Erratum: Phys.Rev.D 16, 1248 (1977)].

[104] C. G. Callan, Jr. and S. R. Coleman, "The Fate of the False Vacuum. 2. First Quantum Corrections," *Phys. Rev. D* **16** (1977) 1762–1768.

[105] I. Dasgupta, "Estimating vacuum tunneling rates," *Phys. Lett. B* **394** (1997) 116–122, `arXiv:hep-ph/9610403`.

[106] A. Kusenko, P. Langacker, and G. Segre, "Phase transitions and vacuum tunneling into charge and color breaking minima in the MSSM," *Phys. Rev. D* **54** (1996) 5824–5834, `arXiv:hep-ph/9602414`.

[107] F. C. Adams, "General solutions for tunneling of scalar fields with quartic potentials," *Phys. Rev. D* **48** (1993) 2800–2805, `arXiv:hep-ph/9302321`.

[108] R. Apreda, M. Maggiore, A. Nicolis, and A. Riotto, "Gravitational waves from electroweak phase transitions," *Nucl. Phys. B* **631** (2002) 342–368, `arXiv:gr-qc/0107033`.

[109] C. L. Wainwright, "CosmoTransitions: Computing Cosmological Phase Transition Temperatures and Bubble Profiles with Multiple Fields," *Comput. Phys. Commun.* **183** (2012) 2006–2013, `arXiv:1109.4189 [hep-ph]`.

[110] A. Masoumi, K. D. Olum, and B. Shlaer, "Efficient numerical solution to vacuum decay with many fields," *JCAP* **01** (2017) 051, `arXiv:1610.06594 [gr-qc]`.

[111] **LHCb** Collaboration, R. Aaij *et al.*, "First observation of the decay $B^+ \to \pi^+\mu^+\mu^-$," *JHEP* **12** (2012) 125, `arXiv:1210.2645 [hep-ex]`.

[112] **LHCb** Collaboration, R. Aaij *et al.*, "First measurement of the differential branching fraction and *CP* asymmetry of the $B^\pm \to \pi^\pm\mu^+\mu^-$ decay," *JHEP* **10** (2015) 034, `arXiv:1509.00414 [hep-ex]`.

[113] **LHCb** Collaboration, R. Aaij *et al.*, "Observation of the suppressed decay $\Lambda_b^0 \to p\pi^-\mu^+\mu^-$," *JHEP* **04** (2017) 029, `arXiv:1701.08705 [hep-ex]`.

[114] **LHCb** Collaboration, R. Aaij *et al.*, "Physics case for an LHCb Upgrade II - Opportunities in flavour physics, and beyond, in the HL-LHC era," `arXiv:1808.08865 [hep-ex]`.

[115] A. Ali, A. Y. Parkhomenko, and A. V. Rusov, "Precise Calculation of the Dilepton Invariant-Mass Spectrum and the Decay Rate in $B^\pm \to \pi^\pm\mu^+\mu^-$ in the SM," *Phys. Rev. D* **89** no. 9, (2014) 094021, `arXiv:1312.2523 [hep-ph]`.

[116] W.-S. Hou, M. Kohda, and F. Xu, "Rates and asymmetries of B→$\pi\ell^+\ell^-$ decays," *Phys. Rev. D* **90** no. 1, (2014) 013002, `arXiv:1403.7410 [hep-ph]`.

[117] M. Beneke, T. Feldmann, and D. Seidel, "Systematic approach to exclusive $B \to Vl^+l^-$, $V\gamma$ decays," *Nucl. Phys. B* **612** (2001) 25–58, `arXiv:hep-ph/0106067`.

[118] G. Duplancic, A. Khodjamirian, T. Mannel, B. Melic, and N. Offen, "Light-cone sum rules for B —> pi form factors revisited," *JHEP* **04** (2008) 014, `arXiv:0801.1796 [hep-ph]`.

[119] C. Hambrock, A. Khodjamirian, and A. Rusov, "Hadronic effects and observables in $B \to \pi\ell^+\ell^-$ decay at large recoil," *Phys. Rev. D* **92** no. 7, (2015) 074020, `arXiv:1506.07760 [hep-ph]`.

[120] A. Khodjamirian, T. Mannel, A. A. Pivovarov, and Y. M. Wang, "Charm-loop effect in $B \to K^{(*)}\ell^+\ell^-$ and $B \to K^*\gamma$," *JHEP* **09** (2010) 089, `arXiv:1006.4945 [hep-ph]`.

[121] R. N. Faustov and V. O. Galkin, "Rare $B \to \pi l\bar{l}$ and $B \to \rho l\bar{l}$ decays in the relativistic quark model," *Eur. Phys. J. C* **74** no. 6, (2014) 2911, `arXiv:1403.4466 [hep-ph]`.

[122] G. Buchalla, G. Isidori, and S. J. Rey, "Corrections of order Λ_{QCD}^2/m_c^2 to inclusive rare B decays," *Nucl. Phys. B* **511** (1998) 594–610, `arXiv:hep-ph/9705253`.

[123] B. Grinstein, D. R. Nolte, and I. Z. Rothstein, "A Method for extracting cos alpha," *Phys. Rev. Lett.* **84** (2000) 4545–4548, `arXiv:hep-ph/9910245`.

[124] B. Grinstein and D. Pirjol, "Exclusive rare $B \to K^*\ell^+\ell^-$ decays at low recoil: Controlling the long-distance effects," *Phys. Rev. D* **70** (2004) 114005, `arXiv:hep-ph/0404250`.

[125] M. Beylich, G. Buchalla, and T. Feldmann, "Theory of $B \to K^{(*)}\ell^+\ell^-$ decays at high q^2: OPE and quark-hadron duality," *Eur. Phys. J. C* **71** (2011) 1635, `arXiv:1101.5118 [hep-ph]`.

[126] **Fermilab Lattice, MILC** Collaboration, J. A. Bailey *et al.*, "$B \to \pi\ell\ell$ form factors for new-physics searches from lattice QCD," *Phys. Rev. Lett.* **115** no. 15, (2015) 152002, `arXiv:1507.01618 [hep-ph]`.

[127] A. J. Buras and M. Munz, "Effective Hamiltonian for B —> X(s) e+ e- beyond leading logarithms in the NDR and HV schemes," *Phys. Rev. D* **52** (1995) 186–195, `arXiv:hep-ph/9501281`.

[128] H. M. Asatrian, K. Bieri, C. Greub, and M. Walker, "Virtual corrections and bremsstrahlung corrections to b —> d l+ l- in the standard model," *Phys. Rev. D* **69** (2004) 074007, `arXiv:hep-ph/0312063`.

[129] C. Greub, V. Pilipp, and C. Schupbach, "Analytic calculation of two-loop QCD corrections to $b \to sl^+l^-$ in the high q^2 region," *JHEP* **12** (2008) 040, `arXiv:0810.4077 [hep-ph]`.

[130] C. Bobeth, M. Misiak, and J. Urban, "Photonic penguins at two loops and m_t dependence of $BR[B \to X_s l^+l^-]$," *Nucl. Phys. B* **574** (2000) 291–330, `arXiv:hep-ph/9910220`.

[131] C. Bobeth, P. Gambino, M. Gorbahn, and U. Haisch, "Complete NNLO QCD analysis of anti-B —> X(s) l+ l- and higher order electroweak effects," *JHEP* **04** (2004) 071, `arXiv:hep-ph/0312090`.

[132] M. B. Voloshin, "Large O (m(c)**-2) nonperturbative correction to the inclusive rate of the decay B —> X(s) gamma," *Phys. Lett. B* **397** (1997) 275–278, `arXiv:hep-ph/9612483`.

[133] U. Egede, T. Hurth, J. Matias, M. Ramon, and W. Reece, "New physics reach of the decay mode $\bar{B} \to \bar{K}^{*0}\ell^+\ell^-$," *JHEP* **10** (2010) 056, `arXiv:1005.0571 [hep-ph]`.

[134] C. Bobeth, G. Hiller, D. van Dyk, and C. Wacker, "The Decay $B \to K\ell^+\ell^-$ at Low Hadronic Recoil and Model-Independent $\Delta B = 1$ Constraints," *JHEP* **01** (2012) 107, `arXiv:1111.2558 [hep-ph]`.

[135] C. M. Bouchard, G. P. Lepage, C. Monahan, H. Na, and J. Shigemitsu, "$B_s \to K\ell\nu$ form factors from lattice QCD," *Phys. Rev. D* **90** (2014) 054506, `arXiv:1406.2279 [hep-lat]`.

[136] **Fermilab Lattice, MILC** Collaboration, J. A. Bailey *et al.*, "$|V_{ub}|$ from $B \to \pi\ell\nu$ decays and (2+1)-flavor lattice QCD," *Phys. Rev. D* **92** no. 1, (2015) 014024, `arXiv:1503.07839 [hep-lat]`.

[137] J. A. Bailey *et al.*, "$B \to Kl^+l^-$ Decay Form Factors from Three-Flavor Lattice QCD," *Phys. Rev. D* **93** no. 2, (2016) 025026, `arXiv:1509.06235 [hep-lat]`.

[138] A. Khodjamirian and A. V. Rusov, "$B_s \to K\ell\nu_\ell$ and $B_{(s)} \to \pi(K)\ell^+\ell^-$ decays at large recoil and CKM matrix elements," *JHEP* **08** (2017) 112, `arXiv:1703.04765 [hep-ph]`.

[139] **HFLAV** Collaboration, Y. S. Amhis *et al.*, "Averages of b-hadron, c-hadron, and τ-lepton properties as of 2018," *Eur. Phys. J. C* **81** no. 3, (2021) 226, `arXiv:1909.12524 [hep-ex]`.

[140] **LHCb** Collaboration, R. Aaij *et al.*, "Differential branching fractions and isospin asymmetries of $B \to K^{(*)}\mu^+\mu^-$ decays," *JHEP* **06** (2014) 133, `arXiv:1403.8044 [hep-ex]`.

[141] M. Bartsch, M. Beylich, G. Buchalla, and D. N. Gao, "Precision Flavour Physics with $B \to K\nu\bar{\nu}$ and $B \to Kl^+l^-$," *JHEP* **11** (2009) 011, `arXiv:0909.1512 [hep-ph]`.

[142] U. Nierste, "Three Lectures on Meson Mixing and CKM phenomenology," in *Helmholz International Summer School on Heavy Quark Physics*. March, 2009. `arXiv:0904.1869 [hep-ph]`.

[143] U. Nierste, M. Tabet, and R. Ziegler, "Cornering Spontaneous *CP* Violation with Charged-Higgs-Boson Searches," *Phys. Rev. Lett.* **125** no. 3, (2020) 031801, `arXiv:1912.11501 [hep-ph]`.

[144] M. Kobayashi and T. Maskawa, "CP Violation in the Renormalizable Theory of Weak Interaction," *Prog. Theor. Phys.* **49** (1973) 652–657.

[145] T. D. Lee, "A Theory of Spontaneous T Violation," *Phys. Rev. D* **8** (1973) 1226–1239.

[146] M. Nebot, "Bounded masses in two Higgs doublets models, spontaneous *CP* violation and $\mathbb{Z}$ symmetry," *Phys. Rev. D* **102** no. 11, (2020) 115002, `arXiv:1911.02266 [hep-ph]`.

[147] G. Barenboim, M. Gorbahn, U. Nierste, and M. Raidal, "Higgs Sector of the Minimal Left-Right Symmetric Model," *Phys. Rev. D* **65** (2002) 095003, `arXiv:hep-ph/0107121`.

[148] E. Gildener and S. Weinberg, "Symmetry Breaking and Scalar Bosons," *Phys. Rev. D* **13** (1976) 3333.

[149] K. Lane and W. Shepherd, "Natural stabilization of the Higgs boson's mass and alignment," *Phys. Rev. D* **99** no. 5, (2019) 055015, `arXiv:1808.07927 [hep-ph]`.

[150] Y. L. Wu and L. Wolfenstein, "Sources of CP violation in the two Higgs doublet model," *Phys. Rev. Lett.* **73** (1994) 1762–1764, `arXiv:hep-ph/9409421`.

[151] M. Nebot, F. J. Botella, and G. C. Branco, "Vacuum Induced CP Violation Generating a Complex CKM Matrix with Controlled Scalar FCNC," *Eur. Phys. J. C* **79** no. 8, (2019) 711, `arXiv:1808.00493 [hep-ph]`.

[152] G. C. Branco, P. M. Ferreira, L. Lavoura, M. N. Rebelo, M. Sher, and J. P. Silva, "Theory and phenomenology of two-Higgs-doublet models," *Phys. Rept.* **516** (2012) 1–102, `arXiv:1106.0034 [hep-ph]`.

[153] I. P. Ivanov, "Minkowski space structure of the Higgs potential in 2HDM. II. Minima, symmetries, and topology," *Phys. Rev. D* **77** (2008) 015017, `arXiv:0710.3490 [hep-ph]`.

[154] C. W. Murphy, "NLO Perturbativity Bounds on Quartic Couplings in Renormalizable Theories with ϕ^4-like Scalar Sectors," *Phys. Rev. D* **96** no. 3, (2017) 036006, `arXiv:1702.08511 [hep-ph]`.

[155] **ATLAS** Collaboration, G. Aad *et al.*, "Search for charged Higgs bosons in the $H^\pm \to tb$ decay channel in pp collisions at $\sqrt{s} = 8$ TeV using the ATLAS detector," *JHEP* **03** (2016) 127, `arXiv:1512.03704 [hep-ex]`.

[156] **ATLAS** Collaboration, M. Aaboud *et al.*, "Search for charged Higgs bosons decaying into top and bottom quarks at $\sqrt{s}$ = 13 TeV with the ATLAS detector," *JHEP* **11** (2018) 085, arXiv:1808.03599 [hep-ex].

[157] **ATLAS** Collaboration, G. Aad *et al.*, "Search for charged Higgs bosons decaying into a top quark and a bottom quark at $\sqrt{s}$=13 TeV with the ATLAS detector," arXiv:2102.10076 [hep-ex].

[158] **CMS** Collaboration, V. Khachatryan *et al.*, "Search for a charged Higgs boson in pp collisions at $\sqrt{s}$ = 8 TeV," *JHEP* **11** (2015) 018, arXiv:1508.07774 [hep-ex].

[159] **CMS** Collaboration, A. M. Sirunyan *et al.*, "Search for a charged Higgs boson decaying into top and bottom quarks in events with electrons or muons in proton-proton collisions at $\sqrt{s}$ = 13 TeV," *JHEP* **01** (2020) 096, arXiv:1908.09206 [hep-ex].

[160] **CMS** Collaboration, A. M. Sirunyan *et al.*, "Search for charged Higgs bosons decaying into a top and a bottom quark in the all-jet final state of pp collisions at $\sqrt{s}$ = 13 TeV," *JHEP* **07** (2020) 126, arXiv:2001.07763 [hep-ex].

[161] **CMS** Collaboration, A. M. Sirunyan *et al.*, "Search for a charged Higgs boson decaying to charm and bottom quarks in proton-proton collisions at $\sqrt{s}$ = 8 TeV," *JHEP* **11** (2018) 115, arXiv:1808.06575 [hep-ex].

[162] S. Gori, C. Grojean, A. Juste, and A. Paul, "Heavy Higgs Searches: Flavour Matters," *JHEP* **01** (2018) 108, arXiv:1710.03752 [hep-ph].

[163] D. K. Ghosh, W.-S. Hou, and T. Modak, "Sub-TeV H^+ Boson Production as Probe of Extra Top Yukawa Couplings," *Phys. Rev. Lett.* **125** no. 22, (2020) 221801, arXiv:1912.10613 [hep-ph].

[164] **UTfit** Collaboration, M. Bona *et al.*, "The Unitarity Triangle Fit in the Standard Model and Hadronic Parameters from Lattice QCD: A Reappraisal after the Measurements of Delta m(s) and BR(B —> tau nu(tau))," *JHEP* **10** (2006) 081, arXiv:hep-ph/0606167.

[165] **ATLAS** Collaboration, G. Aad *et al.*, "Search for flavour-changing neutral currents in processes with one top quark and a photon using 81 fb^{-1} of pp collisions at $\sqrt{s}$ = 13 TeV with the ATLAS experiment," *Phys. Lett. B* **800** (2020) 135082, arXiv:1908.08461 [hep-ex].

[166] J. Alwall, R. Frederix, S. Frixione, V. Hirschi, F. Maltoni, O. Mattelaer, H. S. Shao, T. Stelzer, P. Torrielli, and M. Zaro, "The automated computation of tree-level and next-to-leading order differential cross sections, and their matching to parton shower simulations," *JHEP* **07** (2014) 079, arXiv:1405.0301 [hep-ph].

[167] C. Degrande, "Automatic evaluation of UV and R2 terms for beyond the Standard Model Lagrangians: a proof-of-principle," *Comput. Phys. Commun.* **197** (2015) 239–262, arXiv:1406.3030 [hep-ph].

[168] C. Degrande, R. Frederix, V. Hirschi, M. Ubiali, M. Wiesemann, and M. Zaro, "Accurate predictions for charged Higgs production: Closing the $m_{H^\pm} \sim m_t$ window," *Phys. Lett. B* **772** (2017) 87–92, arXiv:1607.05291 [hep-ph].

[169] **ATLAS, CMS** Collaboration, "Addendum to the report on the physics at the HL-LHC, and perspectives for the HE-LHC: Collection of notes from ATLAS and

CMS," *CERN Yellow Rep. Monogr.* **7** (2019) Addendum, `arXiv:1902.10229 [hep-ex]`.

[170] I. Neutelings, "CMS conventional coordinate system with LHC and other detectors," accessed 26 May 2021. `https://wiki.physik.uzh.ch/cms/latex:example_spherical_coordinates`.

[171] **ATLAS** Collaboration, M. Aaboud *et al.*, "Search for low-mass resonances decaying into two jets and produced in association with a photon using pp collisions at $\sqrt{s} = 13$ TeV with the ATLAS detector," *Phys. Lett. B* **795** (2019) 56–75, `arXiv:1901.10917 [hep-ex]`.

[172] T. Sjostrand, S. Mrenna, and P. Z. Skands, "PYTHIA 6.4 Physics and Manual," *JHEP* **05** (2006) 026, `arXiv:hep-ph/0603175`.

[173] T. Sjöstrand, S. Ask, J. R. Christiansen, R. Corke, N. Desai, P. Ilten, S. Mrenna, S. Prestel, C. O. Rasmussen, and P. Z. Skands, "An introduction to PYTHIA 8.2," *Comput. Phys. Commun.* **191** (2015) 159–177, `arXiv:1410.3012 [hep-ph]`.

[174] S. Hoeche, F. Krauss, N. Lavesson, L. Lonnblad, M. Mangano, A. Schalicke, and S. Schumann, "Matching parton showers and matrix elements," in *HERA and the LHC: A Workshop on the Implications of HERA for LHC Physics: CERN - DESY Workshop 2004/2005 (Midterm Meeting, CERN, 11-13 October 2004; Final Meeting, DESY, 17-21 January 2005)*. 2005. `arXiv:hep-ph/0602031`.

[175] M. L. Mangano, M. Moretti, F. Piccinini, and M. Treccani, "Matching matrix elements and shower evolution for top-quark production in hadronic collisions," *JHEP* **01** (2007) 013, `arXiv:hep-ph/0611129`.

[176] J. Alwall, M. Herquet, F. Maltoni, O. Mattelaer, and T. Stelzer, "MadGraph 5 : Going Beyond," *JHEP* **06** (2011) 128, `arXiv:1106.0522 [hep-ph]`.

[177] M. Cacciari and G. P. Salam, "Dispelling the N^3 myth for the k_t jet-finder," *Phys. Lett. B* **641** (2006) 57–61, `arXiv:hep-ph/0512210`.

[178] M. Cacciari, G. P. Salam, and G. Soyez, "FastJet User Manual," *Eur. Phys. J. C* **72** (2012) 1896, `arXiv:1111.6097 [hep-ph]`.

[179] M. Czakon and A. Mitov, "Top++: A Program for the Calculation of the Top-Pair Cross-Section at Hadron Colliders," *Comput. Phys. Commun.* **185** (2014) 2930, `arXiv:1112.5675 [hep-ph]`.

[180] "Expected performance of the ATLAS b-tagging algorithms in Run-2," tech. rep., CERN, Geneva, Jul, 2015. `http://cds.cern.ch/record/2037697`.

[181] G. Cowan, K. Cranmer, E. Gross, and O. Vitells, "Asymptotic formulae for likelihood-based tests of new physics," *Eur. Phys. J. C* **71** (2011) 1554, `arXiv:1007.1727 [physics.data-an]`. [Erratum: Eur.Phys.J.C 73, 2501 (2013)].

[182] M. Bordone, A. Greljo, and D. Marzocca, "Exploiting dijet resonance searches for flavor physics," `arXiv:2103.10332 [hep-ph]`.

[183] **CMS** Collaboration, A. M. Sirunyan *et al.*, "Search for low mass vector resonances decaying into quark-antiquark pairs in proton-proton collisions at $\sqrt{s} = 13$ TeV," *Phys. Rev. D* **100** no. 11, (2019) 112007, `arXiv:1909.04114 [hep-ex]`.

[184] **CMS** Collaboration, A. M. Sirunyan *et al.*, "Search for dijet resonances using events with three jets in proton-proton collisions at $\sqrt{s} = 13$ TeV," *Phys. Lett. B* **805** (2020) 135448, `arXiv:1911.03761 [hep-ex]`.

[185] **CMS** Collaboration, A. M. Sirunyan *et al.*, "Search for dijet resonances in proton–proton collisions at $\sqrt{s} = 13$ TeV and constraints on dark matter and other models," *Phys. Lett. B* **769** (2017) 520–542, `arXiv:1611.03568 [hep-ex]`. [Erratum: Phys.Lett.B 772, 882–883 (2017)].

[186] **ATLAS** Collaboration, M. Aaboud *et al.*, "Search for low-mass dijet resonances using trigger-level jets with the ATLAS detector in pp collisions at $\sqrt{s} = 13$ TeV," *Phys. Rev. Lett.* **121** no. 8, (2018) 081801, `arXiv:1804.03496 [hep-ex]`.

[187] H. An, R. Huo, and L.-T. Wang, "Searching for Low Mass Dark Portal at the LHC," *Phys. Dark Univ.* **2** (2013) 50–57, `arXiv:1212.2221 [hep-ph]`.

[188] C. Shimmin and D. Whiteson, "Boosting low-mass hadronic resonances," *Phys. Rev. D* **94** no. 5, (2016) 055001, `arXiv:1602.07727 [hep-ph]`.

[189] **ATLAS** Collaboration, M. Aaboud *et al.*, "Search for light resonances decaying to boosted quark pairs and produced in association with a photon or a jet in proton-proton collisions at $\sqrt{s} = 13$ TeV with the ATLAS detector," *Phys. Lett. B* **788** (2019) 316–335, `arXiv:1801.08769 [hep-ex]`.

[190] **CMS** Collaboration, A. M. Sirunyan *et al.*, "Search for low mass vector resonances decaying into quark-antiquark pairs in proton-proton collisions at $\sqrt{s} = 13$ TeV," *JHEP* **01** (2018) 097, `arXiv:1710.00159 [hep-ex]`.

[191] **CMS** Collaboration, A. M. Sirunyan *et al.*, "Search for low-mass resonances decaying into bottom quark-antiquark pairs in proton-proton collisions at $\sqrt{s} = 13$ TeV," *Phys. Rev. D* **99** no. 1, (2019) 012005, `arXiv:1810.11822 [hep-ex]`.

[192] **ATLAS** Collaboration, M. Aaboud *et al.*, "Measurement of the photon identification efficiencies with the ATLAS detector using LHC Run 2 data collected in 2015 and 2016," *Eur. Phys. J. C* **79** no. 3, (2019) 205, `arXiv:1810.05087 [hep-ex]`.

[193] W. G. Hollik, M. Linster, and M. Tabet, "A Study of New Physics Searches with Tritium and Similar Molecules," *Eur. Phys. J. C* **80** no. 7, (2020) 661, `arXiv:2004.11274 [hep-ph]`.

[194] S. Weinberg, "A New Light Boson?," *Phys. Rev. Lett.* **40** (1978) 223–226.

[195] S. Knapen, T. Lin, and K. M. Zurek, "Light Dark Matter: Models and Constraints," *Phys. Rev. D* **96** no. 11, (2017) 115021, `arXiv:1709.07882 [hep-ph]`.

[196] J. A. Dror, G. Elor, and R. Mcgehee, "Directly Detecting Signals from Absorption of Fermionic Dark Matter," *Phys. Rev. Lett.* **124** no. 18, (2020) 18, `arXiv:1905.12635 [hep-ph]`.

[197] J. A. Dror, G. Elor, and R. Mcgehee, "Absorption of Fermionic Dark Matter by Nuclear Targets," *JHEP* **02** (2020) 134, `arXiv:1908.10861 [hep-ph]`.

[198] V. Silveira and A. Zee, "SCALAR PHANTOMS," *Phys. Lett. B* **161** (1985) 136–140.

[199] J. McDonald, "Gauge singlet scalars as cold dark matter," *Phys. Rev. D* **50** (1994) 3637–3649, `arXiv:hep-ph/0702143`.

[200] J. Jaeckel and S. Roy, "Spectroscopy as a test of Coulomb's law: A Probe of the hidden sector," *Phys. Rev. D* **82** (2010) 125020, `arXiv:1008.3536 [hep-ph]`.

[201] C. Delaunay, C. Frugiuele, E. Fuchs, and Y. Soreq, "Probing new spin-independent interactions through precision spectroscopy in atoms with few electrons," *Phys. Rev. D* **96** no. 11, (2017) 115002, `arXiv:1709.02817 [hep-ph]`.

[202] J. C. Berengut *et al.*, "Probing New Long-Range Interactions by Isotope Shift Spectroscopy," *Phys. Rev. Lett.* **120** (2018) 091801, `arXiv:1704.05068 [hep-ph]`.

[203] M. P. A. Jones, R. M. Potvliege, and M. Spannowsky, "Probing new physics using Rydberg states of atomic hydrogen," *Phys. Rev. Res.* **2** no. 1, (2020) 013244, `arXiv:1909.09194 [hep-ph]`.

[204] G. G. Raffelt, "Astrophysical methods to constrain axions and other novel particle phenomena," *Phys. Rept.* **198** (1990) 1–113.

[205] G. G. Raffelt, *Stars as laboratories for fundamental physics: The astrophysics of neutrinos, axions, and other weakly interacting particles.* 5, 1996.

[206] G. G. Raffelt, "Astrophysical axion bounds," *Lect. Notes Phys.* **741** (2008) 51–71, `arXiv:hep-ph/0611350`.

[207] P. F. Depta, M. Hufnagel, and K. Schmidt-Hoberg, "Robust cosmological constraints on axion-like particles," *JCAP* **05** (2020) 009, `arXiv:2002.08370 [hep-ph]`.

[208] G. Carugno, Z. Fontana, R. Onofrio, and C. Rizzo, "Limits on the existence of scalar interactions in the submillimeter range," *Phys. Rev. D* **55** (1997) 6591–6595.

[209] T. A. Wagner, S. Schlamminger, J. H. Gundlach, and E. G. Adelberger, "Torsion-balance tests of the weak equivalence principle," *Class. Quant. Grav.* **29** (2012) 184002, `arXiv:1207.2442 [gr-qc]`.

[210] G. L. Klimchitskaya and V. M. Mostepanenko, "Constraints on axion and corrections to Newtonian gravity from the Casimir effect," *Grav. Cosmol.* **21** no. 1, (2015) 1–12, `arXiv:1502.07647 [hep-ph]`.

[211] G. L. Klimchitskaya and V. M. Mostepanenko, "Constraints on axionlike particles and non-Newtonian gravity from measuring the difference of Casimir forces," *Phys. Rev. D* **95** no. 12, (2017) 123013, `arXiv:1704.05892 [hep-ph]`.

[212] E. J. Salumbides, J. C. J. Koelemeij, J. Komasa, K. Pachucki, K. S. E. Eikema, and W. Ubachs, "Bounds on fifth forces from precision measurements on molecules," *Phys. Rev. D* **87** no. 11, (2013) 112008, `arXiv:1304.6560 [physics.atom-ph]`.

[213] E. J. Salumbides, W. Ubachs, and V. I. Korobov, "Bounds on fifth forces at the sub-Angstrom length scale," *J. Molec. Spectrosc.* **300** (2014) 65, `arXiv:1308.1711 [hep-ph]`.

[214] W. G. Hollik, "Finding hints of New Physics in Tritium molecular spectra?," September, 2019. `https://indico.desy.de/event/22536/contributions/46973/`. DESY Theory Workshop 2019 "Quantum field theory meets gravity". Talk accessed 26 May 2021.

[215] W. Heitler and F. London, "Wechselwirkung neutraler Atome und homöopolare Bindung nach der Quantenmechanik," *Zeitschrift für Physik* **44** no. 6, (Jun, 1927) 455–472. `https://doi.org/10.1007/BF01397394`.

[216] M. Born and R. Oppenheimer, "Zur Quantentheorie der Molekeln," *Annalen der Physik* **389** no. 20, 457–484.
https://onlinelibrary.wiley.com/doi/abs/10.1002/andp.19273892002.

[217] W. Kołos and L. Wolniewicz, "Nonadiabatic Theory for Diatomic Molecules and Its Application to the Hydrogen Molecule," *Rev. Mod. Phys.* **35** (Jul, 1963) 473–483.
https://link.aps.org/doi/10.1103/RevModPhys.35.473.

[218] K. Pachucki and J. Komasa, "Nonadiabatic corrections to the wave function and energy," *The Journal of Chemical Physics* **129** no. 3, (2008) 034102.
https://doi.org/10.1063/1.2952517.

[219] M. Puchalski, J. Komasa, P. Czachorowski, and K. Pachucki, "Nonadiabatic QED correction to the dissociation energy of the hydrogen molecule," *Phys. Rev. Lett.* **122** no. 10, (2019) 103003, arXiv:1812.02980 [physics.atom-ph].

[220] M. Puchalski, J. Komasa, P. Czachorowski, and K. Pachucki, "Nonadiabatic QED Correction to the Dissociation Energy of the Hydrogen Molecule," *Phys. Rev. Lett.* **122** (Mar, 2019) 103003.
https://link.aps.org/doi/10.1103/PhysRevLett.122.103003.

[221] M. Puchalski, J. Komasa, A. Spyszkiewicz, and K. Pachucki, "Dissociation energy of molecular hydrogen isotopologues," *Phys. Rev. A* **100** (Aug, 2019) 020503.
https://link.aps.org/doi/10.1103/PhysRevA.100.020503.

[222] M. Puchalski, J. Komasa, P. Czachorowski, and K. Pachucki, "Complete $\alpha^6 m$ Corrections to the Ground State of H_2," *Phys. Rev. Lett.* **117** (Dec, 2016) 263002.
https://link.aps.org/doi/10.1103/PhysRevLett.117.263002.

[223] M. Puchalski, J. Komasa, and K. Pachucki, "Relativistic corrections for the ground electronic state of molecular hydrogen," *Phys. Rev. A* **95** (May, 2017) 052506.
https://link.aps.org/doi/10.1103/PhysRevA.95.052506.

[224] M. Puchalski, A. Spyszkiewicz, J. Komasa, and K. Pachucki, "Nonadiabatic Relativistic Correction to the Dissociation Energy of H_2, D_2, and HD," *Phys. Rev. Lett.* **121** (Aug, 2018) 073001.
https://link.aps.org/doi/10.1103/PhysRevLett.121.073001.

[225] M. Puchalski, J. Komasa, P. Czachorowski, and K. Pachucki, "Complete $\alpha^6 m$ corrections to the ground state of H_2," *Phys. Rev. Lett.* **117** no. 26, (2016) 263002, arXiv:1608.07081 [physics.chem-ph].

[226] P. Czachorowski, M. Puchalski, J. Komasa, and K. Pachucki, "Nonadiabatic relativistic correction in H2 , D2 , and HD," *Phys. Rev.* **A98** no. 5, (2018) 052506, arXiv:1810.02604 [physics.atom-ph].

[227] P. Czachorowski, J. Komasa, G. Lach, K. Pachucki, and M. Puchalski, "H2Spectre ver. 7.0." https://www.fuw.edu.pl/~krp/codes.html;
https://qcg.home.amu.edu.pl/H2Spectre.html.

[228] P. Czachorowski, *Relativistic nonadiabatic corrections to the ground state of molecular hydrogen*. PhD thesis, University of Warsaw, 2019.

[229] J. Komasa, M. Puchalski, P. Czachorowski, G. Lach, and K. Pachucki, "Rovibrational energy levels of the hydrogen molecule through nonadiabatic perturbation theory," *Phys. Rev. A* **100** (Sep, 2019) 032519.
https://link.aps.org/doi/10.1103/PhysRevA.100.032519.

[230] W. Kołos and L. Wolniewicz, "Accurate Adiabatic Treatment of the Ground State of the Hydrogen Molecule," *The Journal of Chemical Physics* **41** no. 12, (1964) 3663–3673. https://doi.org/10.1063/1.1725796.

[231] K. Pachucki and J. Komasa, "Nonadiabatic corrections to the wave function and energy," *The Journal of Chemical Physics* **129** no. 3, (Jul, 2008) 034102. http://dx.doi.org/10.1063/1.2952517.

[232] H. M. James and A. S. Coolidge, "The Ground State of the Hydrogen Molecule," *The Journal of Chemical Physics* **1** no. 12, (1933) 825–835. https://doi.org/10.1063/1.1749252.

[233] K. Pachucki, "Born-Oppenheimer potential for H_2," *Phys. Rev. A* **82** (Sep, 2010) 032509. https://link.aps.org/doi/10.1103/PhysRevA.82.032509.

[234] K. Pachucki, M. Zientkiewicz, and V. Yerokhin, "H2SOLV: Fortran solver for diatomic molecules in explicitly correlated exponential basis," *Computer Physics Communications* **208** (07, 2016) .

[235] M. Schlösser, X. Zhao, M. Trivikram, W. Ubachs, and E. J. Salumbides, "CARS spectroscopy of the $(v = 0 \rightarrow 1)$ band in T_2," *Journal of Physics B: Atomic, Molecular and Optical Physics* **50** no. 21, (Oct, 2017) 214004. http://dx.doi.org/10.1088/1361-6455/aa8d80.

[236] T. M. Trivikram, M. Schlösser, W. Ubachs, and E. J. Salumbides, "Relativistic and QED Effects in the Fundamental Vibration of T_2," *Phys. Rev. Lett.* **120** (Apr, 2018) 163002. https://link.aps.org/doi/10.1103/PhysRevLett.120.163002.

[237] K.-F. Lai, P. Czachorowski, M. Schlösser, M. Puchalski, J. Komasa, K. Pachucki, W. Ubachs, and E. J. Salumbides, "Precision tests of nonadiabatic perturbation theory with measurements on the DT molecule," *Phys. Rev. Research* **1** (Nov, 2019) 033124. https://link.aps.org/doi/10.1103/PhysRevResearch.1.033124.

[238] K.-F. Lai, V. Hermann, T. M. Trivikram, M. Diouf, M. Schlösser, W. Ubachs, and E. J. Salumbides, "Precision measurement of the fundamental vibrational frequencies of tritium-bearing hydrogen molecules: T2, DT, HT," *Physical Chemistry Chemical Physics* **22** no. 16, (2020) 89738987. http://dx.doi.org/10.1039/D0CP00596G.

[239] F. Biraben, "The first decades of Doppler-free two-photon spectroscopy," *Comptes Rendus Physique* **20** no. 7, (2019) 671 – 681. http://www.sciencedirect.com/science/article/pii/S1631070519300283. La science en mouvement 2 : de 1940 aux premières années 1980 â Avancées en physique.

[240] G. D. Dickenson, M. L. Niu, E. J. Salumbides, J. Komasa, K. S. E. Eikema, K. Pachucki, and W. Ubachs, "Fundamental Vibration of Molecular Hydrogen," *Phys. Rev. Lett.* **110** (May, 2013) 193601. https://link.aps.org/doi/10.1103/PhysRevLett.110.193601.

[241] F. M. J. Cozijn, P. Dupré, E. J. Salumbides, K. S. E. Eikema, and W. Ubachs, "Sub-Doppler Frequency Metrology in HD for Tests of Fundamental Physics," *Phys. Rev. Lett.* **120** (Apr, 2018) 153002. https://link.aps.org/doi/10.1103/PhysRevLett.120.153002.

[242] M. Niu, E. Salumbides, G. Dickenson, K. Eikema, and W. Ubachs, "Precision spectroscopy of the X1Σg+,v=01(J=02) rovibrational splittings in H2, HD and D2,"

Journal of Molecular Spectroscopy **300** (2014) 44–54.
https://www.sciencedirect.com/science/article/pii/S0022285214000630.

[243] R. Z. Martínez, D. Bermejo, P. Wciso, and F. Thibault, "Accurate wavenumber measurements for the S0(0), S0(1), and S0(2) pure rotational Raman lines of D2," *Journal of Raman Spectroscopy* **50** no. 1, (2019) 127–129. https://analyticalsciencejournals.onlinelibrary.wiley.com/doi/abs/10.1002/jrs.5499.

[244] P. D. Maker and R. W. Terhune, "Study of Optical Effects Due to an Induced Polarization Third Order in the Electric Field Strength," *Phys. Rev.* **137** (Feb, 1965) A801–A818. https://link.aps.org/doi/10.1103/PhysRev.137.A801. [Erratum Phys. Rev. 148, 990 (1966)].

[245] M. N. Slipchenko and J.-X. Cheng, *Nonlinear Raman Spectroscopy: Coherent Anti-Stokes Raman Scattering (CARS)*, pp. 1744–1750. Springer Berlin Heidelberg, Berlin, Heidelberg, 2013. https://doi.org/10.1007/978-3-642-16712-6_136.

[246] L. Wolniewicz, "VibrationalRotational Study of the Electronic Ground State of the Hydrogen Molecule," *The Journal of Chemical Physics* **45** no. 2, (1966) 515–523. https://doi.org/10.1063/1.1727599.

[247] P. G. Wilkinson, "The electronic isotope shift in the Lyman bands of H2, HD, and D2," *Canadian Journal of Physics* **46** no. 10, (1968) 1225–1235. https://doi.org/10.1139/p68-156.

[248] M. Galassi *et al.*, *GNU Scientific Library Reference Manual (3rd Ed.)*. ISBN 0954612078.

[249] P. Fadeev, Y. V. Stadnik, F. Ficek, M. G. Kozlov, V. V. Flambaum, and D. Budker, "Revisiting spin-dependent forces mediated by new bosons: Potentials in the coordinate-space representation for macroscopic- and atomic-scale experiments," *Phys. Rev. A* **99** no. 2, (2019) 022113, arXiv:1810.10364 [hep-ph].

[250] V. Silveira and A. Zee, "Scalar Phantoms," *Physics Letters B* **161** no. 1, (1985) 136–140. https://www.sciencedirect.com/science/article/pii/0370269385906240.

[251] R. D. Peccei and H. R. Quinn, "CP Conservation in the Presence of Instantons," *Phys. Rev. Lett.* **38** (1977) 1440–1443.

[252] R. D. Peccei and H. R. Quinn, "Constraints Imposed by CP Conservation in the Presence of Instantons," *Phys. Rev. D* **16** (1977) 1791–1797.

[253] F. Wilczek, "Problem of Strong *P* and *T* Invariance in the Presence of Instantons," *Phys. Rev. Lett.* **40** (1978) 279–282.

[254] J. Preskill, M. B. Wise, and F. Wilczek, "Cosmology of the Invisible Axion," *Phys. Lett. B* **120** (1983) 127–132.

[255] Y. Chikashige, R. N. Mohapatra, and R. D. Peccei, "Are There Real Goldstone Bosons Associated with Broken Lepton Number?," *Phys. Lett. B* **98** (1981) 265–268.

[256] G. Feinberg and J. Sucher, "Long-Range Forces from Neutrino-Pair Exchange," *Phys. Rev.* **166** (1968) 1638–1644.

[257] S. D. H. Hsu and P. Sikivie, "Long range forces from two neutrino exchange revisited," *Phys. Rev. D* **49** (1994) 4951–4953, arXiv:hep-ph/9211301.

[258] J. A. Grifols, E. Masso, and R. Toldra, "Majorana neutrinos and long range forces," *Phys. Lett. B* **389** (1996) 563–565, arXiv:hep-ph/9606377.

[259] Y. V. Stadnik, "Probing Long-Range Neutrino-Mediated Forces with Atomic and Nuclear Spectroscopy," *Phys. Rev. Lett.* **120** no. 22, (2018) 223202, arXiv:1711.03700 [physics.atom-ph].

[260] A. Yelkhovsky, "Quantum electrodynamics of the helium atom," *Phys. Rev. A* **64** (2001) 062104, arXiv:hep-ph/0103241.

[261] A. Czarnecki, K. Melnikov, and A. Yelkhovsky, "Positronium hyperfine splitting: Analytical value at O(m alpha**6)," *Phys. Rev. Lett.* **82** (1999) 311–314, arXiv:hep-ph/9809341.

[262] A. Czarnecki, K. Melnikov, and A. Yelkhovsky, "Positronium S state spectrum: Analytic results at O(m alpha**6)," *Phys. Rev. A* **59** (1999) 4316, arXiv:hep-ph/9901394.

[263] M. Ghosh, Y. Grossman, and W. Tangarife, "Probing the two-neutrino exchange force using atomic parity violation," *Phys. Rev. D* **101** no. 11, (2020) 116006, arXiv:1912.09444 [hep-ph].

[264] G. Arcadi, M. Lindner, J. Martins, and F. S. Queiroz, "New physics probes: Atomic parity violation, polarized electron scattering and neutrino-nucleus coherent scattering," *Nucl. Phys. B* **959** (2020) 115158, arXiv:1906.04755 [hep-ph].

[265] F. Ferrer and M. Nowakowski, "Higgs and Goldstone bosons mediated long range forces," *Phys. Rev. D* **59** (1999) 075009, arXiv:hep-ph/9810550.

[266] Y. Kamiya, K. Itagami, M. Tani, G. N. Kim, and S. Komamiya, "Constraints on New Gravitylike Forces in the Nanometer Range," *Phys. Rev. Lett.* **114** (2015) 161101, arXiv:1504.02181 [hep-ex].

[267] H. E. Haber *et al.*, "The CP-Violating Two-Higgs Doublet Model," in *Meeting on CP Violation and Non-standard Higgs Physics*. 2006.

[268] F. Herren and M. Steinhauser, "Version 3 of RunDec and CRunDec," *Comput. Phys. Commun.* **224** (2018) 333–345, arXiv:1703.03751 [hep-ph].

[269] **UTfit** Collaboration, "Unitary Triangle fit," accessed 26 May 2021. http://utfit.org/UTfit/ResultsSummer2016SM.

[270] **Particle Data Group** Collaboration, M. Tanabashi *et al.*, "Review of Particle Physics," *Phys. Rev. D* **98** no. 3, (2018) 030001.

[271] K. G. Chetyrkin, J. H. Kuhn, A. Maier, P. Maierhofer, P. Marquard, M. Steinhauser, and C. Sturm, "Addendum to "Charm and bottom quark masses: An update"," *Phys. Rev. D* **96** (2017) 116007, arXiv:1710.04249 [hep-ph]. [Addendum: Phys.Rev.D 96, 116007 (2017)].

[272] K. G. Chetyrkin, J. H. Kuhn, A. Maier, P. Maierhofer, P. Marquard, M. Steinhauser, and C. Sturm, "Charm and Bottom Quark Masses: An Update," *Phys. Rev. D* **80** (2009) 074010, arXiv:0907.2110 [hep-ph].

[273] **Flavour Lattice Averaging Group** Collaboration, S. Aoki *et al.*, "FLAG Review 2019: Flavour Lattice Averaging Group (FLAG)," *Eur. Phys. J. C* **80** no. 2, (2020) 113, arXiv:1902.08191 [hep-lat].

[274] V. M. Braun, D. Y. Ivanov, and G. P. Korchemsky, "The B meson distribution amplitude in QCD," *Phys. Rev. D* **69** (2004) 034014, `arXiv:hep-ph/0309330`.

[275] **RQCD** Collaboration, G. S. Bali, V. M. Braun, S. Bürger, M. Göckeler, M. Gruber, F. Hutzler, P. Korcyl, A. Schäfer, A. Sternbeck, and P. Wein, "Light-cone distribution amplitudes of pseudoscalar mesons from lattice QCD," *JHEP* **08** (2019) 065, `arXiv:1903.08038 [hep-lat]`. [Addendum: JHEP 11, 037 (2020)].

[276] S. Cheng, A. Khodjamirian, and A. V. Rusov, "Pion light-cone distribution amplitude from the pion electromagnetic form factor," *Phys. Rev. D* **102** no. 7, (2020) 074022, `arXiv:2007.05550 [hep-ph]`.

[277] M. J. Baker, J. Fuentes-Martín, G. Isidori, and M. König, "High-p_T signatures in vector–leptoquark models," *Eur. Phys. J. C* **79** no. 4, (2019) 334, `arXiv:1901.10480 [hep-ph]`.

[278] F. M. J. Cozijn, P. Dupré, E. J. Salumbides, K. S. E. Eikema, and W. Ubachs, "Sub-Doppler Frequency Metrology in HD for Tests of Fundamental Physics," *Phys. Rev. Lett.* **120** (Apr, 2018) 153002. `https://link.aps.org/doi/10.1103/PhysRevLett.120.153002`.

[279] C.-F. Cheng, Y. R. Sun, H. Pan, J. Wang, A.-W. Liu, A. Campargue, and S.-M. Hu, "Electric-quadrupole transition of H_2 determined to 10^{-9} precision," *Phys. Rev. A* **85** (Feb, 2012) 024501. `https://link.aps.org/doi/10.1103/PhysRevA.85.024501`.

[280] T. M. Trivikram, M. L. Niu, P. Wcislo, W. Ubachs, and E. J. Salumbides, "Precision measurements and test of molecular theory in highly excited vibrational states of H2 ($v = 11$)," *Applied Physics B* **122** no. 12, (2016) 294. `https://doi.org/10.1007/s00340-016-6570-1`.

[281] R. Z. Martínez, D. Bermejo, P. Wcisło, and F. Thibault, "Accurate wavenumber measurements for the S0(0), S0(1), and S0(2) pure rotational Raman lines of D2," *Journal of Raman Spectroscopy* **50** no. 1, 127–129. `https://onlinelibrary.wiley.com/doi/abs/10.1002/jrs.5499`.

Acknowledgements

First of all, I would like to thank Prof. Ulrich Nierste for offering me the opportunity to pursue a PhD at the TTP. I like to thank him for suggesting the research topics I worked on but also leaving me much freedom to pursue my own ideas. I also want to thank Prof. Matthias Steinhauser for agreeing to be the second supervisor of my thesis and for his helpful comments during the final phases of this work.

I am grateful to Harun Acaroğlu and Martin Lang for proofreading a large part of this thesis. In this regard, I also would like to thank Martin Gabelmann for the discussion on the MSSM Higgs mass corrections during the final stage of this work.

I also like to thank Wolfgang G. Hollik, Matthias Linster, Ulrich Nierste, and Robert Ziegler for our collaborations that lead to the works in References [143, 193] and for the works in process.

A big thanks goes to Simon Kast and Marta Moscati who reserved and offered me the free desk in their office, with the coffee room being just around the corner, before I officially started my PhD studies. In this respect, I would like to thank my other office mates, Abdur Rehman and Harun Acaroğlu, as well as Matthias Linster, David Wellmann, Daniel Baranowski, and Martin Lang for the many random (coffee) breaks and discussions on physics and beyond. I also want to thank the members of the institute for the enjoyable atmosphere during the last years.

Another thanks goes to my previous and current admin colleagues, Konstantin Asteriadis, David Wellmann, Martin Gabelmann, and Martin Lang. I also wish our new admins and successors Vitaly Magerya and Fabian Lange much fun and patience, which they will surely need.

Finally, a huge thanks goes to my family for all the support which made many things so much easier.